



UNIVERSITÀ
DEGLI STUDI
FIRENZE

DOTTORATO DI RICERCA IN SCIENZE CHIMICHE

CICLO XXX

COORDINATORE Prof. ANDREA GOTI

NANOSTRUCTURED GELS AND SENSORS FOR PREVENTIVE AND
SUSTAINABLE CONSERVATION OF WORKS OF ART

GEL E SENSORI NANOSTRUTTURATI PER LA CONSERVAZIONE PREVENTIVA E
SOSTENIBILE DI OPERE D'ARTE

Settore Scientifico Disciplinare CHIM/02

Dottorando

Dott. Chiara Berlangieri

Tutore

Prof. Luigi Dei

Coordinatore

Prof. Andrea Goti

Anni 2014/2017

CONTENTS

List of Abbreviations	v
I Introduction	1
1 Introduction	3
II Fundamentals	7
2 Gels and gel-like systems: properties and applications in Cultural Heritage conservation	9
2.1 Definition and Properties of Gel	10
2.1.1 Chemical and physical gels	11
2.2 Characterization of gels	12
2.2.1 Rheology	12
2.2.2 Small Angle X-Ray Scattering (SAXS)	14
2.3 Gels and gel-like systems in conservation	16
2.3.1 Cleaning works of art surfaces	16
2.3.2 Advantages of confining cleaning fluids in a gel phase . .	17
2.3.3 Gels as cleaning tools: an overview	18
2.4 Aim of the dissertation	24
2.4.1 HPG-based gel-like systems	25
2.4.2 Removal of a degradation patina	25
3 SPR and LSPR (bio)sensing	27
3.1 SPR and LSPR	28
3.1.1 Propagating SPR	28
3.1.2 Localized SPR	28
3.1.3 SPR and LSPR Biosensors	31
3.2 PDMS-Gold nanocomposites	31
3.2.1 Biosensors in the field of Cultural Heritage	33
3.3 Work description	34
III Results and Discussion	37
4 Results and discussions	39
5 Hydroxypropyl guar based gel-like systems	41

6 Appendix	67
6.1 Further Investigations on HPG based systems	68
6.1.1 Glycerol Effect: Creep recovery tests	68
6.1.2 Glycerol Effect: Extensional tests	70
6.1.3 Organic solvents uploading	73
7 Chelators confined into 80pvac-borax highly viscous dispersions	79
8 Gold nanostructures at a PDMS surface	93
IV Conclusions	113
9 Conclusions	115
10 Bibliography	119

LIST OF ABBREVIATIONS

ACRY/BIS acrylamide–bisacrylamide

AuNPs Gold Nanoparticles

EGDMA ethyleneglycol dimethacrylate

HEMA hydroxyethylmethacrylate

HPG Hydroxypropyl guar gum

LSP Localized Surface Plasmon

LSPR Localized Surface Plasmon Resonance

MEK Methyl ethyl ketone

mNPs metal nanoparticles

p(HEMA) poly(2-hydroxyethylmethacrylate)

PAA polyallylamine

PDMS Polydimethylsiloxane

PEI polyethylenimine

PrOH Propanol

PVP poly(vinylpyrrolidone)

SAXS Small Angle X-Ray Scattering

semi-IPN semiinterpenetrating networks

SPR Surface Plasmon Resonance

SPs Surface Plasmons

PREFACE

This thesis was submitted to the University of Florence as a requirement to obtain the PhD degree. The presented work was carried out in the years 2014-2017 at CSGI laboratories, Department of Chemistry "Ugo Schiff", University of Florence.

THESIS OBJECTIVES

The final aim of this project is to study, from different points of view, the potentiality of new technologies in the field of the diagnostic, restoration and conservation of cultural heritage. In particular soft matters and sensors are the main topics of this project. The objectives of this work can be summarized as follow:

1. development and characterization of an aqueous soft system containing hydroxypropyl guar crosslinked by borax, with the addition of glycerol as plasticizer, having potential applications in the cleaning of artistic surfaces;
2. assessment of the efficacy of recently developed highly viscous dispersions in the removal of a gypsum degradation patina from carbonatic stones, after the embedding with chelating agents.
3. development of a smart and cheap sensor, exploring the tunability of gold nanostructures at a PDMS surface through a double-growth approach.

THESIS OUTLINE

This dissertation is divided into four parts: introduction, fundamentals, results and discussion and conclusions.

The **Introduction part** presents the topic of the present work and highlights the motivation of the research conducted in this Thesis.

The **Fundamental part** is divided in two Chapters. The first one shows a brief overview about gels and gel-like systems and highlights the advantages that can be achieved through the use of gel systems in cleaning works of art surfaces. In the same chapter an overview on gels already proposed as cleaning tools in restoration procedures and on the most recent developments will also be provided. The second one briefly introduces the fundamental aspects of the SPR and LSPR spectroscopies and explain the application of sensors in the field of cultural heritage that inspired the work in this Thesis.

The **Results and Discussion part** is divided in sections, according to the different tasks which cover the different aspects of the project:

- 1st Task** Hydroxypropyl guar based gel-like systems: structural, rheological and dynamic characterization, focusing on the role of glycerol introduced as plasticizer in the formulation.
- 2nd Task** Chelators confined into 80pvac-borax highly viscous dispersions: rheological characterization and test on cleaning efficacy by means of Ion Chromatography and Inductively Coupled Plasma techniques.
- 3rd Task** Tunable growth of gold nanostructures at a PDMS surface: formation of well exposed and densely-packed 3D conglomerates of spheroids and behavior of plasmon rulers after a second growth.

The results will be reported following the hierarchical order shown here.

Part I

INTRODUCTION

1

INTRODUCTION

Artworks, from a thermodynamic point of view, can be considered open systems, having a constant interaction with the surrounding environment. For this reason, surface materials can undergo to a degradation caused by both natural aging and chemical, physical and biological phenomena due to environmental factors such as the exposure to light, humidity cycles, temperature, insects and microorganisms and also depending on the chemical composition and mechanical properties of the artwork itself. As a result, an artwork can be object of a more or less serious chemical-physical alteration that can result in a loss of its original appearance. Preserving works of art means slowing down the degradation and eliminating its causes, as far as possible, through restoration and conservation treatments, as long as through diagnostic investigation on artworks materials.

In the last decades new technologies were developed and proposed in the field of conservation of cultural heritage, such as advanced diagnostic techniques for the study of artworks and innovative materials and methods for the cleaning, consolidation and protection of different artistic objects. In particular, it is still necessary and unavoidable to submit the works of art to more invasive actions, first of all the cleaning action.

Within the procedures carried out during restoration, cleaning is considered one of the most critical and potentially harmful step. It implies a removal of undesired materials from a surface and it is necessary for the restoration of the original appearance of the object as long as to remove eventual degraded compounds which can cause other alteration phenomena. Moreover cleaning can be a necessary step to perform other interventions, since it allows the access to the artistic substrate. The problems connected to the cleaning action are mainly related to the traditional methods used by the restorers,

that involve the use of free organic solvents, pure or in mixture. Traditional solvents exhibit poor selectivity and poor controllability of the cleaning action, mainly in terms of solubilization power and penetration within the layers of the works of art. For this reason, innovative materials and techniques are continuously demanded.

In this framework, Colloid and Surface Science played a crucial role. In particular, the CSGI consortium (Center for Colloids and Surface Science) in the Chemistry Department of the University of Florence developed and studied some of the most innovative cleaning tools such as micelles, microemulsions and gels for the restoration of works of art. [1–3]

Micelles and microemulsions are water-based nanostructured fluids, exhibiting an effective action in removal of soil coatings from artworks surfaces that are difficult to be removed using traditional cleaning methods. Thanks to their amphiphilic nature these systems, indeed, allow the swelling, solubilization and selective removal of synthetic coatings, such as acrylic and vinyl polymers, deriving from past restoration procedures.

Another class of versatile and intriguing tools proposed in this field is that of gels and gel-like systems. The use of confining systems allows a controlled release of cleaning agents onto the artifact surface, leading to a more selective and controlled treatment. The high viscosity of these materials results in a minimization of the penetration of the cleaning fluids into the porosity of the substrate. The confinement of organic solvents strongly reduces their evaporation rate and so the toxicity drawbacks. Moreover, these materials are very versatile and can upload a large variety of cleaning agents. In addition, their tunable features make them applicable on different supports.

The diagnostic techniques in the field of conservation play a very important role, that often can be undervalued. The assessment of a cleaning treatment is very crucial in order to achieve even more improvement and to investigate the critical issues connected with a particular situation. Traditionally, the characterization of artworks and the study of the progression of the cleaning process are carried out by means of invasive investigations which often require samplings (FTIR, SEM, GC-MS, Fluorimetry etc.). The research in this field is often focused on the development of protocols that can avoid invasive sampling or, even better, on the application of innovative in-situ analysis.

The work presented in this dissertation takes inspiration from the most recent studies on new technologies proposed and in their application in the field of conservation of cultural heritage. The work can be divided into three topics.

The first one is about the development of new materials for the cleaning of artistic surfaces. Among the innovative cleaning tools we focused on gels and gel-like systems. In particular, in this Thesis, we studied and characterized water-based soft systems containing hydroxypropyl guar (HPG) crosslinked by borax, in which glycerol was added in order to tune the mechanical properties.

In particular we studied the viscoelastic and dynamic features that can be tuned by changing the components amount, focusing on the role of glycerol in systems properties and in the network formation.

The second topic is about the evaluation of the efficacy of a cleaning treatment performed using gel-like systems based on partially hydrolyzed poly(vinyl acetate) and borax, previously developed and characterized in CSGI research group. These systems were embedded with chelators and applied for the removal of a gypsum patina from an artificially sulfated travertine tiles. In the frame of this work, one of the goal was the set-up of an analytical protocol for the pre-treatment and the analysis of gel-like systems collected after the cleaning tests, with the aim to obtain a quantitative determination of sulfate removal.

In the perspective of a restoration intervention even more effective and low invasive, a biochemical characterization of artworks can be a very attractive tool. Among new analytical technologies, SPR and LSPR sensing devices have been proposed as versatile and sensitive platform in analytical analysis for biomolecular interactions. The focus of the method is on the sensitivity of active surfaces that can be thin metal layers (in the case of SPR) or made by metal nanoparticles (in the case of LSPR), associated to biomolecular interaction processes. In particular, LSPR sensing has been increasingly used for biological and biomedical assays. Furthermore, recently a great interest started to grow in developing not just biological, but also chemical sensing applications of this technology. [4, 5] During the last decade biotechnological applications to artwork preservation have been introduced with promising results. Recently, the successful combination of the SPR (bio)sensing technology with gels as innovative cleaning tools in the detection of eggs proteins from a painted surface [6] represented a promising starting point for the development of a new cheap and smart device, with perspectives of application in the field of conservation.

Taking inspiration from this promising perspective, the third section of the work presented in this Thesis regards the fabrication and study of an active substrate. In particular it focused on plasmonic composite substrates for LSPR sensing, using PDMS as a cheap and versatile polymeric substrate for the in-situ growth of Au nanoparticles (AuNPs). The intriguing task is to obtain a devices easier to use, versatile and sensitive at the same time. In particular, the fabrication process was performed by modifying disposable UV-Vis cuvettes with a PDMS film and performing the in-situ growth of AuNPs, obtaining the unique advantage of a stable device that can be interrogated by conventional or portable spectrophotometers.

Part II

FUNDAMENTALS

2

GELS AND GEL-LIKE SYSTEMS: PROPERTIES AND APPLICATIONS IN CULTURAL HERITAGE CONSERVATION

This Chapter shows a brief overview about gels and gel-like systems and highlights the advantages that can be achieved through the use of gel systems in cleaning works of art surfaces. Moreover, an overview on gels already proposed as cleaning tools in restoration procedures and on the most recent developments will also be provided.

Contents

2.1	Definition and Properties of Gel	10
2.1.1	Chemical and physical gels	11
2.2	Characterization of gels	12
2.2.1	Rheology	12
2.2.2	Small Angle X-Ray Scattering (SAXS)	14
2.3	Gels and gel-like systems in conservation	16
2.3.1	Cleaning works of art surfaces	16
2.3.2	Advantages of confining cleaning fluids in a gel phase	17
2.3.3	Gels as cleaning tools: an overview	18
2.4	Aim of the dissertation	24
2.4.1	HPG-based gel-like systems	25
2.4.2	Removal of a degradation patina	25

2.1 Definition and Properties of Gel

The definition of "gel" has always been matter of discussion. As a very famous statement of Jordan Lloyd says: "*..the colloid condition, the gel, is easier to recognize than to define*". [7] Brinker and Scherer defined a gel as a material made by a continuous solid scheleton in which a continuous liquid phase is contained.[8] At least we can define gels as soft materials consisting of interconnected polymer chains or colloidal particles that entrap a fluid. The physical properties of gels are intermediate between those of a solid and of a liquid. As a matter of fact a gel contains a solid dispersed into a fluid (that can be a liquid or gas) forming a three-dimensional network and, finally, an exhaustive definition was given by the International Union of Pure and Applied Chemistry (IUPAC), that defines a gel a "*non-fluid colloidal network or polymer network that is expanded through its whole volume by a fluid*".[9] We can consider a gel as a bicontinuous fluid phase. The concept of continuity refers to the possibility to go across the whole solid phase from one side of the system to the other, without touching the liquid phase, and viceversa. We are surrounded by gels and gel-like systems in our daily life because of their versatility and different applications, from food (jam, ketchup, puddings etc.) to cosmetic products (toothpastes, hair gels etc.), soft contact lenses, and so on.

The properties of a gel strictly depend on the structure of the polymeric network and on its interaction with the solvent. The macromolecules can have a high motility thanks to the huge amount of trapped solvent, and this motility is limited only by the entangled structure. The gels can also exchange material and energy with the surrounding, and that's why they can be considered active materials having responsiveness to different stimuly, such as pH, light, temperature and so on.[10–13] For what concern the mechanical properties of these systems, we can say that a gel has viscoelastic properties, due to its double nature of solid dispersed in a liquid phase.

There are different ways to classify gels. In example, polymer-based gels are the major class of gels and the formation of the 3D network is due to the polymerization with a crosslinker. Another class of gels are the so-called organogels, in which the 3D network exist in equilibrium with a non-polar solvent. In hydrogels water is the continuum phase, while in aerogels the fluid is air or other gas medium. In the perspective of this work, we can say that both hydrogels and organogels can be applied to works of art cleaning: hydrogels are useful to control the cleaning action on water-sensitive substrates, while organogels could be useful for the cleaning of substrates that would be

damaged upon interaction with water.

However, the fundamental classification is based on the nature of the crosslinking. Within this classification chemical and physical gels are the two main categories.

2.1.1 Chemical and physical gels

In physical gels the aggregation usually involves non-covalent interactions, such as hydrogen bonds, hydrophobic, ionic or van der Waals interactions, and also physical entanglement of the gellant molecules. [14] These systems are characterized by an energy of interaction much lower than that of covalent bonds, so one of the main properties of the physical gels is the reversibility. Indeed, if we heat them up to the gelation temperature (T_g , depending on the chemical composition) the structure melts and the resulting liquid system is called "sol". The system can turn to the previous gel by cooling down the temperature, in a process called sol-gel transition. In the field of cleaning of artistic surfaces, an example of physical gel is the "solvent gel" developed by Wolbers [15], that proposed a method to gel organic solvents, using polyacrylic acid in the formulation.

In a chemical gel the gelation process occurs through the formation of covalent bonds. In this case gels are thermally irreversible. If we increase the temperature above a critical value we induce the breaking of the bonds and the system does not turn the original structure by cooling. Hydrogels based on acrylamide–bisacrylamide (ACRY/BIS) have been used recently in cultural heritage cleaning [16] for applications on water-sensitive artifacts. An example of a chemical gel is polyhydroxyethylmethacrylate crosslinked with ethylenglycol dimethacrylate (HEMA/EGDMA) used for soft contact lenses.[17]

Comparing the properties of these two kind of systems in view of a restoration application, it is clear that chemical gels, characterized by covalent bonds that determine strong cohesive forces, can be applied on a surface without leaving residues. On the other hand, physical gels can be easily shaped, with the advantage of a homogeneous interaction with the treated surface, but they often leave residues. The problem of residues is very critical, because they must be removed by mechanical action or using solvents, which might redisperse the solubilized material within the porous matrix of the substrate. [1]

2.2 Characterization of gels

In order to study the structure and main properties of gels, usually a multi-technique approach is necessary, mainly because we are studying a very complex system, whose properties result from various parameters. In the frame of this work we studied structural and mechanical properties of gels containing hydroxypropyl guar crosslinked by borax, and two main techniques were used: rheology for the mechanical properties and SAXS for the gel structure.

2.2.1 Rheology

Rheology studies the deformation of a material due to the application of a force.[18] Rheological measurements are usually performed by applying a force to the sample and registering the resulting response in terms of deformation. As previously mentioned, gels present viscoelastic properties that characterize the response of the material to external mechanical stimuli. [19]

The viscoelastic behavior is described by two different rheological parameters: the storage modulus G' and the loss modulus G'' . The storage modulus describes the elastic behavior of the material, taking into account the energy stored by the system during the perturbation, and it is also called elastic modulus. The loss modulus describes the viscous nature of the system, considering the energy dissipated by the material, and it is also called viscous modulus. A purely elastic material exhibits a $G' \neq 0$ and a viscous modulus $G'' = 0$. On the opposite, purely viscous material has a zero elastic modulus and a non-zero viscous modulus. [18]

The rheological study of this material is very interesting and useful in predicting the gel behavior during its application and can give fundamental informations about their use in the treatment of artistic surfaces. In particular, by means of frequency sweep measurements, it is possible to quantify the viscoelastic behavior of the system. In fact, applying an oscillating perturbation, by varying the perturbation frequency and keeping constant its amplitude, we can obtain a plot in which the elastic and storage moduli are plotted as a function of the perturbation frequency. The value of G' , specially at high frequency, is a fundamental parameter to consider in view of an application in artistic surface treatment. If this value reaches a sort of plateau at high frequency, we can associate it to the shear modulus of the system G_0 , correlated to the density of the entanglement between polymeric chains. The viscoelastic behavior

of the gel and gel-like systems gives us important informations about their macroscopic behavior. In particular, previous studies showed that, in order to have a system that can be easily peeled off the surface after a treatment, a minimum G_0 value of 200 Pa is needed at high perturbation frequencies. [20] From a rheological point of view, we can consider a system a gel only if $G' > G''$. [21] So other similar materials that have a viscoelastic behavior are, more correctly, highly viscous polymeric dispersions (HVPD). These gel-like systems are often characterized by a crossover between G' and G'' in the frequency sweep plot, especially water based systems. In the frame of the first task of this Thesis we are going to study systems containing hydroxypropyl guar crosslinked by borax in which glycerol was added to tune the viscoelastic behavior. These systems can be associated to the gel class for lower glycerol contents, while they start behave as HVPD for higher glycerol concentrations. In the second part of the present work we are going to study the efficacy of a cleaning treatment performed with previously developed systems containing partially hydrolyzed poly(vinyl acetate) and borax as crosslinker, that are classified as HVPD.



Figure 2.1: TA Instrument Hybrid Rheometer DISCOVERY HR-3 used for rheological measurements reported in this Thesis. Image reproduced from the web site <http://www.tainstruments.com/dhr-3/>

2.2.2 Small Angle X-Ray Scattering (SAXS)

Small Angle X-Ray Scattering belongs to the group of techniques in which an elastic diffusion of an incident radiation on a sample (in this case X-Rays) occurs and the resulting scattering pattern is registered and analyzed in order to reach informations about dimensions, shape and orientation of the scattering objects in the sample.

A SAXS instrumentation includes the X-Ray source, a monochromator, a collimation system, a sample chamber and a detection system. [22] SAXS, but in general scattering techniques, is non-destructive and the sample preparation

is minimal. In a typical small angle scattering experiment an angular distribution of the scattering intensity takes place, due to the inhomogeneities at the nanometre scale (i.e. 1–100 nm) that are referred to a change in the dimensional range investigated.

For what concern gels and gel-like systems, an important parameter to consider for their use is the mesh size or correlation length, that is associated to the size of the pores in the network and that can be studied by means of SAXS. This parameter gives us informations about the crosslinking density and, in particular, as reported in literature, [23] in a semi-diluted polymeric solution, the mesh size corresponds to the average distance between neighboring entanglement points of the 3D polymeric network. In this Thesis we used SAXS measurements in order to better understand the role of the components on the structure of the studied systems, taking into account the differences between the mesh size values.



Figure 2.2: SAXS Hecus S-3 Micro. Image reproduced from the web site <http://www.anarghyainnotech.com/hecus.html>

2.3 Gels and gel-like systems in conservation

2.3.1 Cleaning works of art surfaces

Within the procedures involved in conservation treatments, cleaning is one of the most delicate and potentially harmful step; the removal of undesired materials from a surface is the main aim of the cleaning operation and can become a very critical issue if we are talking about artistic or historical surfaces. A conservator can face a very large range of materials to be removed, such as dirt, soil, biological coatings, synthetic coatings that can produce aesthetic alteration with aging, but that can also be cause of chemical and physico-chemical damage degrading over time. In addition, each typology of artifact requires different specific treatments. Being an irreversible step, cleaning can cause many risks for the artwork itself: the materials to be removed can co-exist with those belong to the artifact in complex layered structures of few hundred of microns, thus a very high control of the cleaning action is of a crucial importance. [24]

In the past, a great variety of materials was used for cleaning (soaps, vinegar, lemon juice, saliva). In the last decades, the traditional cleaning methods involved principally the use of neat organic solvents, in most cases coupled with mechanical action. However, the use of solvents can lead to undesired effects connected to the physical mechanism involved in the process. One of the main concerns is the lack of control on their penetration within the substrate, which can result in solubilization and alteration of materials belonging to the artwork, or the transport of dissolved matter through porous matrices, so to detrimental effects. Moreover, their use in cleaning represents a risk also for the operator and for the safety of working environment, because of the drawbacks related to solvents toxicity. As a result, much research has been carried out in the last decades on more innovative systems in which aqueous cleaning systems or solvents can be confined in a polymer network, such as gels. [3]

2.3.2 Advantages of confining cleaning fluids in a gel phase

Gels as innovative, effective and versatile tools in the field of cultural heritage conservation were extensively studied in various research works and the role of these materials in the cleaning of works of art has become central. Gel and gel-like formulations have been used to minimize the drawbacks connected to the use of "free" cleaning fluids, allowing a controlled release on the artifact surface. In particular, the several advantages of these innovative systems are summarized as follow [3, 24]:

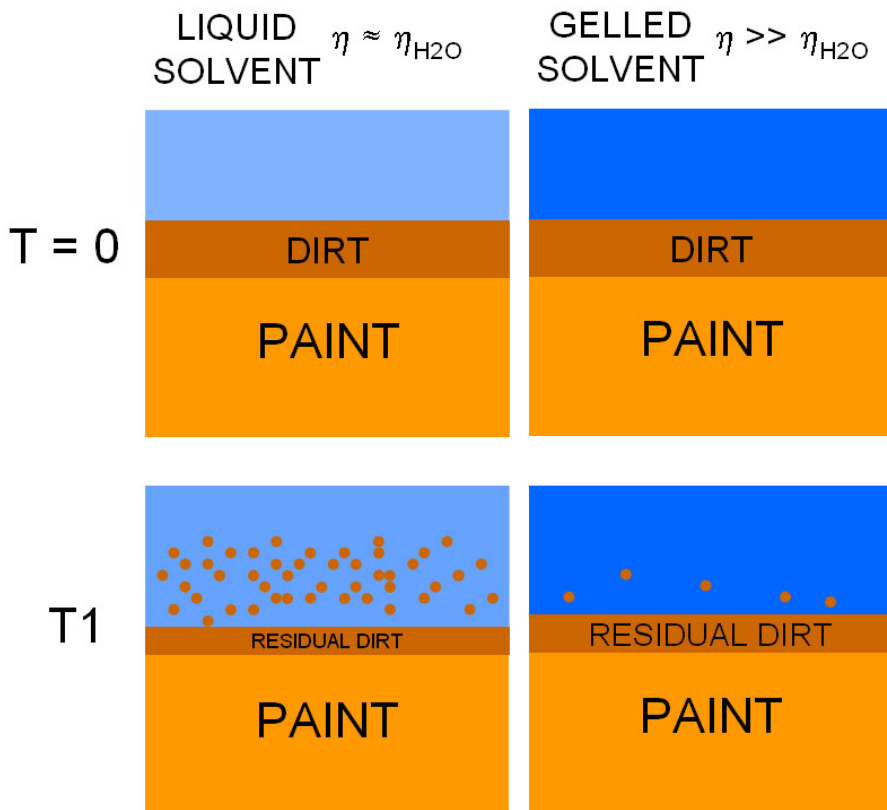


Figure 2.3: Schematic representation of the effects of the application of a liquid (A) or a gelled solvent (B) for the cleaning of a painted surface. (A) The low viscosity (η) of the liquid results in a fast solubilization of the dirt layer, with a possible loss of control of the cleaning action. (B) The high viscosity of the gelled solvent allows a slower and much more controllable cleaning. Image reproduced from Baglioni et al. 2013 [24]

- The penetration of the solvent into the porosity of the substrate is

minimized because of the high viscosity of the systems. This resulting in a selective cleaning action involving just the interface between the artifact and the environment.

- The solubilization kinetic is lower with respect to that of a free solvent, as a result of the reduced mobility of solutes inside the gel. The decreased rate of solubilization strongly enhances the control on the cleaning procedure.
- The toxicity drawbacks are minimized thanks to the decrease of the evaporation rate of the liquid phase confined in the gel.
- These materials are very versatile and can upload a large variety of cleaning agents (organic solvents, chelating agents, microemulsions ad so on). In addition, depending on the cleaning fluid uploaded and on their characteristics, gels can be applied on different supports.

There is a vast amount of literature on gels. In particular, colloid and surface science gave a great contribution in the development of innovative systems with specific properties and in the following section a brief overview on the classes of gels used in cleaning of works of art and on the most recent developments in these intriguing systems is provided.

2.3.3 Gels as cleaning tools: an overview

2.3.3.1 Conventional systems

In the past decades, conservators studied several methods for the confinement of solvents, to increase the control of cleaning step, using thickeners and gellants, mainly constituted by water-soluble polymers. For what concern terminology, restorers commonly refer to the overall typologies of confining systems with the term "gel", even if in some cases they do not correspond to definition of gels in its strict sense. Since they all display the macroscopic appearance of gels, for simplicity, we will adopt the terminology in use among restorers.

One of the main classes of materials traditionally used as thickening agents comprises **cellulose ethers**, such as Klucel® and Tylose®, respectively

a hydroxypropyl and hydroxyethyl cellulose. These materials are used to thicken water and polar solvents which can form physical gels, with a consistency similar to a jam, and they can be applied on the surface to be cleaned, as showed in Figure2.4,[24] with the ability to fill and adapt also on rough surfaces. However, their scarce cohesive forces result in leaving residues on the surfaces with which they are put in contact. The residues removal often implies the use of mechanical action, often aggressive and dangerous for the original substrate. [25] In addition, the presence of cellulosic residues might allow microbial proliferation on the surface. Furthermore, the retention features of those systems are not very high, and high solvent evaporation rates can lead to the formation of dry films of solid material on the treated surface.

Another class of physical gels commonly used as cleaning systems is based on gelation of synthetic polymers derived from **polyacrylic acid** (i.e. Carbopol®, Pemulens®), introduced along with the development of "solvent gels", a class of materials proposed in the late 1980s by Richard Wolbers. [15] Solvent gels are based on the combination of the gellant (polyacrylic acid), characterized by the presence of many carboxylic groups, and a non-ionic surfactant (Ethomeen C12 or C15) with weak basic properties. The bases cause deprotonation of carboxylic functions in the acid chains that unfold and form an extended 3D network, in which the solvent is confined. [15, 26] The two surfactants differ for their hydrophilic-lipophilic balance (HLB) and are thus used to induce gelation in solvents or solvent mixtures characterized by different polarities. Ethomeen C12 is used for gelation of low polarity solvents, while C25 is more suitable for highly polar solvents. However, as for other physical gels for cleaning, solvent gels release residues on the surface of works of art after cleaning treatment. Again, mechanical removal and solubilization of the solvent gel deposits are necessary. The degradation phenomena induced by residues of the non-volatile components (polymer, surfactant) are unpredictable, and several studies have been carried out to investigate on the residue question. [27, 28]

Recently, **polysaccharide materials** such as agar and gellan gum have been proposed for residue-free surface cleaning purposes. [29, 30] These materials are applied on the surfaces as a highly viscous solution or as "rigid gels" (see Figure2.5) and allow a cleaning treatment leaving almost no residues. [31] They can support chelating agents, enzymes or surfactants at different pH values [31] and recently they have been used loaded with nanostructured cleaning fluids (microemulsions) for the removal of hydrophobic materials from porous surfaces. [32] Gellan gum gels were proposed for the cleaning of paper artifacts, being able to retain the dirt, and removal occurs without leaving substantial residues. [30] Agar and gellan gum gels allow gentle surface cleaning also on water-sensitive artifacts such as paper; however, in some cases

their water retention features can be not sufficient and leaching or loss of components such as water-soluble colors or inks might occur due to excessive wetting. [33]



Figure 2.4: Application and removal of a Klucel® "gel". Image reproduced from Baglioni et al., 2015. [3]

2.3.3.2 Innovative cleaning tools

Studies on new formulations with enhanced properties are continuously ongoing. In particular, research work is focused on gels with improved mechanical properties, resulting in easy handling materials and with the aim to avoid gel residues on the treated surface. Another important goal is to obtain high retentiveness systems, to fully control the cleaning action especially on sensitive substrates.

In the last decade, the development of several formulations with specific and enhanced properties compared to those discussed in the previous section has been proposed. These innovative tools were successfully used for the cleaning of artistic surfaces and some examples of the main innovative formulations, mainly developed in CSGI research group, will be reported in the following



Figure 2.5: "Rigid gels" obtained from polysaccharide materials: an agar agar gel (2%) loaded with water. Image reproduced from Baglioni et al., 2015. [3]

paragraphs. [3, 24]

- *Stimuli-responsive gels*

One of the most intriguing strategies for the easy and complete removal of gels after cleaning treatment was proposed with the development of stimuli-responsive gels. These systems can be easily and rapidly removed thanks to their responsiveness to a chemical, physical or mechanical "switch". As an example, polyamine (i.e. polyallylamine, PAA, or polyethylenimine, PEI) based rheoreversible gels proposed by Carretti et al. [34, 35] are able to be changed from a solution-form into a gel-form through bubbling CO_2 . The addition of CO_2 to the PAA solution converts into a gel through the formation of polyallylammonium carbamate ($PAACO_2$) characterized by strong inter-chain interactions. The so formed gel can be applied directly on a painted surface and it can be removed by simple decarboxylation, adding in situ a small amount of a weak aqueous solution (0.05M) of acetic acid after the cleaning action. The viscoelastic gel, reverted in this way into a liquid phase, can be wiped away with a cotton swab. Gelled systems of PAA in 1-pentanol were used for the removal of aged varnish from a gilded 19th century frame [36], while PEI based gels were applied for the cleaning of painted surfaces and gilded wood artifacts. [37, 38] [36]

Other type of gels able to respond to an external magnetic field were also proposed. Magnetic nanoparticles were functionalized and associated with acrylamide based gels containing water or aqueous systems. [39, 40] These hydrogels can release aqueous systems such as microemulsions in a controlled way on the surface with which they are put in contact. Thanks to magnetic properties, the removal of the gel can be carried out by using a permanent magnet, so completely avoiding any direct handling. This feature might be particularly useful in case of surfaces that are extremely sensitive to mechanical stress.

- *Chemical hydrogels*

Chemical hydrogels are another class of materials that have recently proved to be promising systems in the cleaning of artifacts. Having enhanced retentiveness they permit a safe and effective cleaning even on highly watersensitive artifacts, providing also residue-free results. Domingues et al. proposed semiinterpenetrating networks (semi-IPN), obtained by embedding poly(vinylpyrrolidone) (PVP) within a poly(2-hydroxyethylmethacrylate) (p(HEMA)) network.[33, 41] In this way it is possible to take advantage of the features of both polymers, in particular of the mechanical strength typical of p(HEMA) and of the PVP's high hydrophilicity. In addition, the gel's features can be tuned by varying the components ratios. These materials are transparent and the preparation allows the obtaining of the particular shape of elastic foils that can be easily handled and removed once the cleaning action is complete (Figure2.6). FTIR analysis showed also that these gels do not leave residues on the treated surface.[33]

Applicative tests using p(HEMA)/PVP hydrogels have been performed on water-sensitive and scarcely cohered painted surfaces, such as *tempera magra* paintings on canvas, where pigments and colorants are mixed with a minimal amount of binder (animal glue). The application of these semi-IPN gels loaded with water succeeded in the gradual and controlled removal of grime trapped into the substrate surface pores, without damaging for the painted layer. The p(HEMA)/PVP gels were also tested on paper samples painted with a water-soluble ink and results showed that the hydrogel did not alter the surface and that the application of the high retentive gel avoided excessive wetting and the diffusion of the colorant through the paper substrate. [33]

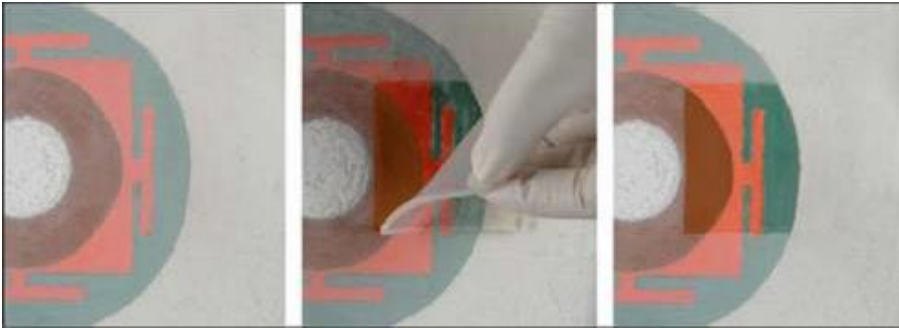


Figure 2.6: Removal of hydrophilic superficial grime using a p(HEMA)/PVP semi-IPN hydrogel loaded with water. Image reproduced from Domingues et al., 2013. [33]

These gels were originally developed for the upload of water-based nanostructured fluids, by simply immersion of 12h, and in this work they have been used in the removal of hydrophilic surface grime [33] and of hydrophobic materials [41]. However, these systems are also able to upload polar solvents like glycols or alcohols and ethanamine.

- *Gel-like systems*

Highly viscous polymeric dispersions (HVPD) are a class of interesting materials that represents another possible approach for the selective removal of coatings from artistic surfaces. As already mentioned in section 2.2.1, these systems cannot be classified as gels based on their rheological behavior, even if they have similar macroscopic features. The HVPD developed in the last decade can be formed by poly(vinyl alcohol) or by partially hydrolyzed poly(vinyl acetate), whose chains are cross-linked by borax, so they have a network structure characterized by the presence of entanglements resulting from hydrogen bonds and borax-induced cross-linking. The gelation properties of PVA-borax HVPD containing water/organic liquid mixtures were extensively studied for their application in cleaning of paintings [42, 43]. The principal feature of these viscoelastic systems, particularly appealing if used as cleaning tools, is their capability to be removed through a simple peeling action and the absence of residues on the treated surface, thanks to their high elastic modulus (Figure 3.1). [20, 43] These systems can upload even water and different organic solvents such as acetone, alcohols, MEK, cyclohexanone and propylene carbonate, so they can be applied in the removal of a large variety of materials. [42, 44] PVA-borax HVPD allow also a gradual and

controlled cleaning of solvent-sensitive surfaces. As an example, a water-loaded formulation was recently used to remove a dark layer constituted by carbonaceous particles (mainly due to atmospheric pollution) from the surface of a delicate painted layer that included water-sensitive substances like gypsum [45].



Figure 2.7: The HVPD containing a PVAc/borate polymeric dispersion was peeled off from the surface of an oil painting on canvas by means of tweezers. Image reproduced from Baglioni et al., 2013. [1]

2.4 Aim of the dissertation

In the present Thesis two main topics are addressed regarding gels and gel-like systems in the field of cultural heritage. On one hand the study and characterization of a new cleaning tool was carried out. On the other hand the assessment of the cleaning action of systems previously developed in CSGI research group.

2.4.1 HPG-based gel-like systems

The first topic is about the development of new materials for the cleaning of artistic surfaces: the main aim is to obtain a cleaning tool that can adapt itself even to the roughness of the surface to be treated and that, at the same time, can be easily removed, allowing a selective and controlled cleaning action. For this purpose we focused on water-based systems containing hydroxypropyl guar (HPG) crosslinked by borax and we studied the viscoelastic and dynamic features that can be tuned by changing the components amount. In particular we deeper investigated systems behavior after the addition of glycerol, focusing on its effect on systems viscoelastic properties and structure, connected to its role in the network formation.

Results regarding this topic is reported in chapter 5, in which is appended the paper *Structural, rheological and dynamics insights of hydroxypropyl guar gel-like systems* (submitted by Berlangieri et al.). Further investigations on the same systems, involving also the uploading of organic solvents, are reported in the Appendix section 6.

2.4.2 Removal of a degradation patina

The second topic is about a study on the effectiveness of a cleaning treatment using aqueous HVPD based on partially hydrolyzed poly(vinyl acetate) and borax, embedded with chelators. These peelable systems, previously developed and characterized in CSGI research group [43], were used as cleaning tools for the removal of a gypsum patina from an artificially sulfated travertine tiles and the efficacy in the cleaning action was assessed by means of Ion Chromatography and Inductively Coupled Plasma analysis on the HVPD samples collected after the cleaning tests. The evaluation of the efficacy of a cleaning treatment is also a very important aspect in the field of conservation of cultural heritage. In the frame of this work, one of the goal was the set-up of an analytical protocol for the pre-treatment and the analysis of samples.

Results regarding this topic are reported in chapter 7, and in particular in the appended paper *Chelators confined into 80pvac-borax highly viscous dispersions for the removal of gypsum degradation layers*. [46]

3

SPR AND LSPR (BIO)SENSING

This Chapter briefly introduces the fundamental aspects of the SPR and LSPR spectroscopies and explains the application of biosensors in the field of cultural heritage that inspired the work in this Thesis.

Contents

3.1	SPR and LSPR	28
3.1.1	Propagating SPR	28
3.1.2	Localized SPR	28
3.1.3	SPR and LSPR Biosensors	31
3.2	PDMS-Gold nanocomposites	31
3.2.1	Biosensors in the field of Cultural Heritage	33
3.3	Work description	34

3.1 SPR and LSPR

3.1.1 Propagating SPR

Surface plasmon resonance (SPR) is a label-free detection method developed in the 1990s. Thanks to its suitable and versatile characteristics it is used as a sensitive platform in analytical analysis for biomolecular interactions. The focus of the method is on the detection of the refractive index changes near thin metal layers due to biomolecular interactions.

A plasmon is a coherent oscillation of the surface conduction electrons in a noble metal. Electromagnetic radiations can optically excite surface plasmons, resulting in a resonance that occurs when an incident photon hits the metal surface at a so-called SPR Angle of incidence. According to this phenomenon, a portion of the light energy couples through the metal coating with the electrons in the metal surface layer, which begin to move due to excitation. [47] The electrons in movement propagate parallel to the metal surface and are called surface plasmons (SPs).

The SPs oscillation generates an electric field having a range of few hundreds of nanometers from the boundary between the metal surface and sample solution. [48, 49] The defined SPR angle, at which resonance takes place, is dependent on the refractive index of the bulk near the metal surface.[49–51]

3.1.2 Localized SPR

If in the SPR technique a homogeneous noble metal layer (Au or Ag) is used as active substrate on a glass surface, in the Local Surface Plasmonic Resonance (LSPR) the surface is covered with particles of noble metal characterized by nanometric dimensions. When the size of a nanoparticle, in which a surface plasmon is confined, is comparable to the wavelength of the electromagnetic radiation, we observe a collective oscillation involving the particle's free electrons and it is defined as a localized surface plasmon (LSP). Due to this LSP we have an enhancement of the electric fields near the particle's surface, this enhancement rapidly decreases with distance. In the case of noble metal nanoparticles, the maximum of the extinction spectrum corresponds to the plasmon resonant frequency and occurs in the visible range of wavelengths.

The dependence of the extinction peak on the surrounding refractive index is the basis for the sensing applications. [4, 52, 53]

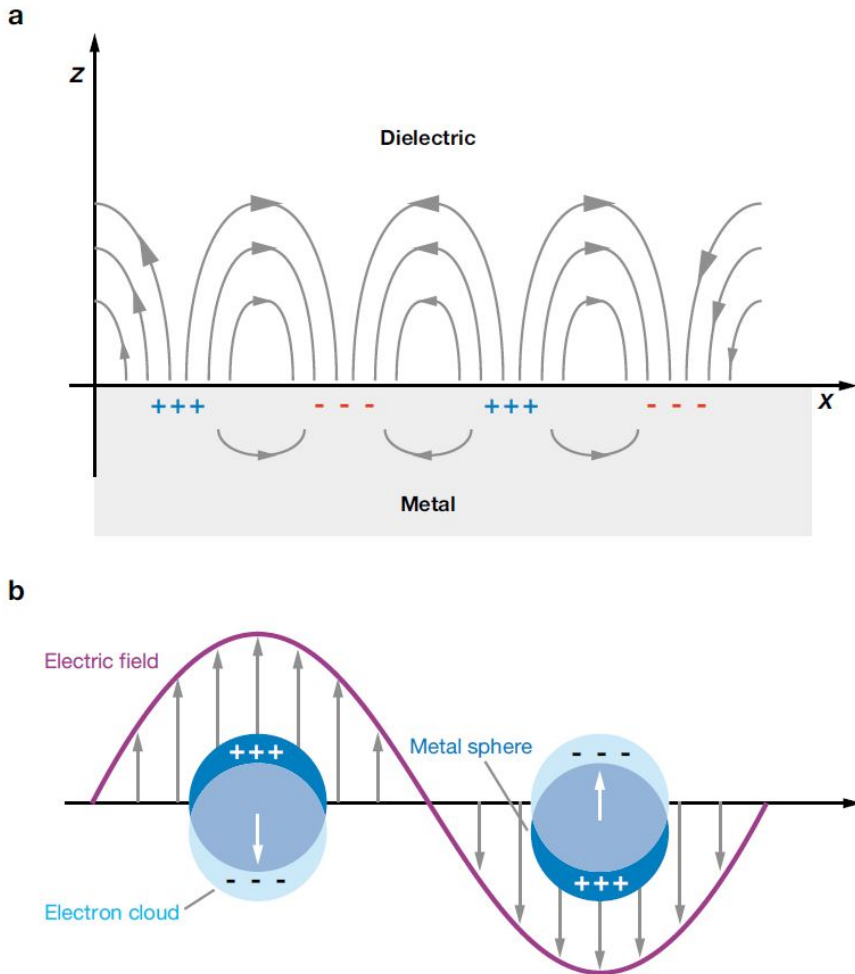


Figure 3.1: Schematic representation of (a) a propagating plasmon and (b) a localized surface plasmon. Image reproduced from Willets et al., 2007. [53]

In particular, in the case of localized surface plasmons, light interacts with nanoparticles smaller than the incident wavelength. As a result, the plasmon oscillates locally around the particle with a frequency called LSPR. [4, 53] Also the LSPR is sensitive to dielectric environment local changes, so one of the sensing application of LSPR-active particles is to register shifts in the LSPR peak wavelength and/or absorbance intensity due to changes in the surrounding bulk refractive index. [4, 52, 53] The registered changes are approximately linear

with changes in refractive index. Therefore, the refractive index sensitivity (RIS) of a particular nanoparticle is usually reported in nanometers of peak shift per refractive index unit (nm/RIU) and calculated according to the Eq 3.1.

$$S = \frac{d\lambda_p}{dn} \quad (3.1)$$

Where $d\lambda_p$ is the difference of the peak wavelength corresponding to the plasmon frequency in two different mediums and dn is the difference in the refractive index of the two bulks.

The main advantages of LSPR sensors are their localized sensing capabilities. As already reported, field enhancements due to LSPR rapidly decrease and decay with distance from the nanoparticle surface, so the recorded shifts of spectral LSPR only refer to a nanoscale region around the particle. As a matter of fact, we can observe local variations such as molecular interactions near the particle surface as a result of the highly localized sensing volume. The relationship between the wavelength shift in the maximum of the LSPR extinction spectrum and the change in the local refractive index is described in Eq3.2 [53]

$$\Delta\lambda_{max} = m\Delta n[1 - \exp(\frac{-2d}{l_d})] \quad (3.2)$$

Where m is the bulk refractive-index response of the nanoparticles; Δn is the refractive index change due to a molecular adsorption; d is the adsorbate layer thickness; and l_d is the characteristic electric field decay length, that is usually approximated as an exponential decay. Various studies demonstrated this relationship for different systems, by varying the bulk refractive index or the length of a molecular adsorbate.[54–56]

Previous studies highlighted the effect of particle shape on LSPR properties. As an example, Mock et al. suggests a correlation between the spectra of silver nanoparticles having similar volumes and different shapes (spheres, triangles, and cubes) and their structure.[57] Other works demonstrated that gold nanoshells had a higher sensitivity if compared to nanospheres with a similar diameter and that particles with a sharp shape, such as bipyramids, stars and nanotriangles, exhibit higher RIS. [58–60] The ability to change parameters such as shape and size of the particles and study the effect on the LSPR is an important experimental challenge.

3.1.3 SPR and LSPR Biosensors

Biosensors based on SPR have been applied in various fields, to study a large variety of molecular interactions including protein-protein [61], protein-DNA [62], receptor-drug [63] among others. In biosensors the ligand (recognition element) or the analyte may have both a biological or synthetic origin. In a typical SPR measurement an analyte is captured by the ligand, that is immobilized on the sensor surface, determining a local change in the refractive index near the metal surface, and, in a simplest case of direct detection, resulting in a measurable signal. At the end of the assay, the sensor can be regenerated by injecting a solution that breaks only the binding between ligand and analyte, leaving the ligand (recognition element) still anchored to the sensor surface. Using LSPR spectroscopy we can reach similar sensitivity comparing with SPR, with the additional advantages of localized sensing volumes and lower cost instrumentation. For these reasons LSPR sensing has been increasingly used for biological and biomedical assays. Furthermore, recently a great interest started to grow in developing not just biological, but also chemical sensing applications of this technology, such as for gas sensors. [4, 5] Furthermore plasmonic nanoparticles in combination with pH-sensitive polymers, have also been used in the development of pH sensors. [64] The ability to produce nanoparticles with different material, shape and size has been a major factor in exploring the great variability of applications of LSPR spectroscopy. In different studies authors tuned the particles polydispersity, shape and size by playing on the chemical synthesis. In particular interesting studies have been performed on the fabrication of a wide variety of shapes, including triangles, cubes, prisms, bipyramids, and even stars by changing the reaction conditions. [65–69]

3.2 PDMS-Gold nanocomposites

The optical properties of metal-polymer nanocomposite films based on gold and silver are of great interest. These nanocomposite materials with inorganic nanoparticles immobilized into a polymer matrix are used in a large number of applications such as color filters, optical sensors, thermo-chromic materials. [70, 71] Polymer composites with embedded metal nanoparticles take advantages from the unique properties of the NPs and make them exploitable for a variety of applications. The advantage is also that the polymer matrix holds and

stabilizes the active particles. Further interesting applications of gold and silver polymer composites in water purification [72], targeted drug release and antimicrobial coatings [73] have been reported as well. The choice of polymer plays an crucial role in determining the functional properties of the composite material. Gold—PDMS nanocomposites belong to this class of composite nanomaterials and are of increasing interest due to their simple preparation procedure, transparency, stability, and nontoxicity.

3.2.0.1 PDMS as polymer matrix in nanocomposites

Polydimethylsiloxane is a transparent and highly flexible polymer, with a low glass transition temperature (T_g) and high thermal and oxidative stability. These attractive features make its use in metal-polymer nanocomposites very advantageous. It is also inert to biological molecules thanks to its high hydrophobicity. The synthesis of nanocomposites can be carried out through different approaches, such as by in-situ methods, or by incorporating pre-made nanoparticles into a polymer matrix.[70, 74, 75]

AuNPs are particularly attractive for sensing applications, due to their strong plasmon band in the visible spectrum. Au-PDMS composites have been synthesized in different ways, in particular various authors reported the synthesis of foams, gels and films for applications in water purification and drug delivery.[72, 76] The advantages deriving from the association of PDMS with AuNPs of various shapes, in the form of nanocomposite materials, result in a successfully utilization of these active surfaces for sensing purposes.

The synthesis conditions of nanocomposites give rise to few parameters that can determine the biosensing properties of the nanocomposite itself, such as the distribution of the metal particles in the polymer matrix. Another important condition that deals with the activity of the device is that the metal nanoparticles must be able to interact with biomolecules, so for polymer matrix has to provide an appropriate environment for this purpose. [77] Indeed, if the gold nanoparticles are completely embedded into the polymer, their mobility may be very low (restricted) and the distance between the active NPs and the biomolecules may be higher respect to the sensing volume of the particle. It is very important to take into account the spatial distribution of AuNPs for an effective sensing ability.

Because of its extreme hydrophobicity, PDMS does not promote the hydrophilic biomolecules to enter the inner domains of the polymer. However, it has been reported recently that, by varying the cross-linker concentration, the free volume of the film can be changed and the enclosure of various molecular entities

can be facilitated.[78]

Various research groups have prepared Au-polymer nanocomposites by in-situ nanoparticle formation methods and obtained well-dispersed nanoparticles. Among others, Zhang et al. have successfully reported an in-situ preparation of gold nanoparticles–PDMS free-standing films, using a simple approach and without the need of additional reducing agent. The synthesis was carried out by immersing the PDMS film in a chloroauric acid diluted solution (HAuCl_4) followed by an incubation for a certain time. [79] Also other authors followed the same approach [80, 81] and succeed in the formation of a well dispersed AuNPs on the polymer surface. Goyal et al. prepared a homogenous mixture of metal salt, silicone elastomer and the curing agent. During the curing process, both the crosslinking of the elastomer and the reduction of the metal salt to form nanoparticles occurred simultaneously, leading to a homogeneous distribution of nanoparticles in the PDMS matrix. [82] The formation of NPs at PDMS surface (NPs@PDMS) is attributed to the residual curing agent present in the PDMS matrix after polymerization, that was able to reduce HAuCl_4 . [79, 81, 82] Gold NPs formed at PDMS surface are generally spherical, with size and surface distribution depending on PDMS preparation (base monomer/curing agent ratio, η), Au(III) concentration, and growth time.

Because of their extreme versatility and tunability, AuNPs@PDMS have been applied in traditional LSPR biosensing, in which mNPs are modified with bioreceptors targeting specific analytes [76, 79, 81], but they also have been exploited for their direct testing upon external chemical/physical stimuli. [83]

3.2.1 Biosensors in the field of Cultural Heritage

Microbiology and biotechnology have played a key role in various fields: medicine, pharmaceutical and chemical industries and food analysis [84, 85]. Furthermore, their potential is still little exploited in the field of preservation and restoration of cultural heritage. During the last decade, biotechnological applications to artwork preservation have been introduced with promising prediction of future innovations. [6]

Studies on the identification and characterization of microorganisms such as bacteria or lichens and of insects that can affect artworks materials (wood, canvas, paper, photographic films and so on) have been carried out [86, 87]. Also, the development of biosensors applied to the study of paper degradation [88] and to the identification of protein ligands of paintings has been introduced [89]. In particular, a nanostructured electrochemical biosensor for detecting egg yolk in tempera paintings, based on the determination of immunoglobulin

IgY, was developed by Bottari et al., while Micheli et al. developed a biosensor coupled to Flow Injection Analysis, for monitoring the degradation of paper through the quantitative determination of glucose, the principal degradation product of cellulose-based materials as a result of attack by fungus. Through this kind of biosensor it is also possible to understand if the microorganism responsible of the degradation has been removed during the cleaning of the sample.

In the perspective of a restoration intervention even more effective and low invasive, a biochemical characterization of artworks can be a very attractive tool. In a recent work [6], an immuno-based SPR biosensor was developed, with the aim to identify and distinguish the different egg proteins belonging to a painted surface. This study allowed to distinguish the protein components belonging respectively to the paint layer (where yolk was used as a binding medium for pigments) and to the protective layer (mainly made by albumen in this specific case of study).

From these points of view, SPR application in cultural heritage diagnosis and conservation has a great unexplored potential, considering its large application to biomolecules identification [49].

3.3

Work description

The recent successful combination of the SPR (bio)sensing technology with some innovative cleaning tools in the detection of eggs proteins from a painted surface [6] represented a promising starting point for the development of a new cheap and smart device, with perspectives of application in the field of conservation. The intriguing task is to obtain devices easier to use, versatile and sensitive at the same time. For this purpose, we started from the study of an active substrate. The third section of the work presented in this Thesis regards the fabrication of plasmonic composite substrates for LSPR (bio)sensing, using PDMS as a cheap and versatile polymeric substrate for the in-situ growth of Au nanoparticles (AuNPs). In particular, the fabrication process was performed by modifying disposable UV-Vis cuvettes with a PDMS film and performing the in-situ growth of AuNPs, obtaining a stable device whose signal can be investigated by conventional or portable spectrophotometers.

The in-situ reduction of Au(III) on PDMS obtained by means of the available protocols leads to spherical NPs of different size and distribution. The NPs can penetrate in depth as function of the curing agent to monomer ratio (η). [76, 79, 81, 82] Using conditions reported in literature the obtained NPs display

negligible RIS and they need cost and time consuming post-processing treatments to improve their features. However, the so obtained substrates reach only moderate RIS (about 70 nm RIU⁻¹).

In this work we explored suitable modifications of the growth strategy to enhance the bulk sensitivity. In particular, a two-steps growth of AuNPs@PDMS is proposed. Results obtained are very interesting in the perspective of understanding and controlling metal NPs optical properties during their in-situ synthesis @PDMS surface, and represent a valid alternative to time and cost expensive existing approaches. Furthermore, the optical responsivity to chicken ovalbumin and to the binding of the specific antibody (anti-OVA IgG) make these stimuli-responsive substrates promising devices also for application in the diagnostic studies of cultural heritage materials.

A complete description of this work is reported in chapter 8 in the paper *Tunable growth of gold nanostructures at a PDMS surface to obtain plasmon rulers with enhanced optical features* . [90]

Part III

RESULTS AND
DISCUSSION

4

RESULTS AND DISCUSSIONS

In the following sections results obtained for the three topics are reported. In particular, the published and submitted papers regarding the work already carried out are appended, together with an appendix containing further investigations regarding the study of systems containing HPG.

LIST OF PAPERS

- I Berlangieri, C., Poggi, G., Murgia, S., Monduzzi, M., Baglioni, P., Dei, L. and Carretti, E.
Structural, rheological and dynamics insights of hydroxypropyl guar gel-like systems
Under review (**2017**).
- II Berlangieri, C., Andrina, E., Matarrese, C., Carretti, E., Traversi, R., Severi, M., Chelazzi, D., Dei, L. and Baglioni, P.
Chelators confined into 80pvc-borax highly viscous dispersions for the removal of gypsum degradation layers
Pure Appl. Chem. (**2017**), 89(1), 97-109.
- III Scarano, S., Berlangieri, C., Carretti, E., Dei, L. and Minunni, M.
Tunable growth of gold nanostructures at a PDMS surface to obtain plasmon rulers with enhanced optical features
Microchim. Acta (**2017**), 184(9), 3093–3102.

5

HYDROXYPROPYL GUAR BASED GEL-LIKE SYSTEMS

This Chapter summarizes the results of the study and characterization of HPG based gel-like systems conducted in this Thesis, focusing on the role of glycerol introduced as plasticizer in the formulation.

Structural, rheological and dynamics insights of hydroxypropyl guar gel-like systems

Chiara Berlangieri^a, Giovanna Poggi^a, Sergio Murgia^b, Maura Monduzzi^b, Piero Baglioni^a, Luigi Dei^a and Emiliano Carretti^{a§}

a.Department of Chemistry “Ugo Schiff” & CSGI Consortium, University of Florence, via della Lastruccia, 3, 50019 Sesto Fiorentino (Florence), Italy. Address here.

b.Department of Chemical and Geological Sciences and CSGI, University of Cagliari, ss 554 bivio Sestu, 09042 Monserrato (Cagliari), Italy.

§ Corresponding author. E-mail: carretti@csgi.unifi.it

Abstract

A dynamic, rheological, and structural characterization of aqueous gel-like systems containing hydroxypropyl guar gum (HPG), borax and glycerol is presented in this paper. The role of glycerol, which is introduced as a plasticizer in the formulation, is investigated by means of ¹¹B-NMR and ¹H-NMR PGSTE measurements in order to clarify its contribution to the gel network formation and its interaction with borax, with whom it forms a complex. The effect of gels components on the rheological behavior and on the activation energy related to the relaxation process of the system was assessed by means of rheology. The results obtained suggest that the mechanical properties of these gels can be tuned and controlled by modulating the formulation in a wide range of compositions. Moreover, a structural characterisation has been also carried out by means of Small Angle X-ray Scattering (SAXS) to highlight the role of the various components on the mesh size of the network. The structural and mechanical characteristics of these systems suggest their potential use for applicative purposes. In this regard, one of the gel set up has been successfully tested as cleaning agent on the surface of a XIX stucco fragment coming from the La Fenice theatre (Venice, Italy) for the removal of a dirt layer composed by dust and particulated matter originated during a fire in 1996.

Keywords

Guar gum, borax, hydrogel, cleaning, cultural heritage conservation.

Introduction

Hydroxypropyl guar gum (HPG) is a derivative of guar gum in which several free hydroxyls are substituted by hydroxypropyl groups upon etherification (**Figure 1A**). It is a natural polysaccharide extracted from the seeds of *Cyamopsis tetragonoloba*, and it is composed by a linear chain of mannose units linked by β -1,4 bonds. This backbone is functionalized by galactose residues α -1,6-

linked, randomly attached, forming short side-branches. It is cheap, non-toxic, biocompatible, biodegradable, easy available and soluble in water, where it forms viscous solutions even at low concentrations.[1–5] For these reasons guar gum has several applications in food, paper, textile, pharmaceutical and petroleum industries.

HPG together with similar polysaccharides have been recently used for the formulation of versatile and well-performing materials with various fields of application.[1,6–10] Gel-like systems containing ionic surfactants and modified guar covalently crosslinked have also been proposed as agents for removing solid particles, able to perform a gentle mechanical surface cleaning of sensitive materials such as ceramic, wood, glass and metals.[11] Hydrogels made by guar and HPG crosslinked with ions such as titanate and borax are widely used in the oil and gas industry, mainly as a proppant transport agent in hydraulic fracturing process.[1,6–10]

Furthermore, the efficacy of borax as crosslinker for polymers bearing hydroxyl groups is well known (see **Figure 1B**). [12,13] The nature of linkage has been subject of debates: according to the model proposed by Shibayama for polyvinyl alcohol[14] and for scleroglucans,[15,16] mixed physical/chemical linkages occur; nevertheless, more recent studies suggest the presence of chemical crosslinks only between borax and polymeric chains with the formation of chemical bridges by transient covalent bonds.[17,18] Moreover, as indicated by rheology, being the lifetime of these covalent crosslinks in the order of seconds,[13,19] that makes the guar-borate networks are usually characterized by self-healing properties.

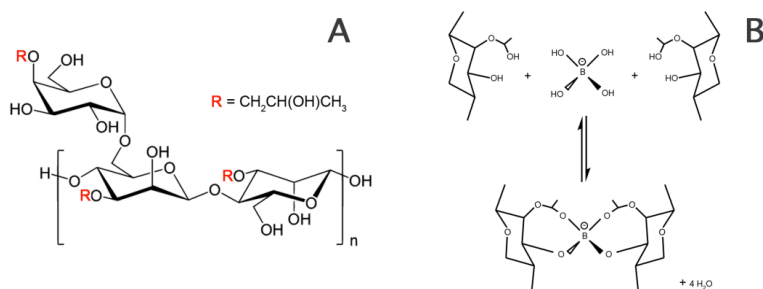


Figure 1. (A) Chemical structure of hydroxypropyl guar (HPG). (B) Crosslinking reaction leading to the formation of a gelator network.

It is well known that glycerol increases the flexibility of polymeric materials by increasing the interchain spacing; for this reason and due also to its large availability, glycerol is used as plasticizer for polymeric materials in many fields, as food packaging [20,21] or to improve the plasticity of protein and polysaccharides based films.[20,21] It can also lead to an increase of the elongation at break of materials, resulting in systems that can resist to a certain stretching before breaking. [20,21]

In this paper, a dynamic, rheological, and structural characterization of aqueous gel-like systems containing HPG, borax and glycerol is presented. In the last decades, several papers focusing on the study of the mechanical properties and the applicative performances of HPG aqueous solutions [22] and gel-like systems [8–10,23,24] have been published. However, to our knowledge, a systematic study of the simultaneous role of both borax and glycerol on the structural and on the mechanical properties of aqueous HPG based gels, which is the main subject of this paper, is still lacking. The role of glycerol in the crosslinking mechanism and its interactions with borax were studied here systematically for the first time by using a combined approach based on both by

means of $^{11}\text{B-NMR}$, $^1\text{H-NMR}$ PGSTE and rheological measurements. In particular, rheological investigations allowed for the first time to obtain informations also on the effect of gels components on the viscoelastic behaviour, on the activation energy related to the relaxation process of the system and on the critical polymeric concentration, above which an extended three-dimensional polymer network is formed. Further, information about the role of all the components on the structure of HPG-based systems, were obtained by a Small Angle X-ray Scattering (SAXS) investigation.

This approach allowed to identify several of the key factors that control the nature of the materials and the results obtained suggest that the mechanical properties of these gel-like fluids can be tuned by modulating their composition. The extended structural and mechanical characterization of these gel-like systems shows that their properties can be widely controlled and tuned, by tuning the concentration of the components. This feature has important applicative implications mainly in the field of Cultural Heritage conservation where the HPG/glycerol/borax systems can be used for the selective and gentle cleaning of painted surfaces of historical and artistic interest. In this regard, a preliminary applicative test was carried out on a sample collected from a *stucco* decoration of La Fenice theatre, in Venice. A gel-like formulation was successfully used for the removal of a dark *patina* resulted from the fire that almost destroyed the theatre in 1996.

Materials and Methods

Chemicals

Hydroxypropyl guar gum (HPG, Mw = 90 KDa) with a substitution level of 1.2 was kindly provided by Ametech Srl; glycerol (Merck, purity 99%) and sodium tetraborate decahydrate, (Sigma Aldrich, purity 99.5-100%) was used as received by the suppliers.

Samples Preparation

Samples without plasticizer were prepared through the following procedure: HPG was placed in water and then stirred and heated at 65° C to favour solubilization. An aqueous solution of borax at 4% was then added and the sample was stirred with a Vortex to obtain a homogenous gelation. For samples containing the plasticizer, HPG was added to a glycerol aqueous solution. In all the samples containing borax, the ratio polymer/borax was fixed to 4/1 as reported in literature for the formulation of crosslinked systems,[10,23] except for the series in which the crosslinker effect was investigated.

Rheological tests

Oscillatory shear measurements were carried out on a TA Instrument Hybrid Rheometer DISCOVERY HR-3, using a plate-plate geometry (Flat Plate 40mm diameter) and a Peltier for temperature control. The minimum gap between the plates at zero radial position was 500 μm . The cell was closed by lowering the head to the measuring position in the z axis force controlled mode; the maximum squeezing force was 1.0 N. Before starting the experiments, the samples were left to equilibrate for 30 min at 25 °C. Frequency sweep measurements were carried out within the linear viscoelastic range (5% strain), determined by means of an amplitude sweep test (see Figure S1). The storage and loss moduli (G' and G'') were measured over the frequency range of 0.001 to 100 Hz.

Time Temperature Superposition (TTS) procedure was carried out to observe the temperature-dependence of the mechanical properties of the viscoelastic materials. In these experiments, the Storage modulus (G') and Loss modulus (G'') were monitored as a function of frequency in the linear viscoelastic region at various temperatures by means of isothermal frequency sweep tests. TTS principle implies that curves obtained at various temperatures can be superimposed by shifting the data in the vertical and/or horizontal directions; all the curves can be combined in a single master curve choosing a reference temperature (T_0). All the systems were analysed by keeping 25 °C as the reference temperature. The shape of the master curve does not change shape with temperature, but the curve appears to be only shifted.[23,25] The master curve generated by the software (TRIOS Data Analysis, TA Instrument) represents the time response of the material at the reference temperature. The software can analyse the shift factors using the Arrhenius equation (1) to calculate the Activation Energy of the relaxation process:

$$\ln a_T = \left(-\frac{E}{R}\right)\left(\frac{1}{T} - \frac{1}{T_0}\right) \quad (1)$$

where a_T is the shift factor, E is the Activation Energy associated to the relaxation process, R is the gas constant, T is the measurement temperature and T_0 is the reference temperature.

NMR measurements

^1H and ^{11}B NMR measurements were carried out in deuterated water at 25 °C using a Bruker Advance 300 MHz (7.05 T) spectrometer at the operating frequencies of 300.13 and 96.29 MHz, respectively. ^{11}B NMR chemical shifts were referenced with respect to an external $\text{BF}_3\text{-OEt}_2$ standard at 0.0 ppm.

A standard BVT 3000 variable temperature control unit with an accuracy of ± 0.5 °C was used. Self-diffusion coefficients were determined using a Bruker DIFF30 probe supplied by a Bruker Great 1/40 amplifier that can generate field gradients up to 1.2 T m^{-1} . The pulse-gradient stimulated echo (PGSTE) sequence was used.[26,27] Self-diffusion coefficients were obtained by varying the gradient strength (g) while keeping the gradient pulse length (δ) and the gradient pulse intervals constant within each experimental run. The data were fitted according to the Stejskal-Tanner equation (2):

$$I/I_0 = \exp(-Dq^2t) \quad (2)$$

where I and I_0 are the signals intensities respectively in the presence and absence of the applied field gradient, $q = \gamma g \delta$ is the so-called scattering vector (γ being the gyromagnetic ratio of the observed nucleus), $t = (\Delta - \delta/3)$ is the diffusion time, Δ is the delay time between the encoding and decoding gradients, and D is the self-diffusion coefficient to be extracted. Errors on the self-diffusion coefficients were estimated around 2% on the basis of repeated measurements. Areas of the ^{11}B NMR resonances, assuming they were Lorentzian in shape, were calculated using the program Microcal™ Origin™ from Microcal Software (Northampton, MA). Typically, errors on areas were estimated around 5%.

SAXS experiments

SAXS measurements were carried out with a HECUS S3-MICRO camera (Kratky-type) equipped with a position-sensitive detector (OED 50M) containing 1024 channels of width 54 mm. Cu $K\alpha$ radiation ($\lambda = 1.542 \text{ \AA}$) was provided by an ultrabright point micro-focus X-ray source (GENIX-Fox 3D, Xenocs, Grenoble), operating at a maximum power of 50 W (50 kV and 1 mA). The sample-to-detector distance was 281 mm. The space between the sample and the detector was kept under

vacuum during the measurements to minimize scattering from the air. Scattering curves were obtained in the q -range between 0.01 and 0.54 \AA^{-1} . Gel samples were placed into 1 mm demountable cells having Kapton films as windows. The temperature was maintained at $25 \pm 0.1^\circ$ C by a Peltier controller. All SAXS curves were modelled according to a Lorentzian model (eq. 3).

$$I(q) = \frac{I_0}{1+(qL)^2} + bkg \quad (3)$$

where I_0 is the scattering intensity at $q=0$, L is the correlation length which corresponds in a semi-diluted solution to the average distance between neighbouring entanglement points and bkg is a q -independent instrumental background term.[28–30]

Results and Discussion

Formulation and characterization

The dynamic mechanical properties of HPG-based systems were investigated by means of frequency sweep oscillation tests. They provide information about the dependence of the storage modulus (G') and of the loss modulus (G'') on the frequency of the applied shear perturbation. **Figure 2A** shows the trend of the storage modulus G' and the loss modulus G'' at a constant strain of 5% as a function of the applied shear perturbation. The polymer concentration in both samples was 3 wt% while the ratio HPG wt%/Borax wt% was fixed at 4/1 as reported in literature for the formulation of similar crosslinked systems.[10,23]

The mechanical behaviour of HPG/water system was investigated before and after the addition of borax that acts as crosslinker. Borate anions induce the formation of covalent intermolecular junctions between the polymer chains through a di-diol condensation reaction. This results in a more rigid network and in a decrease of the viscous character of the samples: these covalent crosslinking, together with the intramolecular and intermolecular hydrogen bonding interactions that occur between the hydroxyl groups of the HPG chains, lead to an increase of the elastic behaviour and of systems stiffness. From the rheological point of view, the increase of borax determines the increase of the solid like behaviour of the system, with a huge increase in the Storage modulus G' as clearly indicated by the frequency sweep curves reported in **Figure S2**.

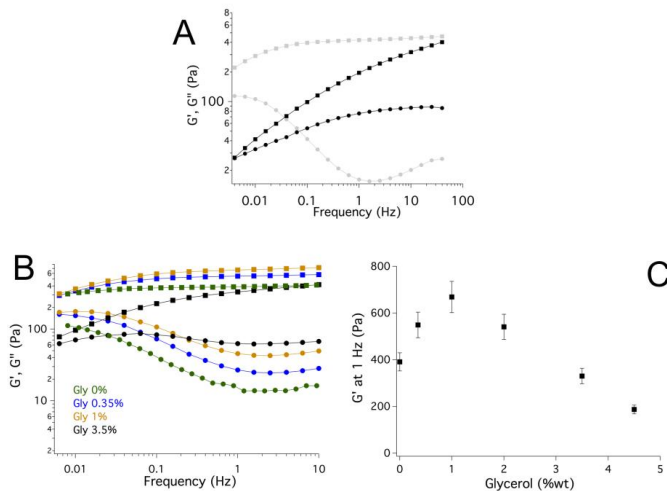


Figure 2. A) Frequency sweep measurements on HPG/water sample before (black curves) and after borax addition (gray curves). The ratio HPG wt%/Borax wt% was fixed at 4/1. The oscillation amplitude was 5%. G' (■), G'' (●). (B) Frequency sweep measurements on samples with increasing amount of glycerol, HPG 3 wt% and a ratio HPG wt%/Borax wt% fixed at 4/1. The oscillation amplitude was 5%. G' (■), G'' (●). (C) Storage modulus values at 1Hz plotted against glycerol concentration.

To modify the system's stiffness, tuning the mechanical behaviour of the sample, glycerol was introduced as plasticizer, and its role in the viscoelastic properties of the formulation was systematically investigated by means of oscillating rheological test. Frequency sweep tests were carried out on systems containing different glycerol concentrations, while keeping HPG at 3 wt% and borax at 0.75 wt%. The trend of the Storage and of the Loss moduli G' and G'' , at a constant strain of 5% (in the linear viscoelastic range), as a function of the frequency is reported in **Figure 2B**, where the change of the elasticity of the systems induced by the addition of glycerol can be observed. In **Figure 2C**, the Storage modulus (G') at 1Hz is plotted as a function of glycerol concentration. The presence of two different regimes is evident: at glycerol concentrations lower than 1wt%, a progressive increase of the stiffness of the system is observed indicating a structuring role of this additive. Above this threshold, the plasticizing effect of glycerol prevails as indicated by the decrease of G' .

Systems containing different glycerol amounts were deeper investigated as a function of temperature between 25°C and 60°C by means of the Time Temperature Superposition (TTS) approach, to observe the temperature-dependence of viscoelastic properties of these fluids and, according to Equation 1, to calculate the Activation Energy associated to the relaxation process. In **Figures S3-S7** the isothermal frequency sweep measurements and the master curves for samples containing HPG (3 wt%)/borax (0.75 wt%)/water and increasing amounts of glycerol are reported. The Activation Energy trend is reported in **Figure 3A**: we observed that the E_a progressively decreases as glycerol concentration increases above 1wt% confirming that above this threshold the driving factor is the plasticizing role of glycerol that cause a decrease of the E_a of the investigated systems.

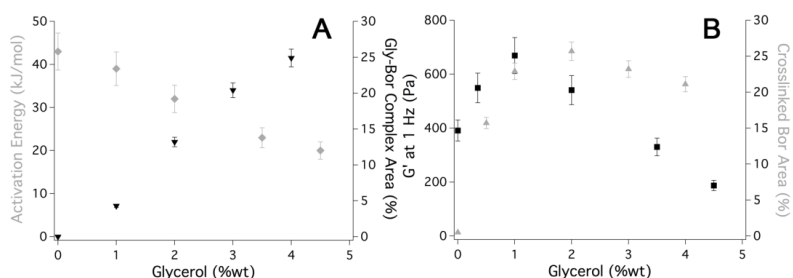


Figure 3. (A) Activation Energy values obtained from rheological measurements (◆) and Glycerol-Borate complex Area obtained from ^{11}B NMR measurements (▼) are plotted against glycerol concentration. All samples contain 3 wt% of HPG and 0.75 wt% of borax. (B) Storage modulus values at 1Hz obtained from rheological measurements (■) and Crosslinked Borate Area obtained from NMR measurements (▲) are plotted against glycerol concentration.

With the aim of clarifying the role of glycerol in the crosslinking mechanism, an extensive ^{11}B -NMR study was carried out on samples containing increasing amount of glycerol. There are several papers in literature about the interaction between borax and hydroxyl groups.[31] Several of them focus on crosslinked systems such as gel-like materials based on poly(vinyl alcohol) (PVA)[18,32] and on borax-galactomannan based gels.[12]

As shown in **Figure 4A**, the ^{11}B NMR spectrum of the polymer/borax system in water is characterized by one intense resonance at 11.5 ppm and a small resonance emerging at 5.5 ppm, being the downfield resonance due to the free borate/boric acid molecular species, and the other to the cross-linked borate.[33] The addition of glycerol caused strong alterations of the NMR spectrum, with a downfield shift of the free boron species resonance at 13.88 ppm, the appearance of a new NMR signal at 9.77 ppm, and a dramatic increase of the cross-linked borate signal with respect to the free borate/boric acid, as determined by the ratio between the area of the two NMR signals (see **Table S1**). Differently from the other two resonances, the signal belonging to the non-complexed boron shifts further downfield as more glycerol is added, indicating a change in the borate/boric acid ratio, with an increase in the uncharged species. Such a phenomenon was previously suggested to be related to the less attractive environment to borate ions originated by the addition of organic liquids.[18] The removal of the borate ions may be connected to the new resonance at 9.77 ppm, associated with the formation of the glycerol borate complex.[33]

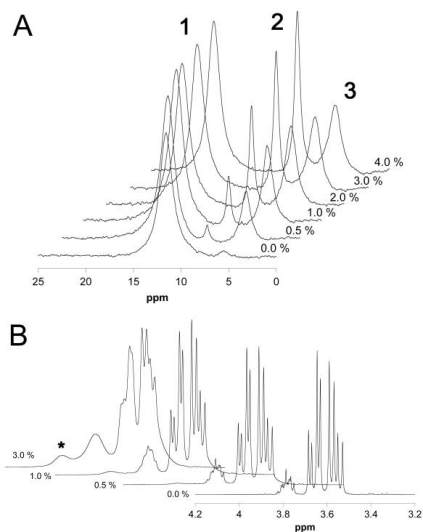


Figure 4. A) ^{11}B NMR stacked plot spectra of the polymer/water system containing 3 wt % of HPG, 0.75 wt% of borax and increasing amounts of glycerol (indicated as wt%). Peaks attribution: non-complexed boron (1), glycerol/borate complex (2), crosslinked borate (3). B) ^1H NMR stacked plot spectra of the glycerol/water system containing increasing amounts of borax (wt%). The star indicates a new resonance attributed to the glycerol borate complex.

In other words, the borate/boric acid equilibrium is altered because of the anion sequestered for the formation of the complex. Remarkably, while increasing the glycerol content, the amount of the glycerol borate complex increases at the expenses of the cross-linked borate, probably due to the higher mobility of the glycerol molecule with respect to the rigid polymer matrix that favours the glycerol/borate ions. As reported in **Table S1**, a strong increase of crosslinked borate can be observed after the addition of a small amount of glycerol (0.5 wt%): this can be explained with the decrease of the dielectric constant of the system that leads to the borax tendency to exist in the crosslinking form rather than in the ionic one. The value gradually increases up to 1% of glycerol, where it reaches a sort of threshold. On the other hand, the glycerol-borate complex keeps increasing with increasing amount of glycerol. This trend allows us to deeper understand the meaning of rheological data. In Figure 5 a comparison between rheological and ^{11}B -NMR results as a function of glycerol concentration is reported. From **Figure 3B** we observe how the addition of glycerol up to 1% induced an increase of entanglement density resulting in an increase of system elastic behaviour, while a strong decrease of G' occurred at higher concentrations. In the same graph, we can see that the area of the crosslinked borax, measured by ^{11}B -NMR, follows the same trend, indicating that a fraction of borax is not anymore acting as a crosslinker in the polymeric network.

This behaviour may be ascribed to a possible double role of glycerol in the crosslinking mechanism. On one hand, at low concentrations, glycerol molecules seem to act as a structuring agent, inducing the crosslinking of borax and improving the elastic behaviour of the system. On the other hand, at concentration higher than 1 wt%, glycerol seems to behave mainly as a plasticizer, reducing the density of the covalent borate bridges and then causing a decrease in the sample stiffness. The trend of $\tan\delta$ (where $\tan\delta = G''/G'$) at 1 Hz, reported in Figure S8, confirms a

change in the viscoelastic behaviour for HPG/H₂O/borax based systems upon increasing the amount of glycerol. In particular, above 1%, an increase of G'' modulus is observed, resulting in less rigid samples.

Moreover, the glycerol borate complex area increases with glycerol (**Figure 3A**), confirming that borax is sequestered from the glycerol to create a complex. This leads to a decrease of the Activation Energy in the relaxation processes (**Figure 3A**). When the complex formation begins to be much favoured, by increasing the amount of available glycerol, we see a sharp decline in the modulus G' in rheological measurements, and a slight decrease of crosslinked boron fraction in ¹¹B-NMR measurements (**Figure 3B**). The two phenomena, which contribute to the variation of G', seem to proceed in the same direction up to a glycerol concentration between 1% and 2%, then the formation of the glycerol-borate complex becomes favoured over the borax crosslinking mechanism.

To confirm the glycerol-borate complex formation, glycerol aqueous solutions were investigated before and after borax addition measuring the self-diffusion coefficient *D* of glycerol by ¹H PGSTE NMR. In the analysed samples glycerol was maintained at a fixed concentration in deuterated water, while the amount of borax was increased. As reported in **Table S2** the strong interaction between glycerol and borate induces an evident decrease in the glycerol motions that can be already observed at low glycerol-to-borate molecular ratio, and becomes more significant as the borate concentration increases. Interestingly, upon the addition of borax a new downfield resonance started to grow (see **Figure 4B**). It is worth noticing that borax in (deuterated) water does not show any ¹H NMR signal. Therefore, the new signal was attributed to the glycerol borate complex, and implicitly accounts for its high stability, being the fingerprint of a stable complex rather than a loose assembly in fast exchange between the bound and free form. In addition, the formation of the glycerol borate complex is confirmed by the progressive broadening of the width at half high and the consequent coalescence of the NMR signals observed in the ¹H NMR spectra as the borax concentration is increased (**Figure 4B**). Indeed, such a loss of resolution is related to the more rapid spin-spin relaxation rates, in turn, caused by a) the reduced mobility experienced by the glycerol molecules because of the formation of the complex with borate ions, and particularly by b) the effect of the quadrupolar relaxation of the boron nucleus on the nearby nuclei.

After the dynamical characterization of systems containing increasing amount of glycerol, we focused on the role of the polymer in our formulations. To understand the effect of HPG concentration on the mechanical properties of the HPG based systems, frequency sweep measurements were carried out on a series of samples prepared with different amount of HPG (**Figure 5**), while keeping the HPG/borax ratio at 4/1 and glycerol at 3.5 wt%. This value was selected in view of a potential application.[18]

Figure 5A indicates that the increase in HPG concentration doesn't significantly alter the shape of the shear moduli although its value increases upon increasing the HPG concentration, as also indicated by the decrease in the tanδ values (see **Figure S9**). Moreover, for HPG concentrations lower than 3 wt%, two different regimes can be observed (**Figure 5A**): at $\omega > \omega_c$ (where ω_c is the crossover frequency between the G' and G'' curves), $G' > G''$, meaning that the elastic behaviour prevails; at $\omega < \omega_c$ where $G' < G''$, the viscous character is predominant. **Figure 5A** also shows that upon increasing the HPG concentration the crossover between G' and G'' curves shifts towards lower frequency values, indicating an increase of the mean relaxation time; furthermore, for a HPG content higher than 3 wt%, the crossover between G' and G'' disappears, indicating an increase of the solid-like character of the system. Moreover the increase of G' observed by increasing the HPG concentration indicates an increase in the complexity of the structure of the investigated systems and an increase in the strength of the 3D network due to the increase of the

spatial density of the borate-modulated cross-linking (ρ_e) between the HPG chains.[34] **Figure 5B** reports the trend of the elastic modulus G' at 1 Hz as a function of the HPG concentration; the graph shows that G' (1 Hz) is nearly constant up to 2 wt% of HPG, while above this threshold (indicated as C^*), the drastic increase in G' (1 Hz), that reaches a value of 600 Pa at 4 wt% HPG, indicates the formation of an extended 3D polymer network.

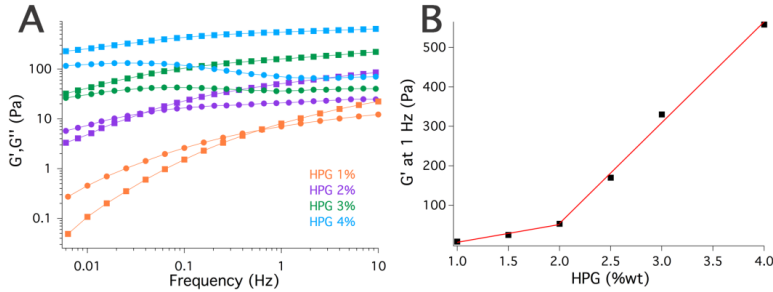


Figure 5. Frequency sweep measurements on samples with HPG (from 1 to 4%), glycerol 3.5% and the ratio HPG wt%/Borax wt% fixed at 4/1. The oscillation amplitude was 5%. G' (■), G'' (●). **B:** Storage modulus values at 1Hz as a function of HPG concentration.

There is a considerable literature on the dependence of the G' modulus on polymer concentration in solution.[35] In most cases, the dependence of G' is described by a power law: $G' \propto \phi^n$ (4) where ϕ is the polymer concentration expressed as wt%.[36] For rigid networks having a fibrillary morphology the exponent n is strictly related to the fractal dimension D_F of the object connecting at the junction (5). [36–38]

$$G' \propto \phi^n \quad (4)$$

$$G' \propto \phi^{(3+D_F)/(3-D_F)} \quad (5)$$

In **Figure S10** the trend of the G' values at 1 Hz are plotted on a log/log scale as a function of the polymer concentration. From the obtained slope (n), a fractal dimension (DF) of 1.6 is calculated, and this suggests, accordingly to Jones and Marques theory,[37] a network with objects connected by rigid junctions, for which an *enthalpic* elasticity occurs.[36]

The rheological properties of a selected system containing HPG 3%/borax 0.75%/glycerol 3.5% were also investigated as a function of temperature between 25 °C and 60 °C, to investigate the temperature-dependence of viscoelastic properties of these fluids and to obtain the activation energy (E_a) associated to the relaxation process through the TTS approach (equation 1). The frequency sweep curves and the master curves for samples investigated are reported in **Figures S3, S6, S11 and S12**, while the activation energy values for samples with and without glycerol and borax are listed in **Table S3**.

The addition of borax to the HPG dispersion in water (sample 2 and sample 1, respectively) lead to an increase of the E_a value, confirming the ability of borax in increasing the systems' stiffness (see Figure 2). The addition of glycerol to sample 2 determined a significant decrease of the E_a value (sample 3). It is worth noting that both the formulations containing glycerol (samples 3 and 4), are characterized by activation energy values that are much lower than those of the corresponding systems that don't contain glycerol (system 2 and 1, respectively). As a matter of fact, over 2 wt%, glycerol creates a stable complex with borate, resulting in less rigid systems, as shown by NMR

measurements. NMR results are also confirmed by the comparison between E_a values of samples 3 and 4: the addition of borax to a system containing glycerol does not increase significantly the activation energy of the relaxation process, differently from what happened for samples 2 and 1. This is due to the fact that borate is partially sequestered by glycerol and it is not entirely involved in the crosslinking of HPG.

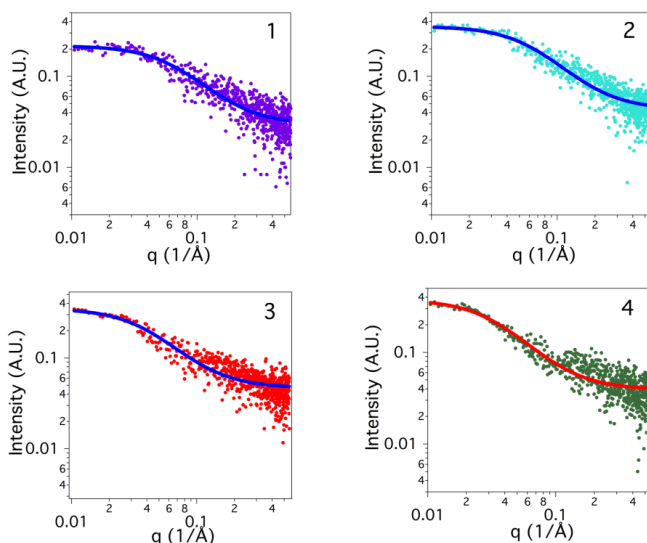


Figure 6. Comparison between SAXS curves samples containing HPG/water (**1**), HPG/borax/water (**2**), HPG/glycerol/borax/water (**3**) and HPG/glycerol/water (**4**).

SAXS curves have been collected on HPG aqueous binary solutions before and after the addition of the plasticizer and the crosslinker to better understand the role of the components on the structure of the studied systems. In **Figure 6**, SAXS profiles and the best fitting curves according to Eq. 3 are reported. Fitting results are reported in **Table 1**. As reported in literature,[30] in a semi-diluted polymeric solution, the mesh size (indicated by the Screening Length (L)) corresponds to the average distance between neighbouring entanglement points of the 3D polymeric network.

For what concern samples 1 and 2, the addition of borax does not significantly change the mesh size of the HPG aqueous dispersion. On the contrary, in the presence of glycerol (sample 3 and 4), borax leads to a significant decrease in the screening length of the polymeric network. Moreover, the addition of glycerol leads to a huge increase of the mesh size (compare sample 1 with sample 4 and sample 2 with sample 3), confirming the ability of this additive to interpose among HPG chains, reducing the entity of the interactions between the HPG monomers (mainly due to H bonds), therefore acting as a plasticizer.

Table 1. Lorentz parameters associated with the best fits to the SAXS curves for samples containing HPG and HPG/glycerol aqueous dispersion, with and without borax as crosslinker.

SAMPLE	COMPOSITION	Scale factor I0	Screening Length L (Å)	Bkg
1	HPG 3 wt% in water	0.19 ± 0.03	14.5 ± 0.4	0.03
2	HPG 3 wt%/borax/water	0.31 ± 0.04	15.2 ± 0.3	0.04
3	HPG 3 wt%/Glycerol 3.5 wt%/borax/water	0.30 ± 0.06	24.5 ± 0.6	0.05
4	HPG 3 wt%/Glycerol 3.5 wt% in water	0.34 ± 0.07	28.9 ± 0.7	0.04

Application Test

In the last decades, several advanced and innovative systems for the conservation of cultural heritage have been proposed.[39–41] In particular hydro and organogels have been proposed as a feasible alternative to overcome the limits of traditional methods for the selective removal of patinas from surfaces of artistic and historical interest.[42–46]

The characterization of HPG/glycerol/borax gel-like systems shows that their properties can be tuned, even dramatically, by varying the concentration of the components. From the applicative point of view this is a very attractive feature of these systems. Therefore, a preliminary applicative test using a gel-like formulation with HPG (3 wt%), borax (0.75 wt%), and glycerol (3.5 wt%) was carried out. This system was chosen because it can be stretched without breaking (see **Figure S13**), which is an appealing feature for the application on curved surfaces. Moreover, the value of the intrinsic elastic modulus of this system allows its peeling from the cleaned surface in one step.[18] After the fire that almost destroyed La Fenice theatre (Venice) in 1996, artworks and decorations that belonged to the beautiful historical building were altered by a dark coating, resulted from dust and particulate matter generated from the fire. The *stucco* of La Fenice theatre is a rough, porous material, as can be seen from **Figure 7A**. The first attempt to remove the surface patina was carried out by following a traditional procedure based on the use of a cotton swab soaked with demineralized water. In that way, it was possible to obtain the softening of the dirt layer, which was then absorbed by the porous matrix, resulting in an unsatisfactory cleaning of the decoration (**Figure 7B**). A second cleaning test was then carried out by means of a gel-like HPG-system that, according to the Washburn equation, due to its high viscosity, allowed the minimization of the penetration of the water into the porous support. The HPG/glycerol/borax system was applied on the stucco surface with a spatula and left on the surface for about 1 minute (see **Figure 7B**); after the application, the system was removed in one step through a simple peeling action. The comparison between the cleaning action of our system and that of neat water applied by means of a wet cotton swab can be observed in **Figure 7C**. The promising results of this preliminary test suggest a possible application of this formulation for the selective cleaning of the surface making these gel-like systems particularly interesting in the field of restoration.

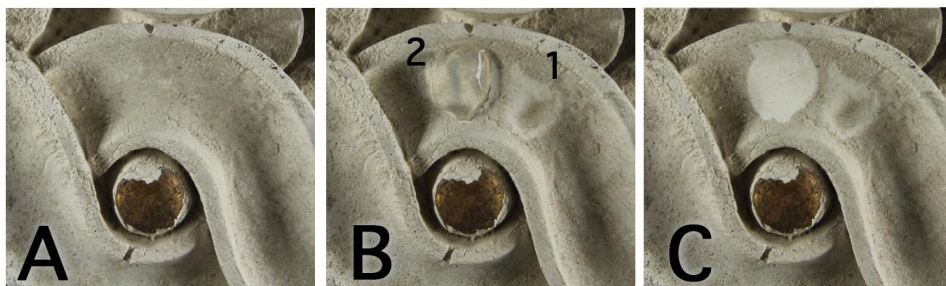


Figure 7. Detail of the sample region before (A), during (B) and after (C) the application as described in the text. Comparison between the cleaning performance of a wet cotton swab (1) and of the HPG based system (2).

Conclusions

A rheological, dynamic, and structural characterization of water based gel-like systems containing hydroxypropyl guar gum (HPG), borax, and glycerol is reported. From rheological measurements, we observed that the addition of borax to aqueous HPG dispersions lead to systems with increased stiffness, being borax a well-known efficient crosslinker for hydroxyl-rich polymers. With the aim of tuning the mechanical properties of HPG/borax gel-like systems, variable amounts of glycerol were added and the overall effect on the systems was studied. Surprisingly, at low concentration (below 1%), glycerol acts a structuring agent, increasing the storage modulus. Above 1%, it behaves as a plasticizer, as it might be expected. We then decided to deepen the role of glycerol in network formation and its interactions with borax, using ^{11}B -NMR and ^1H -NMR PGSTE. In particular, from ^{11}B -NMR, the formation of a glycerol-borate complex was observed. When glycerol is higher than 1%, the complex formation act as a driving force and occurs at the expenses of the crosslinking between borax and polymer chains, resulting in the decrease of the Storage modulus, as observed from rheological measurements. The formation of a stable glycerol-borate complex was confirmed by ^1H PGSTE NMR measurements, from which we calculated the diffusion of glycerol in borax aqueous solutions. The activation energies of the relaxation process obtained by Time Temperature Superposition (TTS) allow us to calculate the fractal dimension of the investigated systems that resulted to be the one typical of a network with objects connected by rigid junctions. A structural characterization carried out by SAXS experiments provided insight about the mesh size, which is influenced by both the presence of borax and glycerol. A preliminary applicative test for the removal of a dark patina from a *stucco* decoration belonging to La Fenice theatre (Venice) was then performed. The promising results obtained suggest a possible application of these formulations in the field of restoration.

Funding: this work was supported by CSGI and by the European Union's Horizon 2020 research and innovation programme under grant agreement No 646063 [Nanorestart Project].

Conflict of interest: none.

References

- [1] R.K. Proud'homme, V. Costien, S. Knoll, The effect of shear hystory on the rheology of hydroxypropyl guar gels, *Polym. Aqueous Media Perform. through Assoc.* (1989) 89–112.
- [2] J.E. Fox, Seed gums, *Thick. Gelling Agents Food.* (1997) 262–283.
- [3] C.H. Kucera, D.N. DeMott, Drilling fluid containing crosslinked polysaccharide derivative, US patent 4257903, 1981.
- [4] T. Coviello, F. Alhaique, A. Dorigo, P. Matricardi, M. Grassi, Two galactomannans and scleroglucan as matrices for drug delivery : Preparation and release studies, *Eur. J. Pharm. Biopharm.* 66 (2007) 200–209.
- [5] H. Kono, F. Otaka, M. Ozaki, Preparation and characterization of guar gum hydrogels as carrier materials for controlled protein drug delivery, *Carbohydr. Polym.* 111 (2014) 830–840.
- [6] T. Coviello, P. Matricardi, C. Marianecchi, F. Alhaique, Polysaccharide hydrogels for modified release formulations, *J. Control. Release.* 119 (2007) 5–24.
- [7] G. Milcovich, F. E. Antunes, R. Farra, M. Grassi, F. Asaro, Modulating carbohydrate-based hydrogels as viscoelastic lubricant substitute for articular cartilages, *International Journal of Biological Macromolecules.* 102 (2017) 796-804.
- [8] Y. Cheng, K.M. Brown, R.K. Prud'homme, Characterization and Intermolecular Interactions of Hydroxypropyl Guar Solutions, *Biomacromolecules.* 3 (2002) 456–461.
- [9] D. Risica, A. Barbetta, L. Vischetti, C. Cametti, M. Dentini, Rheological properties of guar and its methyl , hydroxypropyl and hydroxypropyl-methyl derivatives in semidilute and concentrated aqueous solutions, *Polymer (Guildf).* 51 (2010) 1972–1982.
- [10] S. Wang, H. Tang, J. Guo, K. Wang, Effect of pH on the rheological properties of borate crosslinked hydroxypropyl guar gum hydrogel and hydroxypropyl guar gum, *Carbohydr. Polym.* 147 (2016) 455–463.
- [11] R. Dietrich, M. Flury, Agent for removing solid particles, US patent 7541325, 2009.
- [12] E. Pezron, A. Ricard, F. Lafuma, R. Audebert, Reversible Gel Formation Induced by Ion Complexation. 1. Borax-Galactomannan Interactions, *Macromolecules.* 21 (1988) 1121–1125.
- [13] T. Coviello, P. Matricardi, F. Alhaique, R. Farra, G. Tesei, S. Fiorentino, et al., Guar gum / borax hydrogel : Rheological , low field NMR and release characterizations, *E-XPRESS Polym. Lett.* 7 (2013) 733–746.
- [14] M. Shibayama, Y. H., H. Kurokawa, H. Fujiwara, M. Nomura, Sol-gel transition of poly(vinyl alcohol)-borate complex, *Polymer (Guildf).* 28 (1988) 2066–2071.
- [15] G. Bocchinfuso, A. Palleschi, C. Mazzuca, T. Coviello, F. Alhaique, G. Marletta, Theoretical and experimental study on a self-assembling polysaccharideforming nanochannels: Static and dynamic effect induced by a soft confinement, *J. Phys. Chem. B.* 112 (2008).
- [16] A. Palleschi, T. Coviello, G. Bocchinfuso, F. Alhaique, Investigation on a new scleroglucan / borax hydrogel : Structure and drug release, *Int. J. Pharm.* 322 (2006) 13–21.
- [17] G. Bocchinfuso, C. Mazzuca, C. Sandolo, S. Margheritelli, F. Alhaique, T. Coviello, et al., Guar Gum and Scleroglucan Interactions with Borax : Experimental and Theoretical Studies of an Unexpected Similarity, *J. Phys. Chem. B.* 114 (2010) 13059–13068.
- [18] L. Angelova, B. Berrie, K. De Ghetaldi, A. Kerr, R.G. Weiss, Partially hydrolised poly(vinyl acetate)-boraxbased gel-like materials for conservation of art: Characterization and applications, *Studies in Conservation.* 60 (2015) 227-244.
- [19] E. Pezron, A. Ricard, L. Leibler, Rheology of Galactomannan-Borax Gels, *J. Polym. Sci. Part B.*

- Polym. Phys. 28 (1990) 2445–2461.
- [20] V. Epure, M. Griffon, E. Pollet, L. Avérous, Structure and properties of glycerol-plasticized chitosan obtained by mechanical kneading, *Carbohydr. Polym.* 83 (2011) 947–952.
- [21] C. Gao, E. Pollet, L. Av, Food Hydrocolloids Properties of glycerol-plasticized alginate fi lms obtained by thermo- mechanical mixing, *Food Hydrocoll.* 63 (2017) 414–420.
- [22] M. Kapoor, D. Khandal, R. Gupta, P. Arora, G. Seshadri, S. Aggarwal, et al., Certain Rheological Aspects of Functionalized Guar Gum, *Int. J. Carbohydr. Chem.* 2013 (2013) 1–15.
- [23] S. Kesavan, R.K. Proud'homme, Rheology of Guar and HPG Cross-linked by Borate, *Macromolecules.* 2 (1992) 2026–2032.
- [24] M. Rietjens, P.A. Steenbergen, Crosslinking mechanism of boric acid with diols revisited, *Eur. J. Inorg. Chem.* (2005) 1162–1174.
- [25] J. Dealy, D. Plazek, Time Temperature Superposition - A User Guide, *Rheol. Bulletin.* 78 (2009) 16–31.
- [26] S. Murgia, M. Monduzzi, F. Lopez, G. Palazzo, Mesoscopic structure in mixtures of water and 1-butyl-3-methyl imidazolium tetrafluoroborate: A multinuclear NMR study, *J. Solution Chem.* 42 (2013) 1111–1122.
- [27] S. Murgia, G. Palazzo, M. Mamusa, S. Lampis, M. Monduzzi, Aerosol-OT in water forms fully-branched cylindrical direct micelles in the presence of the ionic liquid 1-butyl-3-methylimidazolium bromide., *Phys. Chem. Chem. Phys.* 13 (2011) 9238–45.
- [28] E. Carretti, C. Matarrese, E. Fratini, P. Baglioni, L. Dei, Physicochemical characterization of partially hydrolyzed poly(vinyl acetate)-borate aqueous dispersions, *Soft Matter.* (2014).
- [29] M. Shibayama, Structure-mechanical property relationship of tough hydrogels, *Soft Matter.* 8 (2012) 8030–8038.
- [30] P.G. De Gennes, *Scaling concepts in polymer physics*, Cornell University Press, Ithaca, New York, 1979.
- [31] P.J.P. Sci, *Complex Formation in Polymer-Ion Solutions.* 1. Polymer Concentration Effects, (1989) 1169–1174.
- [32] S. G. Chaudri, B. H. Rajai, P. S Singh, Nanoscale homogeneity of silica-poly(vinyl alcohol) membranes by controlled cross-linking via sol-gel reaction in acidified and hydrated ethanol, *RSC Advances.* 5 (2017) 65862–65869.
- [33] M. Bishop, N. Shahid, J. Yang, A.R. Barron, Determination of the mode and efficacy of the cross-linking of guar by borate using MAS 11B NMR of borate cross-linked guar in combination with solution 11B NMR of model systems., *Dalton Trans.* (2004) 2621–2634.
- [34] B. a Schubert, E.W. Kaler, N.J. Wagner, The Microstructure and Rheology of Mixed Cationic/Anionic Wormlike Micelles, *Langmuir.* (2003) 4079–4089.
- [35] P.G. de Gennes, P. Pincus, Scaling theory of polymer adsorption, *J. Phys..* 37 (1976) 1445–1452.
- [36] J.-M. Guenet, Structure versus rheological properties in fibrillar thermoreversible gels from polymers and biopolymers, *J. Rheol. (N. Y. N. Y).* 44 (2000) 947–960.
- [37] J.L. Jones, C.M. Marques, Rigid polymer network models, *J. Phys. France.* 51 (1990) 1113–1127.
- [38] M. Pääkkö, M. Ankefors, H. Kosonen, A. Niskanen, S. Ahola, M. Östeberg, et al., Enzymatic Hydrolysis Combined with Mechanical Shearing and High-Pressure Homogenization for Nanoscale Cellulose Fibrils and Strong Gels, *Biomacromolecules.* 8 (2007) 1934–1941.
- [39] T. Duncan, B. Berrie, R. G. Weiss, Soft, Peelable Organogels from Partially Hydrolyzed Poly(vinyl acetate) and Benzene-1,4-diboronic Acid: Applications to Clean Works of Art, *ACS Applied Materials and Interfaces.* 9 (2017) 28069–28078.
- [40] P. Baglioni, D. Chelazzi, eds., *Nanoscience for the Conservation of Works of Art*, The Royal

Society of Chemistry, London, UK, 2013.

- [41] G. Poggi, N. Toccafondi, D. Chelazzi, P. Canton, R. Giorgi, P. Baglioni, Calcium hydroxide nanoparticles from solvothermal reaction for the deacidification of degraded waterlogged wood., *J. Colloid Interface Sci.* 473 (2016) 1–8.
- [42] E. Carretti, L. Dei, Gels as Cleaning Agents in Cultural Heritage Conservation, in *Molecular Gels: Materials with Self-Assembled Fibrillar Networks*, P. Terech and R. G. Weiss Eds., Springer, 2005, New York, USA, pp. 929-938.
- [43] L. Angelova, M. Leskes, B. Berrie, R.G. Weiss, Selective formation of organo, organo-aqueous, and hydro gel-like materials from partially hydrolysed poly(vinyl acetate)s based on different boron-containing crosslinker., *Soft Matter*. 11 (2015) 5060-5066.
- [44] P. Baglioni, E. Carretti, D. Chelazzi, Nanomaterials for Art Conservation, *Nature Nanotechnology*. 10 (2015) 287-290.
- [45] C. Mazzuca, G. Poggi, N. Bonelli, L. Micheli, P. Baglioni, A. Palleschi, Innovative chemical gels meet enzymes: A smart combination for cleaning paper artworks, *J. Colloid Interface Sci.* 502 (2017) 153–164.
- [46] C. Berlangieri, E. Andrina, C. Matarrese, E. Carretti, R. Traversi, M. Severi, et al., Chelators confined into 80pvac-borax highly viscous dispersions for the removal of gypsum degradation layers, *Pure Appl. Chem.* 89 (2017) 97–109.

SUPPLEMENTARY MATERIAL

Structural, rheological and dynamics insights of hydroxypropyl guar gel-like systems

C. Berlangieri^a, G. Poggi^a, S. Murgia^b, M. Monduzzi^b, P. Baglioni^a, L. Dei^a and E. Carretti^{a§}

a. Department of Chemistry "Ugo Schiff" & CSGI Consortium, University of Florence, via della Lastruccia, 3, 50019 Sesto Fiorentino (Florence), Italy. Address here.

b. Department of Chemical and Geological Sciences and CSGI, University of Cagliari, ss 554 bivio Sestu, 09042 Monserrato (Cagliari), Italy.

§ Corresponding author. E-mail: carretti@csgi.unifi.it

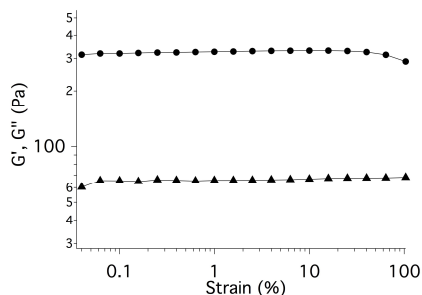


Figure S1. Amplitude sweep measurements on the hydrogel containing HPG 3 wt%/glycerol 3.5 wt%/borax 0.75 wt%/water. G' (●) and G'' (▲) are reported versus strain %. In the graph the linear viscoelastic region can be observed between about 0.1% to 100% strain. The oscillation Frequency was 1Hz.

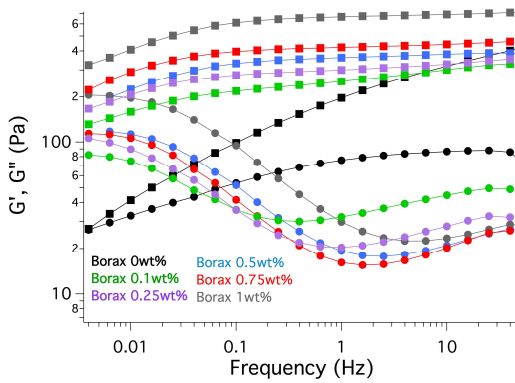


Figure S2: Frequency sweep measurements on HPG/water sample with increasing amount of borax, from 0 to 1 wt%. HPG concentration was 3 wt%. The oscillation amplitude was 5%.

G' (■), G'' (●).

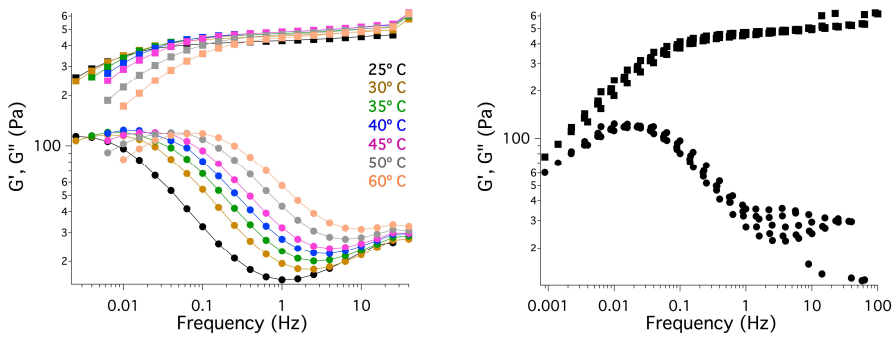


Figure S3. Frequency sweep curves at temperatures from 25 to 60 °C (left) and the final master curve (right) for system containing HPG 3 wt%/ borax 0.75 wt%/water. G' (■), G'' (●).

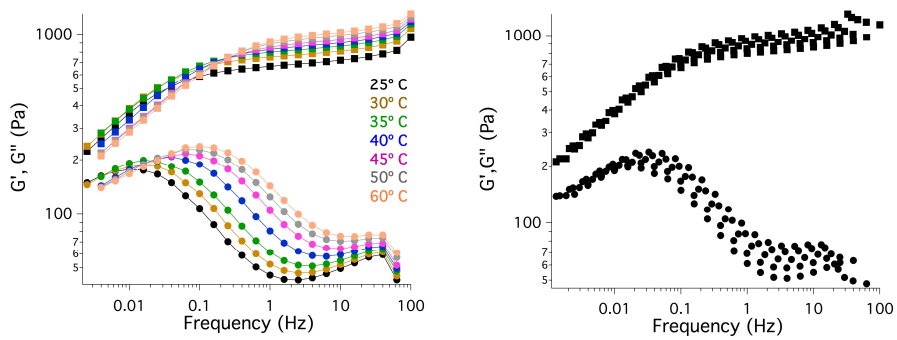


Figure S4. Frequency sweep curves at temperatures from 25 to 60° C (left) and the final master curve (right) for system containing HPG 3 wt%/glycerol 1 wt%/borax 0.75 wt%/water. G' (■), G'' (●).

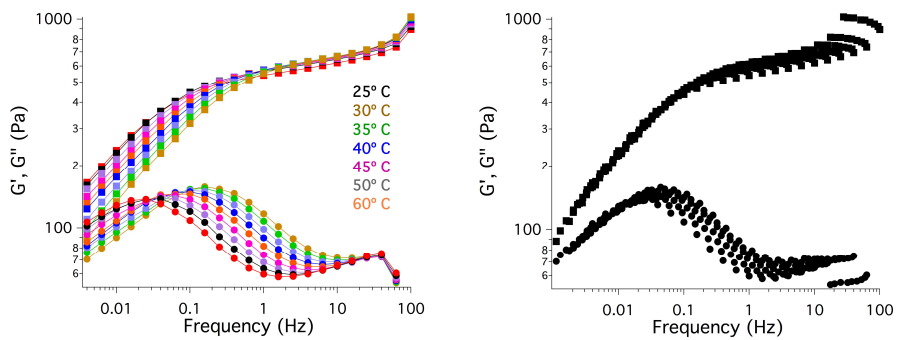


Figure S5. Frequency sweep curves at temperatures from 25 to 60° C (left) and the final master curve (right) for system containing HPG 3 wt%/glycerol 2 wt%/borax 0.75 wt%/water. G' (■), G'' (●).

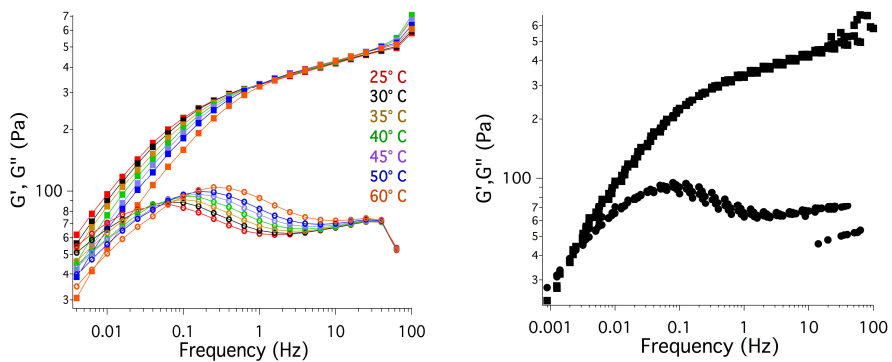


Figure S6. Frequency sweep curves at temperatures from 25 to 60° C (left) and the final master curve (right) for system containing HPG 3 wt%/glycerol 3.5 wt%/borax 0.75 wt%/water. G' (■), G'' (●).

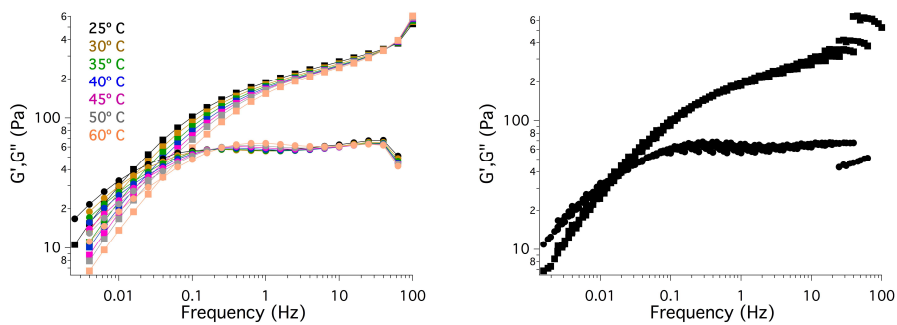


Figure S7. Frequency sweep curves at temperatures from 25 to 60° C (left) and the final master curve (right) for system containing HPG 3 wt%/glycerol 4.5 wt%/borax 0.75 wt%/water. G' (■), G'' (●).

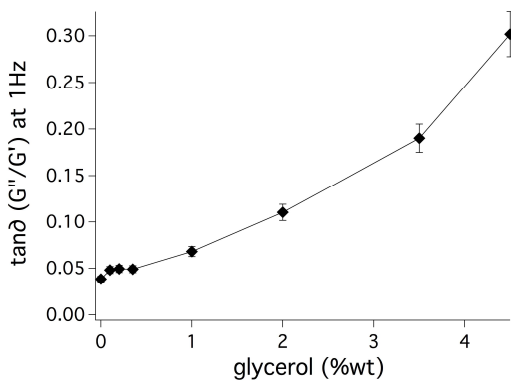


Figure S8. $\tan\delta$ values at Frequency 1 Hz are plotted against Glycerol wt%. The estimated error on these measurements is of 10%.

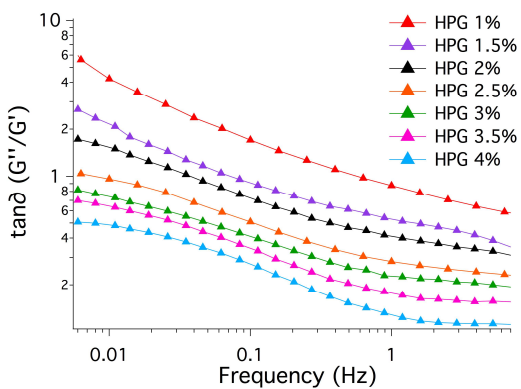


Figure S9. $\tan\delta$ for samples containing different amount of HPG, glycerol 3.5 wt%, borax 0.75 wt% and water

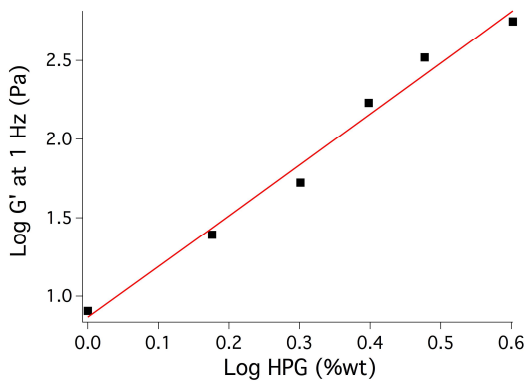


Figure S10: Log G' (1 Hz) as a function of Log HPG wt%. A linear function was used to fit the data.

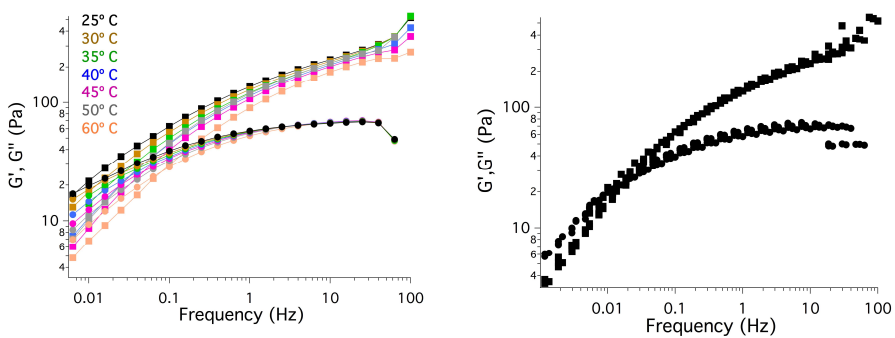


Figure S11. Frequency sweep curves at temperatures from 25 to 60° C (left) and the final master curve (right) for sample containing HPG 3 wt% in water. G' (■), G'' (●).

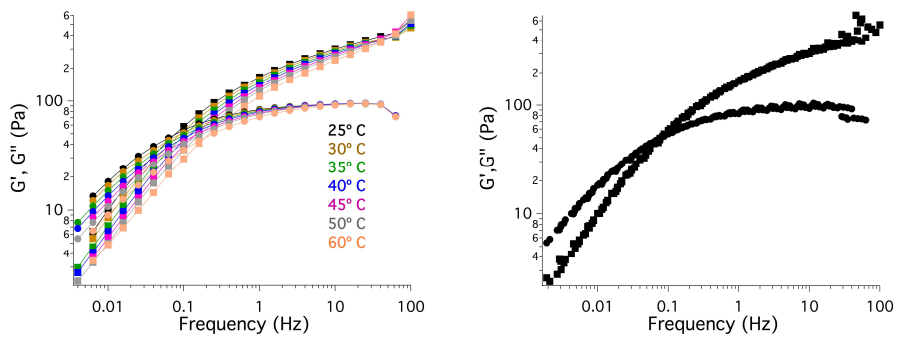


Figure S12. Frequency sweep curves at temperatures from 25 to 60° C (left) and the final master curve (right) for sample containing HPG 3 wt%/glycerol 3.5 wt%/ water. G' (■), G'' (●).



Figure S13. Elasticity of the HPG/glycerol/borax formulation chosen for the preliminary applicative test.

Table S1. Chemical shifts (ppm) and area % of the signals in the ^{11}B NMR spectra of the polymer/water system containing 3 wt% of HPG, 0.75 wt% of borax and increasing amounts of glycerol (indicated as wt%).

Glycerol wt%	ppm (area %)		
	FREE BORATE/BORIC ACID	GLY-BORATE	CROSSLINKED BORATE
0.0	11.6 (96.5)	-----	5.55 (0.5)
0.5	13.88 (83.6)	9.77 (0.7)	5.65 (15.7)
1.0	15.21 (72.8)	9.74 (4.3)	5.71 (22.9)
2.0	17.00 (61.1)	9.71 (13.2)	5.58 (25.7)
3.0	18.02 (56.4)	9.71 (20.4)	5.58 (23.2)
4.0	18.46 (54.0)	9.69 (24.9)	5.71 (21.1)

Table S2. Self-diffusion coefficients (D , $\text{m}^2 \text{s}^{-1}$) of glycerol and glycerol borate complex in water solutions at increasing amounts of borax (expressed as wt%). Chemical shifts (C.S.), reported in ppm, refer to the NMR signal used to calculate the various D .

Borax %wt	0.0	0.5	1.0		3.0	
Species	Gly	Gly	Gly	Gly-Borate	Gly	Gly-Borate
C.S. *	3.65	3.64	3.63	3.94	3.63	3.94
$D \times 10^{-10}$	6.98	6.77	6.57	5.35	5.75	5.32

Table S3. Activation energies calculated using Arrhenius equation. The estimated error on these measurements is of 10%.

SAMPLE	COMPOSITION	Ea (kJ/mol)
1	HPG 3 wt% in water	29.5 ± 2.9
2	HPG 3 wt%/borax/water	37.7 ± 3.8
3	HPG 3 wt%/Glycerol 3.5 wt%/borax/water	23.4 ± 2.3
4	HPG 3 wt%/Glycerol 3.5 wt% in water	20.7 ± 2.1

6

APPENDIX

Contents

6.1	Further Investigations on HPG based systems	68
6.1.1	Glycerol Effect: Creep recovery tests	68
6.1.2	Glycerol Effect: Extensional tests	70
6.1.3	Organic solvents uploading	73

6.1 Further Investigations on HPG based systems

In this appendix are reported further investigations on systems containing HPG crosslinked by borax. Results and discussion showed in this section are to be considered preliminar.

6.1.1 Glycerol Effect: Creep recovery tests

Samples containing increasing amount of glycerol were studied by means of Creep recovery tests. A Stress of 15 Pa was applied and the response of the systems in terms of displacement was recorded (loading phase). After the removal of the stress, the displacement was recorded during the recovery phase. The recovery % was determined. (Figure 6.1)

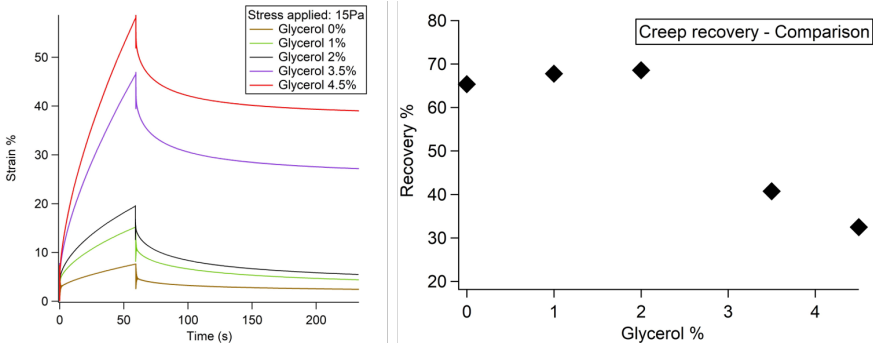


Figure 6.1: Creep recovery curves of samples containing increasing amounts of glycerol (left). Recovery % plotted against the glycerol concentration (right).

The curve related to the load phase for each sample was fitted using the Maxwell and Kelvin-Voigt model (see Figure 6.2), [91] [92] where the overall deformation is described by the equation 6.1.

$$\gamma(t) = \left(\frac{\sigma}{G_1}\right) + \left(\frac{\sigma}{G_2}\right) * \left(1 - e^{-\frac{t}{\tau_2}}\right) + \left(\frac{\sigma}{\eta_1}\right) * t \quad (6.1)$$

Where:

- σ is the stress applied

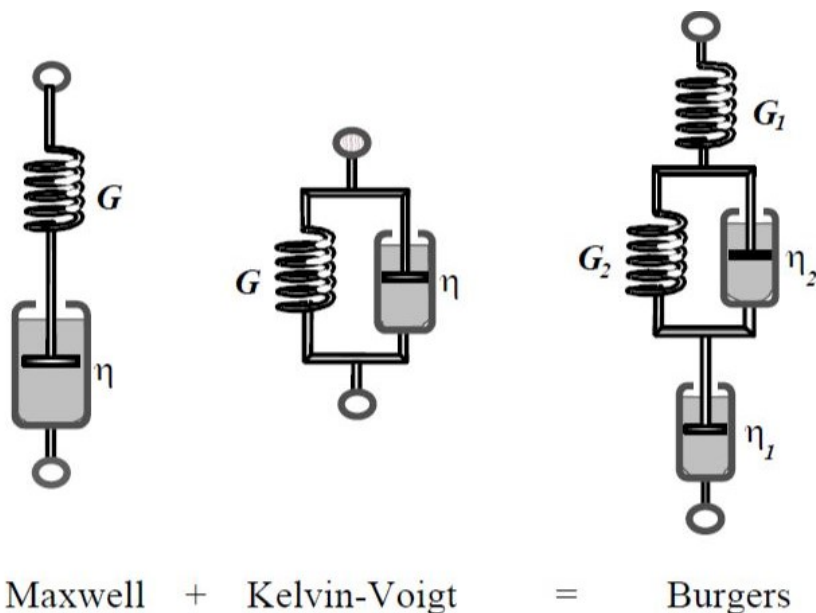


Figure 6.2: Schematic representation of the Maxwell, Kelvin-Voigt and Burgers models. (H. Barnes, *Handbook of Elementary Rheology*, 2000).[91]

- G_1 is the elastic constant of pure elastic response (Shear modulus for the elastic region, related to the crosslinking density of a system).
- G_2 is the elastic constant in the viscoelastic region (Shear modulus of the viscoelastic region)
- η_1 is the viscosity related to the viscous region
- η_2 is the viscosity related to the viscoelastic region

All the samples displayed a permanent deformation, typical of a viscoelastic material. We can already observe that increasing glycerol concentration increases the permanent deformation. In particular, from the figure 6.1 in the graph of the creep recovery we can observe a neat difference between samples containing glycerol up to 2 % and samples with higher glycerol concentrations. While for the first three samples the recovery of the deformation due to the applied stress is almost the same, this parameter strongly decreases for samples containing the highest amounts of glycerol. These samples, indeed, show a more viscous-like behavior. Fitting results are listed in the table below (Table 6.1). G_1 corresponds to the elastic modulus and the decrease of this value with increasing amounts of glycerol suggests a decrease in stiffness and a decrease of crosslinking density. η_1 , also called Voigt viscosity, is associated to the internal friction of polymer chains [93] and its decreasing value indicates a more

permanent deformation of the samples containing higher amount of glycerol, thanks to the high mobility of polymer chains.

Glycerol %	G_1 (KPa)	G_2 (KPa)	η_1 (KPa*s)	η_2 (KPa*s)
0	5.24 ± 0.01	12.5 ± 0.1	246.7 ± 1.4	143.5 ± 1.5
1	3.31 ± 0.01	4.82 ± 0.07	115 ± 1	46.0 ± 0.6
2	3.06 ± 0.01	3.37 ± 0.05	84.7 ± 0.9	25.7 ± 0.4
3.5	2.35 ± 0.02	1.67 ± 0.02	28.0 ± 0.1	13.1 ± 0.2
4.5	2.24 ± 0.01	1.14 ± 0.01	22.8 ± 0.1	9.89 ± 0.1

Table 6.1: Parameters obtained from the fitting of the load phase curve of the creep tests using the MKV model.

6.1.2 Glycerol Effect: Extensional tests

Extensional rheology measurements were made using flat-plate geometry (4 cm diameter) at 25°C. The gap between the plates was 0.5 mm. Samples were loaded between the plates and allowed to equilibrate until the force exerted on the top plate was 0 N. The two plates were then moved progressively farther from each other with a velocity of 5 $\mu\text{m/s}$. Samples investigated were systems containing HPG/borax/water and increasing amounts of glycerol (from 0 to 3.5%). In Figure 6.3 the extensional rheological curves are reported.

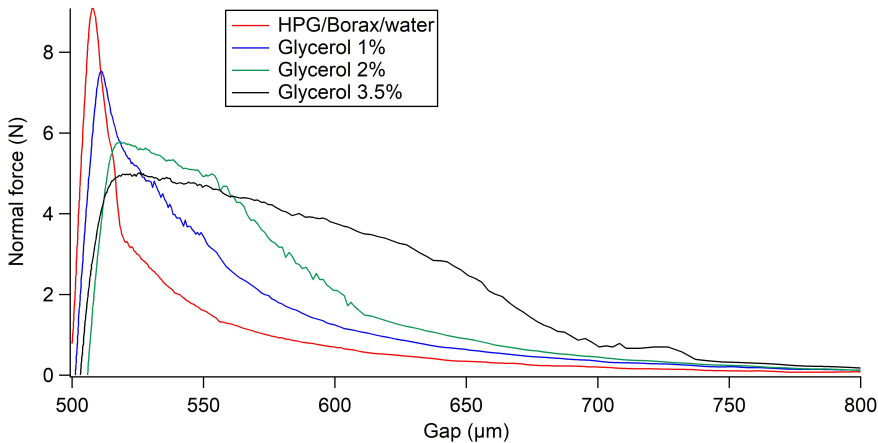


Figure 6.3: Extensional rheological curves for samples containing increasing amounts of glycerol.

First results show a decrease in the strength of the networks as the amount of glycerol is increased. Indeed we can observe a decrease of the maximum

normal force, correlated to system cohesion. [20] As a matter of fact, increasing the glycerol concentration, the maximum force needed to pull the sample apart decreases (Table 6.2).

Glycerol %	Normal Force Maxima (N)
0	9.08
1	7.64
2	6.05
3.5	5.31

Table 6.2: Values of the maximum force for samples investigated.

Also the Young's Modulus associated to each sample, measured performing a linear fitting of the first part of the curve, confirm this trend. The Young's Modulus (E) is a parameter related to the stiffness due to the chemical-physical properties of the material. This property defines the material resistance against deformation. [92] The Young's Modulus can be defined as the ratio between the normal force (σ , force per unit area) and the strain (ε , ratio of deformation over initial length) along that axis in the elastic portion of the stress-strain curve, that is the initial portion, so in the range in which the material provide a linear response (see Equations 6.2, 6.3, 6.4). [94]

$$E = \frac{\sigma}{\varepsilon} \quad (6.2)$$

$$\sigma = \frac{N}{A} \quad (6.3)$$

$$\varepsilon = \frac{\Delta l}{l_0} \quad (6.4)$$

where l_0 is the initial gap (and actually is the original length of the object), N is the force on an object under tension, A is the area of the cross-section perpendicular to the applied force. As we can see from the Table 6.3 and Figure 6.4 below, the stiffness decreases with glycerol increasing, resulting in a decrease of the systems resistance against deformation. We have a more stretchable and sticky material as long as we add glycerol (See also Figure 6.5).

Glycerol %	Normal Force Maxima (N)
0	1.014 ± 0.003
1	0.745 ± 0.003
2	0.591 ± 0.004
3.5	0.527 ± 0.004

Table 6.3: Values of the Young's modulus resulted from the fitting of the first portion of the extensional curve for the samples investigated.

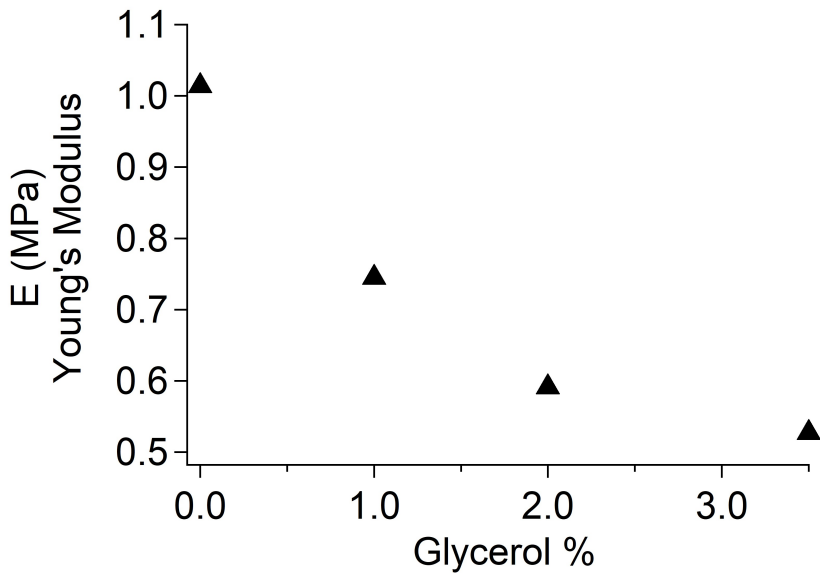


Figure 6.4: In the graph values of Young's modulus for each sample was plotted against the glycerol content.

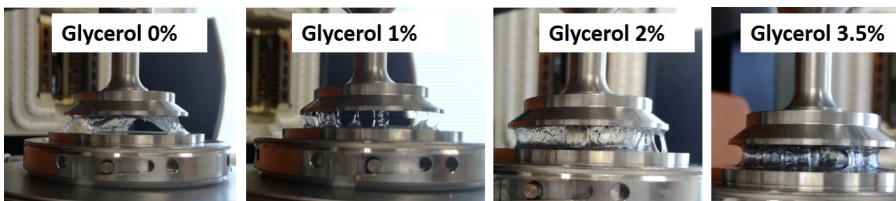


Figure 6.5: Pictures of the samples during extensional rheological measurements.

6.1.3 Organic solvents uploading

The uploading of organic solvents in our new systems containing hydroxypropyl guar is a fundamental aspect for their application in cleaning of artistic surfaces. The most promising system containing HPG/glycerol/borax/water, described in details in chapter5 and in the appended paper, was prepared again including in its composition different amounts of organic solvents. The maximum amount of solvents to be uploaded is determined taking into account the water solubility for each solvent, considering water amount contained in the complete system. For every solvent several attempts are performed, varying solvent and/or glycerol amounts, in order to obtain the best performance. Polymer and borax amounts for every system are retained as usual (respectively 3% and 0.75%). The best results belongs to the formulation reported in the Table 6.4.

Solvent	Glycerol %	Solvent %
1-Propanol	3.75	20
Methylethyl ketone (MEK)	4	15

Table 6.4: Glycerol and organic solvent amounts in the most promising formulations, retaining the best behavior in term of elasticity and elongation ability.

Rheological measurements were performed on samples containing increasing amount of organic solvent, allowing us to investigate how different concentration can influence systems properties. Frequency Sweep measurements have been carried out, at 25°C using a plate-plate geometry, within the linear viscoelastic range (5% strain). The storage and loss moduli (G' and G'') have been measured over the frequency range of 0.001 to 100 Hz. For all the samples the linear viscoelastic region was similar, having the same behavior during the Amplitude Sweep test: a 5% strain is chosen as a medium value in linear viscoelastic range, in which our systems are stable.

In the first experiment different amounts of Propanol were uploaded. The rheological behavior of this systems (Figure6.6) is almost similar, but a gradual separation of G' and G'' curves is observed. As the content of Propanol increases, the G' and G'' moduli increase, but at the same time the two curves separate. In all the cases G' is predominant. The value of G' at a fixed frequency (1 Hz) is similar for samples with increasing amount of solvent.

The same test has been carried out on samples containing increasing amounts of MEK (Figure6.7. From FS tests we can observe how the elastic modulus G' of systems containing MEK up to 10% is quite similar and however it is lower than the elastic modulus of the standard gel (curve in red). Measurements on the sample containing MEK 15% w/w, shows a slight increase of G' . However,

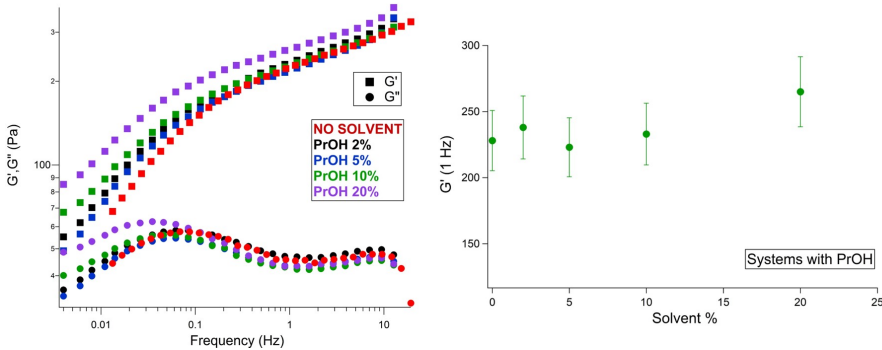


Figure 6.6: (Left) Storage modulus and Loss modulus for samples containing different amount of Propanol. (Right) Storage modulus of samples at 1 Hz VS PrOH concentration.

taking into account the error on these measurements, we can't assume the difference as significant in terms of viscoelastic behavior.

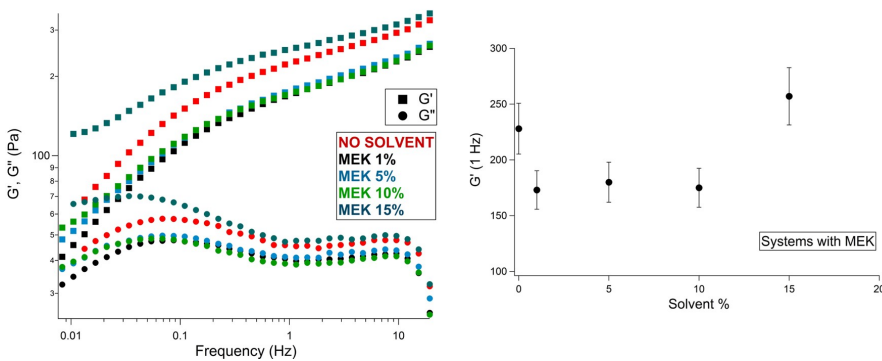


Figure 6.7: (Left) Frequency Sweep measurements for gel containing different amounts of MEK. (Right) Storage modulus of samples at 1 Hz VS solvent concentration.

This preliminary results suggests that the presence of organic solvents does not strongly change the macroscopic mechanical behavior of the samples.

6.1.3.1 SAXS measurements

In order to study the effect of solvents on the systems structure, SAXS measurements on samples before and after solvent addition were performed. On samples containing solvents, other measurements were also performed before

and after the addition of glycerol. SAXS measurements were performed using the Austrian SAXS beamline at Elettra Synchrotron (Trieste, Italy). The gel samples were placed into 1 mm demountable cells having Kapton films as windows. The measurements were recorded at room temperature, on a Mar300-imageplate detector (MarResearch, Norderstedt, Germany), with a 8 keV X-ray beam. 3 second irradiation was repeated 20 times for each sample, to monitor possible radiation damage, and averaged. In the following figures (6.8, 6.9, 6.10) SAXS profiles with the best fitting curves are reported.

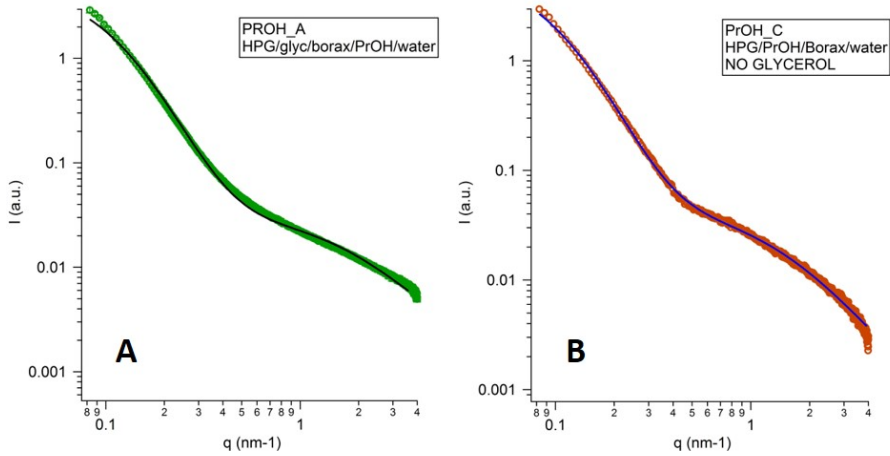


Figure 6.8: SAXS curves for sample containing HPG/glycerol/borax/PrOH/water (A) and for the analogous one without glycerol (B)

In the Table6.5 are listed the best fitting parameters, according to the following Equation6.5 [95]:

$$I(q) = \frac{I_{DB}(0)}{(1 + Inh^2q^2)^2} + \frac{I_{OZ}(0)}{1 + L^2q^2} \quad (6.5)$$

Where $I_{OZ}(0)$ is the scattering intensity of the Ornstein-Zernike (OZ) term, L is the correlation or screening length, $I_{DB}(0)$ is the scattering intensity of the Debye-Bueche term and Inh is the characteristic average dimension of the inhomogeneities. The first term of the equation represents solid-like long-range inhomogeneities, concerning the scattering at low q produced by inhomogeneities, as for example, solid-like polymer domains. The second term describes the liquid-like scattering functions.

As already mentioned in the appended paper (Berlangieri et al. *Structural, rheological and dynamics insights of hydroxypropyl guar gel-like systems*), the Screening Length can be associated to the mesh size of the polymeric network.

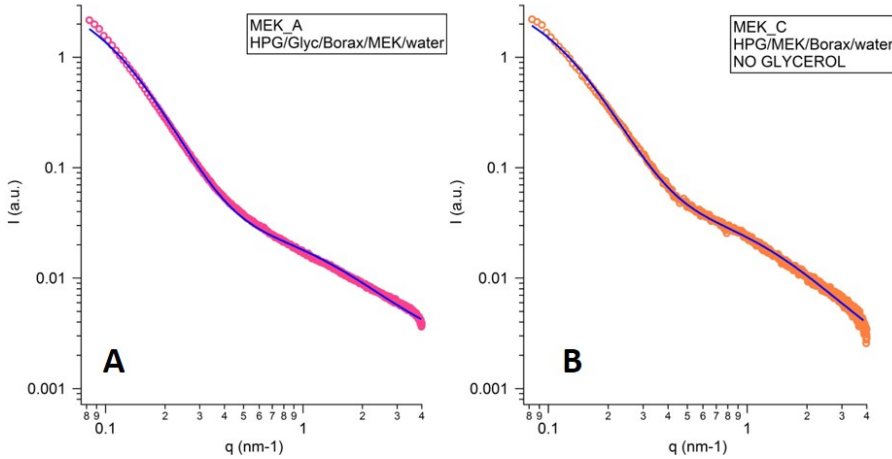


Figure 6.9: SAXS curves for sample containing HPG/glycerol/borax/MEK/water (A) and for the analogous one without glycerol (B)

Sample	Screening Length (\AA)	Inhomogeneities (\AA)
Gel STD	11.63 ± 0.23	96.60 ± 0.23
PrOH A	5.90 ± 0.02	81.80 ± 0.43
PrOH B	7.84 ± 0.08	89.80 ± 1.08
MEK A	7.97 ± 0.05	83.89 ± 0.55
MEK B	8.49 ± 0.12	78.48 ± 1.14

Table 6.5: Parameters associated with the best fits to the SAXS curves.

Fitting results show that this parameter decreases with organic solvent addition, probably due to the decrease of the dielectric constant of the system. For what concern samples containing Propanol, the L value slightly increases for the sample without glycerol, while on the opposites it slightly decreases for the analogous sample containing MEK. The characteristic length of solid-like inhomogeneities, described by the Inh parameter, follows a similar trend.

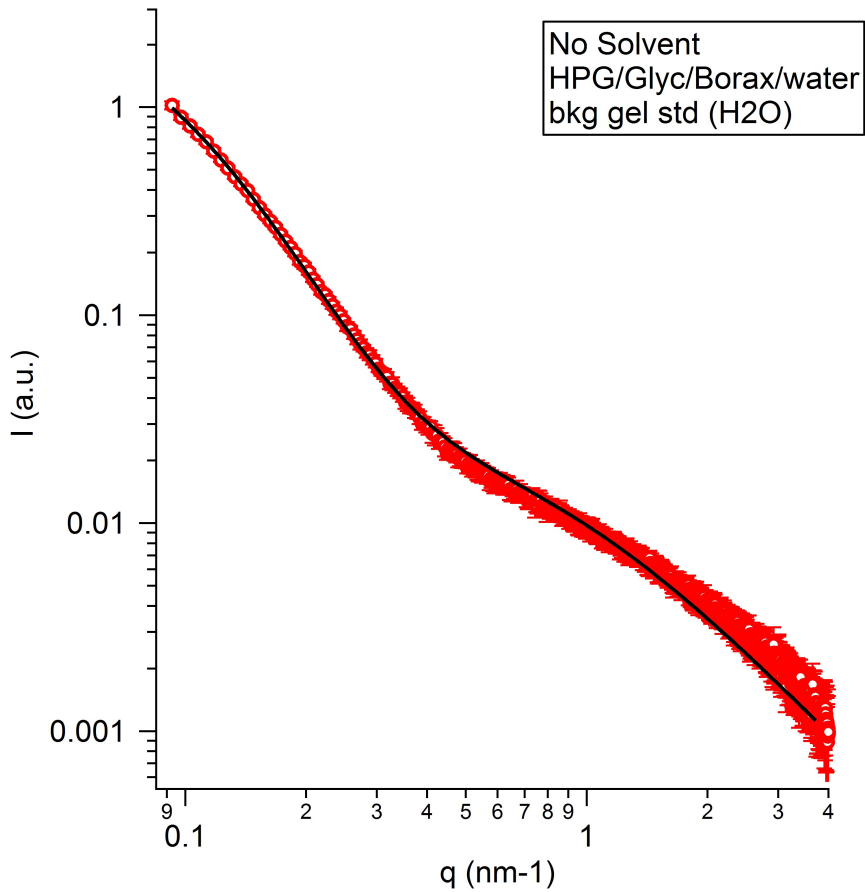


Figure 6.10: SAXS curves for the standard sample HPG/glycerol/borax/water, without organic solvents.

7

CHELATORS CONFINED INTO 80PVAC-BORAX HIGHLY VISCOUS DISPERSIONS

In this Chapter are reported the results on the removal of gypsum degradation layers from carbonatic matrices in cultural heritage conservation, using aqueous HVPD based on partially hydrolyzed poly(vinyl acetate) and borax, embedded with chelators.

Conference paper

Chiara Berlangieri, Elisabetta Andrina, Caterina Matarrese, Emiliano Carretti, Rita Traversi, Mirko Severi, David Chelazzi, Luigi Dei* and Piero Baglioni

Chelators confined into 80pvac-borax highly viscous dispersions for the removal of gypsum degradation layers

DOI 10.1515/pac-2016-0815

Abstract: In this paper a new method for the removal of gypsum degradation layers from carbonatic matrices in cultural heritage conservation, using aqueous Highly Viscous Polymeric Dispersions (HVPDs) based on partially hydrolyzed poly(vinyl acetate) and borax, embedded with chelators, is presented. Due to their interesting viscoelasticity, these systems guarantee a good adhesion to the treated surface and easiness of removal in one step, minimizing the residues. Thus, they can potentially overcome the “residue question” limit associated to traditional methodologies that use thickened solutions of chelators. Here the rheological properties of HVPDs containing different amounts of selected chelating agents are explored and their efficacy in the extraction of gypsum is verified through cleaning tests onto artificially sulfated travertine tiles. The homogeneous removal of gypsum across the surface was checked non-invasively via Fourier Transform Infrared Spectroscopy (FTIR) 2D Imaging. An analytical protocol for the pre-treatment and the analysis of HVPD samples by means of Ion Chromatography (IC) and Inductively Coupled Plasma Atomic Emission Spectroscopy (ICP-AES) was set up and the approximate amount of calcium sulfate removed was determined.

Keywords: chelates; desulphatisation; gypsum layers; POC-16; poly vinyl alcohol-borax; viscoelasticity.

Introduction


Since ancient times, limestones have been used as base material for artworks, statues and mural paintings, constituting the larger part of our cultural heritage for many centuries.

A common degradation that affects artifacts made of natural or artificial carbonatic materials is the sulphatisation, the transformation of calcium carbonate in calcium sulfate dihydrate (gypsum) due mainly to the interaction with the atmospheric sulfur dioxide in the presence of humidity and oxidation catalysts [1]. The elementary cell of gypsum occupies almost a double volume compared to that of calcium carbonate. In the case of carbonatic supports, when this reaction takes place and new crystals of gypsum form inside the porous structure, the consequent volume expansion determine mechanical stresses that cause cracking,

Article note: A collection of invited papers based on presentations at the 16th International Conference on Polymers and Organic Chemistry (POC-16), Hersonissos (near Heraklion), Crete, Greece, 13–16 June 2016.

***Corresponding author: Luigi Dei**, Department of Chemistry “Ugo Schiff” and CSGI Consortium, University of Florence, via della Lastruccia, 3 – 50019 Sesto Fiorentino (Florence), Italy, Tel.: +39 055 4573045, Fax: +39 055 4574913, e-mail: luigi.dei@unifi.it
Chiara Berlangieri, Elisabetta Andrina, Caterina Matarrese, Emiliano Carretti, David Chelazzi and Piero Baglioni: Department of Chemistry “Ugo Schiff” and CSGI Consortium, University of Florence, via della Lastruccia, 3 – 50019 Sesto Fiorentino (Florence), Italy

Rita Traversi and Mirko Severi: Department of Chemistry “Ugo Schiff”, University of Florence, via della Lastruccia, 3 – 50019 Sesto Fiorentino (Florence), Italy

 © 2017 IUPAC & De Gruyter. This work is licensed under a Creative Commons Attribution-NonCommercial-NoDerivatives 4.0 International License. For more information, please visit: <http://creativecommons.org/licenses/by-nc-nd/4.0/>

Brought to you by | Università degli Studi di Firenze
Authenticated
Download Date | 5/16/17 8:11 AM

fissuring and pulverization of the carbonatic matrix [2]. In particular, for frescoes, when the phenomenon is particularly severe, we observe lifting and detachment of the paint layer, with loss of decoration and pigments [3].

One of the most effective traditional treatments for the gypsum removal from carbonatic supports is the Ferroni-Dini method [4], developed in 1966 by Enzo Ferroni, chemistry professor at the University of Florence, and Dino Dini, headmaster in the restoration of frescoes. It's a two-phases treatment consisting in the solubilization of gypsum with a water solution of $(\text{NH}_4)_2\text{CO}_3$ (ammonium carbonate) followed by the application of barium hydroxide that ensures the consolidation of the degraded matrix and at the same time makes the sulfate unreactive and insoluble [5–7].

An alternative, widely used technique for the removal of soluble salts and, in particular, of calcium sulfate from frescoes, mural paintings and plasters consists in the use of ion-exchanger resins [8, 9]. Generally they are synthetic resins that swell when in contact with water and are completely insoluble in it [10]. Due to this feature, when ion-exchangers are in contact with an artwork contaminated by salts, their action is limited to the surface up to a depth of about 70–100 μm , without penetrating into the porosity of the object, thus avoiding the interaction with the original materials to preserve [11].

Other substances used by restorers to treat the efflorescences are chelators. The most diffused are disodium EDTA, Rochelle salt (especially for the cleaning of gilded bronzes because of its mild action that preserve the original gilded foil [12]), citrate salts and benzotriazole [13–17]. Usually they are applied in aqueous solution (1–5% of additive) [18]. The solution pH has a fundamental role for the dissociation equilibria of the chelator and its selectivity towards different ions.

A potential risk in the use of these substances, is that calcium ions coming from the carbonate matrix could be solubilized as well. To limit the penetration of the cleaning agent into the inner layers and to avoid the solubilization of the original material constituting the plaster and the paint layer, chelators aqueous solutions are usually adsorbed into poultices of carboxymethylcellulose or gelled with a thickener as Klucel G [19, 20] or Carbopol [6].

The main drawback of these applicative methods is the “residue question” [21], as the thickened systems release residues onto the treated surface. The necessity of a clearance step with a neat liquid (generally water) and/or extra mechanical action can be critical in presence of fragile or hydrophilic surfaces/materials.

At the Chemistry Department of the University of Florence and CSGI Consortium, innovative peelable poly(vinyl) acetate (PVAc)-borax based Highly Viscous Polymeric Dispersions (HVPDs) for cleaning artistic surfaces were developed and studied [22].

The viscoelastic and cleaning/removing properties of the HVPDs can be modulated by varying the entanglements density of the network [23, 24] and/or the polarity of the continuous phase by incorporating different organic solvents [25–27]. Their high elastic modulus and viscosity allow the minimization of the residues left onto the treated surface and of the penetration of the cleaning agent into the porous matrix of the artwork. The first applicative tests on canvas and wood paintings [22, 28] resulted in a controllable, gradual, selective cleaning action.

Recently, considering the great versatility of these HVPDs, the capability of embedding chelators was explored. This achievement could extend the application field of these systems to mural paintings and metal surfaces, both frequently affected by the presence of foreign patinas like salt efflorescences and corrosions/oxidation deposits, respectively. In fact, it must be noted that this class of HVPDs has a broad range of potential applications that include the cleaning of both classic and modern artifacts (easel/mural paintings, graffiti, metallic and plastic objects), therefore their current implementation will highly benefit from studies concerning their characterization and effectiveness.

In this work three chelating species were selected: disodium EDTA, $(\text{NH}_4)_2\text{CO}_3$ and sodium/potassium tartrate. The maximum loadable amount of each, before observing phase separation, was determined. The viscoelastic properties of HVPDs containing different amounts of chelator were investigated to study how the additive influence their elastic response.

To evaluate the efficacy in the removal of calcium sulfate, these HVPDs embedded with chelators were tested onto artificially sulfated travertine tiles. The qualitative, non-invasive evaluation of the cleaning

treatment was carried out through FTIR 2D Imaging, in order to estimate the homogeneousness of the removal of gypsum across the treated surface. HVPD samples collected after the cleaning tests were analyzed through Ion Chromatography and Inductively Coupled Plasma techniques. The quantification of the gypsum extracted was possible thanks to the set-up of an analytical protocol for the pre-treatment and the analysis of samples that was suitable for IC/ICP.

Materials and methods

Eighty percent hydrolyzed poly(vinyl acetate) was supplied by Kuraray Co., Ltd. as random copolymer ($M_w = 47\,300$) and was used as received. Sodium tetraborate decahydrate (99, 5–100 %, Sigma-Aldrich), $(\text{NH}_4)_2\text{CO}_3$ (Sigma-Aldrich), disodium EDTA dihydrate (99–100 %, ACS reagent, Sigma-Aldrich), potassium sodium tartrate tetrahydrate (99 %, ACS reagent, Sigma-Aldrich), ammonium hydroxide (Sigma, NH_3 content 28–30 %), hydrochloric acid 37 % (CARLO ERBA, min. assay 36.5 %) and sulphuric acid 96 % (96 ± 1 %, CARLO ERBA) were used as received. Water was purified by a Millipore Elix3 apparatus ($R \geq 15 \text{ M}\Omega \text{ cm}$).

Preparation of the polymeric dispersions

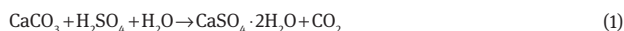
The PVAc was dissolved in a water solution of the chelating agent; then a solution of borax was added and the system was stirred with a VORTEX apparatus until it became rigid in few minutes. The polymer/borax weight ratio was kept to 4 : 1. The pH of all the systems was adjusted in order to warrantee the maximum complexation ability. All the measurements and cleaning tests were carried out 1 week after the samples preparation to ensure their equilibration.

Travertine samples sulfation

The sulfation of the travertine tiles was inducted by soaking one of their surface ($4.8 \times 4.8 \text{ cm}$) into a $5 \text{ M H}_2\text{SO}_4$ solution for 1 h. Then they were let dry until a constant weight was reached.

Gravimetric determination of the calcium sulfate dihydrate formed onto the travertine samples

The average amount (g) of gypsum formed ($W_{\text{CaSO}_4 \cdot 2\text{H}_2\text{O}}$) onto the travertine tiles was determined gravimetrically, according to the stoichiometric equilibrium of the sulfation reaction (1), using the formula (2):



$$W_{\text{CaSO}_4 \cdot 2\text{H}_2\text{O}} = \frac{\Delta W \cdot MW_{\text{CaSO}_4 \cdot 2\text{H}_2\text{O}}}{MW_{\text{CaSO}_4 \cdot 2\text{H}_2\text{O}} - MW_{\text{CaCO}_3}} \quad (2)$$

where ΔW (g) is the difference between the final weight W_f (g) and the initial weight W_i (g) of the travertine tile after the sulfation, $MW_{\text{CaSO}_4 \cdot 2\text{H}_2\text{O}}$ and MW_{CaCO_3} are the molecular weights of $\text{CaSO}_4 \cdot 2\text{H}_2\text{O}$ and CaCO_3 , respectively. The total average amount of $\text{CaSO}_4 \cdot 2\text{H}_2\text{O}$ formed onto the travertine surface was 6.7 mg/cm^2 .

Application of HVPDs embedded with chelators onto the sulfated travertine tiles

A weighed amount (1 g) of an HVPD containing the chelator was applied onto a confined area (2.28 cm^2) of a sulfated travertine tile using a plastic ring, for different contact times: 5, 10, 20, 30, 60 min (Fig. 1). Each test

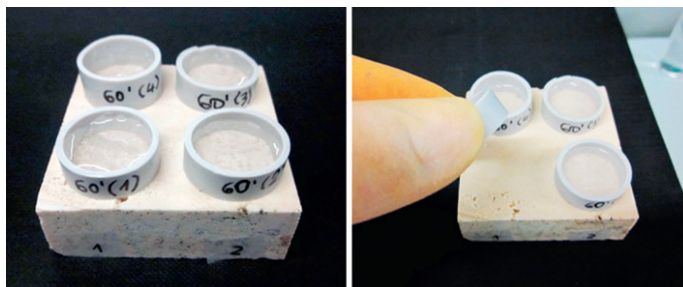


Fig. 1: Exemplifying images showing the four “60 min-long” applications of the HVPD containing EDTA onto the sulfated travertine tile (left) and the ease removal step (right) achieved by confining the HVPD into a plastic ring.

was repeated at least four times. HVPD samples were weighed before and after each application to determine the weight loss. For samples containing $(\text{NH}_4)_2\text{CO}_3$ or Rochelle salt, additional applications lasting 1080 and 1380 min were performed.

Rheological measurements

Oscillatory shear measurements were performed with a Paar Physica UDS200 rheometer working at 25 ± 0.1 °C (Peltier temperature control system) using cone-plate geometry (25 mm diameter and 1° cone angle). The gap between the plates was 0.5 mm. After being loaded, samples were equilibrated for 30 min at 25 °C prior to start the experiments. Frequency sweep measurements were done in the linear viscoelastic region (2–3% strain) based on an amplitude sweep test. The storage modulus G' (Pa) and the loss modulus G'' (Pa) were measured over the frequency range 0.001–100 Hz. The intrinsic elastic modulus G_0 (Pa), represented by the asymptotic value of the elastic shear modulus G' was calculated as the average value of the last five G' points in the *plateau* region of the flow curves.

Ion Chromatography (IC)

IC analyses were performed with a Dionex ICS-90 Ion Chromatography System, using a Dionex AG4A guard-column (4 mm diameter, 5 cm length) and a Dionex AS4A column (4 mm diameter, 20 cm length). The eluent was a buffer solution with Na_2CO_3 (1.8 mM) and NaHCO_3 (1.8 mM) in MilliQ water (1.65 mL/min flow). A 10 mM H_2SO_4 solution was used as the regeneration fluid for the conductivity suppressor (3.36 mL/min flow). The injection loop was 25 μL .

Inductively coupled plasma optical emission spectrometry (ICP-OES)

ICP analyses were performed using a Varian 720-ES ICP-OES spectrometer with an optical detector. The external, auxiliary, and nebulizer flows were 16.5, 1.50, and 0.75 L/min, respectively. A 50 ppm solution of Germanium was used as the internal standard to quantify the analyte of interest.

2D imaging-Fourier transform infrared (FTIR)

The 2D imaging-Fourier transform infrared (FTIR) analysis of the travertine tiles was carried out on a Cary 620–670 FTIR microscope, equipped with an FPA (Focal Plane Array) 128×128 detector (Agilent Technolo-

gies). The spectra were recorded directly on the surface of the samples (or of the Au background) in Reflectance mode, with a spectral resolution of 4 cm^{-1} , acquiring 128 scans for each spectrum. The spatial resolution of each Imaging map is $5.5\text{ }\mu\text{m}$ (i.e. each pixel has dimensions of $5.5 \times 5.5\text{ }\mu\text{m}^2$). Five measurements were carried out on each type of travertine sample (untreated, sulfated, sulfated and cleaned with a HVPD containing 0.5 wt% of $(\text{NH}_4)_2\text{CO}_3$; four consecutive applications with a contact time of 60' each were carried out), and the representative spectra for each sample are shown in this contribution. In order to improve the readability of the spectra, the background noise was reduced using the “smooth” tool (set at 10) of the Igor Pro software, taking care not to alter any diagnostic information deemed useful to this qualitative investigation. In each 2D map, the intensity of the gypsum absorption at 3570 cm^{-1} (OH stretching of water) was imaged as the area of the absorption peak between 3692 and 3542 cm^{-1} . The chromatic scale of the maps shows increasing absorbance of the band as follows: green < yellow < red.

Results and discussion

Being the use of monophasic systems an essential condition to control the cleaning action of the HVPDs, the maximum amount of EDTA, Rochelle salt and $(\text{NH}_4)_2\text{CO}_3$ loadable in the 80PVAc-borax systems before observing phase separation was determined. The obtained values were 0.5 wt%, 1 wt% and 0.5 wt%, respectively.

In a previous paper it was observed that to warrant an adequate performance in terms of ease of application and complete removal through a peeling action [27], the HVPDs should preserve adequate elastic properties even upon addition of additives active against the foreign patinas of the artifacts. In particular their intrinsic elastic modulus G_0 values should be always higher than 400 Pa. To verify if these features were preserved after the addition of chelators, the mechanical properties of the HVPDs set up were explored. Figure 2 shows that upon the addition of $(\text{NH}_4)_2\text{CO}_3$ (A) or Rochelle salt (B), the mechanical behavior of the HVPDs is invariant for chelator concentrations, respectively up to 0.5 and 0.9 wt%. Figure 3 displays that a further increase of Rochelle salt concentration up to 1 wt% determines the formation of a gel (the shear elastic modulus G' is higher than the shear viscous modulus G'' over the entire range of frequencies explored) [29].

The frequency sweeps of the HVPDs containing different amounts of $(\text{NH}_4)_2\text{CO}_3$ or Rochelle salt normalized to the crossover point between the G' and the G'' curves (Fig. 4) indicate that even if changes occur in the timescale of the relaxation process when the concentration of the chelator is increased, the mechanism associated with the relaxation remains almost the same.

Figure 5 shows the trends of the G_0 values as a function of $(\text{NH}_4)_2\text{CO}_3$ (A) and Rochelle salt (B) content; for concentrations around 0.3 wt% and 0.9 wt%, respectively, the salts addition has a structuring effect on the systems as indicated by the increase of their elasticity. In presence of a higher amount of additive, the lowering of G_0 indicates a reduction of the entanglements density of the PVA network.

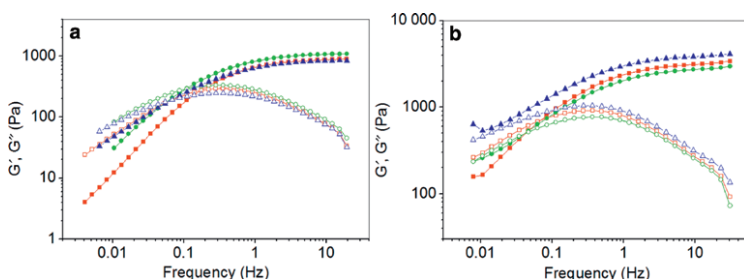


Fig. 2: Flow curves of the G' (●▲) and G'' moduli (○□) for the HVPDs containing: (a) 0.1 wt% (■□), 0.3 wt% (●○), 0.5 wt% (▲△) of $(\text{NH}_4)_2\text{CO}_3$; (b) 0.5 wt% (■□), 0.7 wt% (●○), 0.9 wt% (▲△) of Rochelle salt.

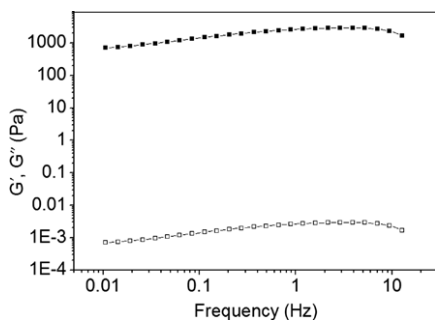


Fig. 3: Trend of G' (■) and G'' moduli (□) for the HVPD sample with 1 wt% Rochelle salt, showing the rheological behavior typical of a gel ($G' \gg G''$).

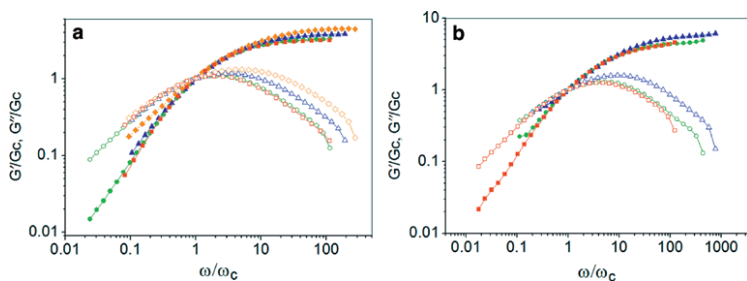


Fig. 4: Normalized mechanical histograms for the 80PVAc-borax with: (a) 0 wt% (■□), 0.1 wt% (●○), 0.3 wt% (▲△) and 0.5 wt% (◆◇) of $(\text{NH}_4)_2\text{CO}_3$; (b) 0 wt% (■□), 0.5 wt% (●○) and 0.7 wt% (▲△) of Rochelle salt. Symbols ■●▲◆ indicate the G'/G_c ratios; symbols □○△◇ indicate the G''/G_c ratios. G_c (Pa) and ω_c (Hz) are the coordinates of the crossover point.

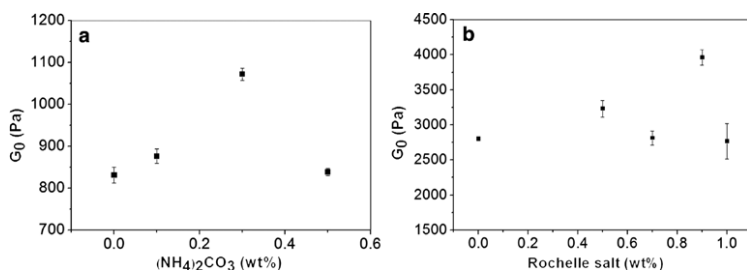


Fig. 5: Intrinsic elastic modulus G_0 of 80PVAc-borax HVPDs as a function of $(\text{NH}_4)_2\text{CO}_3$ (a) and Rochelle salt (b) concentrations (wt%).

Finally, the addition of EDTA determines a significant increase in the intrinsic elasticity (G_0) due to a structuring role of the salt. This behavior was ascribed to a combination of salt and pH effect, assuming that the EDTA tetra-anionic species Y^{4-} [30] ($\sim 50\%$ at pH ~ 11 as that of our EDTA-containing systems), mediates some cross-links between the hydroxyl groups of 80PVAc chains (Matarrese et al., paper submitted).

Even if traditional gel systems used for the conservation of artistic surfaces contain higher concentrations of chelators (1–5 wt%), the ones achievable with the 80PVAc-borax HVPDs, although significantly lower, were

expected to be still adequate for cleaning purposes. An auxiliary benefit of the lower chelator concentrations is that the cleaning action is more gradual and controllable, favoring the preservation of the original layers of the artifacts.

The HVPDs selected for the application tests on sulfated travertine tiles, contained 0.25 wt% EDTA (pH=11), 0.5 wt% $(\text{NH}_4)_2\text{CO}_3$ and 1 wt% Rochelle salt, respectively (Table 1). The aim was to evaluate their efficacy in the gypsum patina removal as a function of both the additive type and the application time. To better confine the cleaning action, the systems were applied into plastic rings that ensured also a quick and easy removal step (Experimental Section, Fig. 1).

To verify the retentive capability of the HVPDs towards the liquid fraction confined into them once in contact with the porous matrixes, the HVPDs weight was monitored before and after each test. To eliminate the contribution due to the water evaporation, a “blank” adsorption was recorded by weighing a HVPD kept close to the samples on which the cleaning tests were carried out without being in contact with the porous matrix. The weight loss of the blank was subtracted to the one registered for the HVPDs applied onto the tiles [31]. The ratio between the water content before and after the test gives the Absorption Index (A.I.%):

$$\text{A.I.}\% = \frac{W_{\text{Abs}} - W_{\text{Ref}}}{W_i - W_{\text{Ref}}} \times 100 \quad (3)$$

where W_{Abs} is the weight of the absorbed water, W_{Ref} is the weight of the evaporated water, W_i is the initial weight of the water in the HVPDs in contact with the travertine surface. Figure 6 shows the A.I.% as a function of the application times of the HVPDs containing the different chelators.

The weight loss undergone by the system due to the migration of the liquid fraction (water solution) into the porous structure of the stone resulted very low: around 4 % after 60 min of application for samples containing $(\text{NH}_4)_2\text{CO}_3$ and Rochelle salt and around 3 % for those with EDTA. These data confirmed the very good retentive properties of the HVPDs, even when embedded with chelators.

Optical micrographs (Fig. 7) of the sulfated travertine surfaces before (B) and after (C) the application of the HVPDs loaded with $(\text{NH}_4)_2\text{CO}_3$ 0.5 wt% (contact time 60') indicate that the system is effective in the superficial removal of the gypsum patina.

Table 1: Composition of the HVPDs used for the cleaning tests on sulfated travertine tiles.

HVPD	PVAc (wt%)	Borax (wt%)	Additive (wt%)	H ₂ O (wt%)
System A	3 %	0.75 %	Disodium EDTA	0.25 %
			NH_3	0.45 %
System B	3 %	0.75 %	$(\text{NH}_4)_2\text{CO}_3$	0.5 %
System C	4 %	1 %	Rochelle salt	1 %

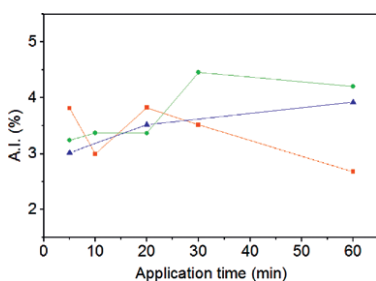


Fig. 6: Absorption Index (%) as a function of the application time for the system containing 0.25 wt% EDTA (■), 0.5 wt% $(\text{NH}_4)_2\text{CO}_3$ (●) and 1 wt% Rochelle salt (▲).

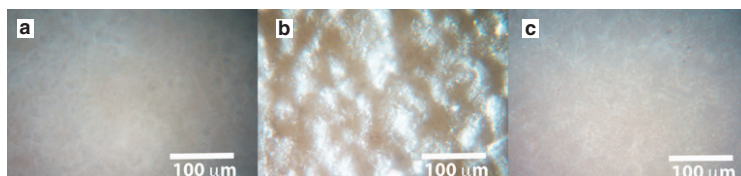


Fig. 7: Optical micrographs (20× magnification) of the travertine surface before the sulfation treatment (a), the sulfated surface before (b) and after (c) the cleaning test with the HVPD containing 0.5 wt% $(\text{NH}_4)_2\text{CO}_3$.

To quantitatively evaluate the amount of sulfates removed, IC analyses were performed and a measuring protocol for the preparation and the analyses of the samples was developed as follow.

Standard solutions for calibrations were freshly prepared in precleaned polyethylene vials by diluting a stock standard solution (1000 mg L^{-1}) purchased from Merck (Darmstadt, Germany). To take into account the matrix effect, a “blank” HVPD sample without the analyte of interest (the sulfate ion) was dissolved with HCl (37% mol), diluted 1 : 100 in MilliQ ultrapure water and added in each standard solution. The sample had previously been applied for 5 min onto a no-sulfated travertine tile, so that the standard solutions contained all the components present in the unknown samples except for the analyte of interest. Before being analyzed, the HVPD samples containing the extracted calcium sulfate dihydrate (~1 g) were solubilized with 50 μL of HCl 37% and diluted 1 : 100 using MilliQ ultrapure water. The sulfate concentration was determined from the calibration curve based on the signal intensity (μS) of the analyte. Considering that the retention time of the sulfate ion and, thus, the instrument sensitivity can slightly change due to measurement conditions or to the matrix complexity, the calibration curve was constructed for each measuring session.

Figure 8 shows the IC chromatograms of the HVPD samples embedded with EDTA after the different cleaning tests. Sulfate shows a retention time of 4.30 min while the ionic species responsible for the peak at 4.70 min could not be identified but did not represent a drawback for the reliable measurement of sulfate peak.

Sulfate peak increased with the contact time between the sulfated surface and the HVPD, whatever was the chelator supported by the system (Table 2).

As regard samples containing Rochelle salt, IC technique was not suitable for the sulfates detection. The peak at 4.35 min due to the tartrate ions significantly overlapped with the sulfate peak at around 4.15 min (Fig. 9); thus, the quantification of the sulfates extracted was affected by a big error. Then, for these samples, the sulfates concentration was determined just by ICP. In particular, as expected, IC data regarding Rochelle

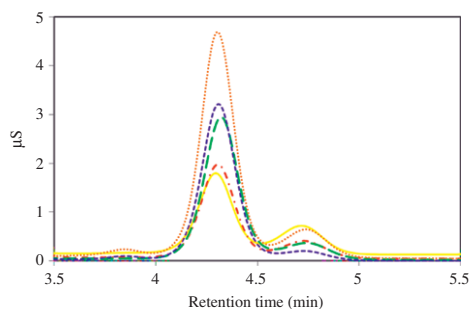


Fig. 8: IC chromatograms for the EDTA-containing samples after being applied onto the travertine tile for 5' (yellow solid), 10' (red dash-dot), 20' (green dashed), 30' (purple short dashed) and 60' (orange dotted). The peak coming from the sulfate ions is at ~4.30 min.

Table 2: IC results displaying the amount of sulfates extracted (ppm) at different contact times for the HVPD containing 0.25 wt% EDTA, 0.5 wt% $(\text{NH}_4)_2\text{CO}_3$ and 1 wt% Rochelle salt.

Contact time	EDTA		$(\text{NH}_4)_2\text{CO}_3$	
	ppm	St. dev.	ppm	St. dev.
5'	2.76	0.21	4.30	0.26
10'	3.51	0.15	5.13	0.35
20'	5.19	0.16	8.52	1.14
30'	6.03	0.30	9.55	1.30
60'	8.92	0.30	25.11	3.62

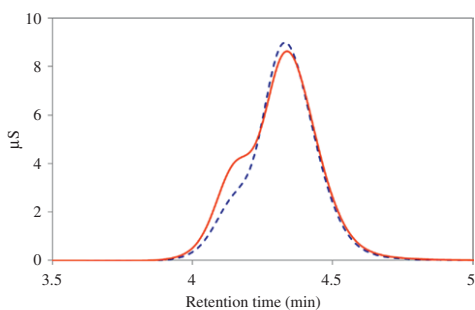


Fig. 9: IC chromatograms for the Rochelle salt-containing samples after being applied onto the travertine tile for 5' (blue dashed) and 60' (red solid). The peak coming from the sulfate ions is at ~4.15 min while the peak at 4.35 min comes from the tartrate ions.

salt-containing HVPDs were overestimated. I.e. according to ICP analyses, only 6.58% of sulfates were extracted after a 60 min-long treatment against the 21.29% calculated on the basis of IC analyses.

On the basis of the results obtained by means of IC and ICP, the percent of sulfates removed by the additives was determined and compared (Table 3) and $(\text{NH}_4)_2\text{CO}_3$ resulted the most effective for the thinning of the gypsum patina.

A more accurate quantification of the sulfates extracted by the HVPDs containing 1 wt% Rochelle salt was achieved via ICP analyses by measuring the sulfur contained in samples collected after being applied for 60', 1080' and 1380'. To make a comparison, cleaning tests of the same duration were carried out also using the HVPD with 0.5 wt% $(\text{NH}_4)_2\text{CO}_3$ (that had resulted the most performing according to the previous tests)

Table 3: Sulfates extracted per unit area (%) at different contact times for the HVPDs containing 0.25 wt% EDTA, 0.5 wt% $(\text{NH}_4)_2\text{CO}_3$ and 1 wt% Rochelle salt.

Contact time	% of sulfates removed per unit area (2.28 cm ²)	
	EDTA	$(\text{NH}_4)_2\text{CO}_3$
5'	1.91	3.04
10'	2.45	3.68
20'	3.81	6.04
30'	4.45	6.81
60'	6.67	18.43

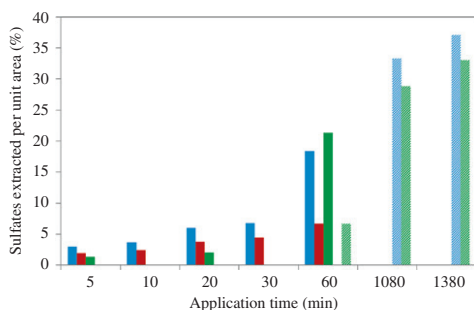


Fig. 10: Sulfates extracted per unit area (%) at different contact times based on IC (filled histograms) and ICP (striped histograms) results for the HVPD containing 0.5 wt% (NH₄)₂CO₃ (light blue), 0.25 wt% EDTA (dark red) and 1 wt% Rochelle salt (green).

and the samples were analyzed through ICP technique as well. Also for ICP analyses a measuring protocol was developed. Before being analyzed, the HVPD samples (~1 g) were solubilized with 50 μL of HCl (37%) and diluted 1:100 using MilliQ ultrapure water. A standard solution with 1000 ppm of SO₄²⁻ was used to obtain standard solutions with different SO₄²⁻ concentrations in which 100 μL of a solution containing Ge as internal standard was then added. For each sample, a triplicate measurement was carried on. The sulfur concentrations (ppb) were determined as the average in ppb recorded at two different detection wavelengths (180.669 nm and 181.972 nm). The concentration of sulfate anions SO₄²⁻ present in the diluted HVPD samples was determined from the sulfur concentration given by the instrument, based on stoichiometric calculations (assuming that the detected sulfur came exclusively from the sulfates extracted by HVPD). Considering the 1:100 dilution, the effective concentration C_e (ppm) of sulfur removed resulted from equation (4):

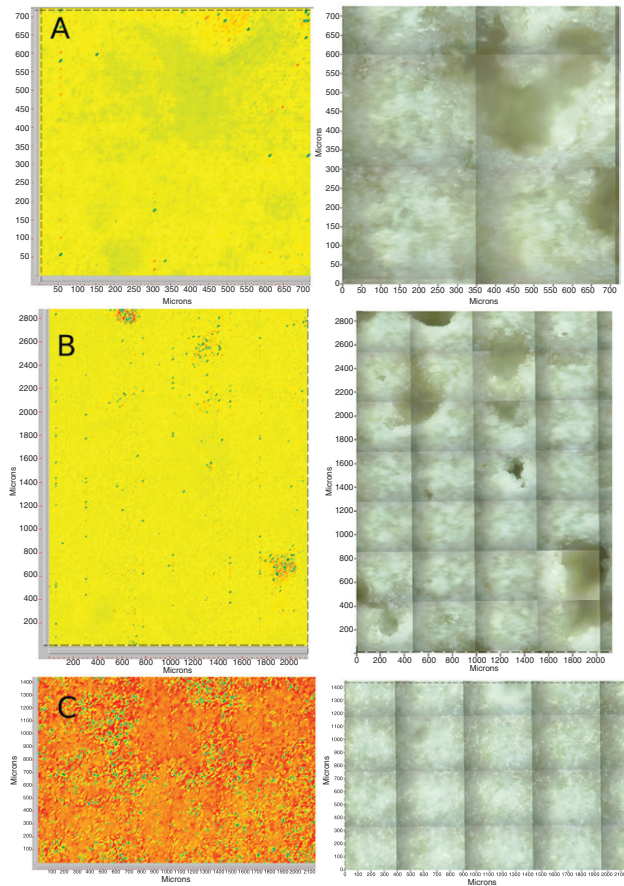
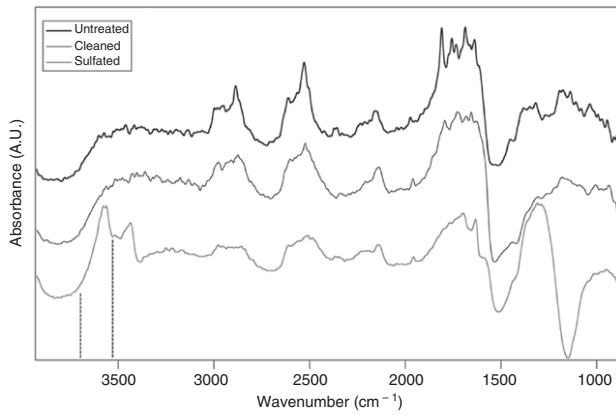
$$C_e = \frac{C_d \cdot P_i}{P_e} \cdot 100 \quad (4)$$

where P_i is the initial amount of HVPD sample used for the cleaning test (mg), C_d is the amount of sulfate anion (ppm) measured in the diluted HVPD sample, P_e is the effective amount (mg) of the HVPD sample collected after the cleaning test and actually used for the ICP analysis.

Comparing both IC and ICP analyses, the most performing additive for the extraction of gypsum still resulted (NH₄)₂CO₃, removing 37% of sulfates after an application of 1380' (Fig. 10). Regardless of the additive, the extraction power increased with the contact time. Systems containing (NH₄)₂CO₃ and Rochelle salt gave significantly better performances when applied for 60' or more.

In order to evaluate the homogeneity of the gypsum removal across the surface, 2D FTIR Imaging was carried out on travertine samples before sulfation, after sulfation, and after sulfation and application of the HVPDs loaded with (NH₄)₂CO₃ 0.5 wt% (four consecutive applications were carried out with a contact time of 60 mins each). Figure 11 shows the obtained results. The intense absorption bands in the spectrum of the sulfated travertine tile, respectively at 3572, 3437 (ν₃ and ν₁ H₂O of gypsum) [32], and 1152 cm⁻¹ (ν₃ SO₄, which looks inverted in the reflectance spectrum), are no longer clearly observable in the spectra of both the

Fig. 11: FTIR spectra of travertine tiles. The top panel shows the comparison between the Reflectance spectra of tiles that were: (i) untreated; (ii) sulfated and then cleaned with the HVPDs; (iii) sulfated. Each spectrum relates to a single pixel (5.5 × 5.5 μm²) of the corresponding 2D Imaging maps shown in the bottom panels (A–C). The intensity of the gypsum absorption at 3570 cm⁻¹ (OH stretching of water) was imaged in the chromatic maps as the area of the peak between 3692 and 3542 cm⁻¹. The chromatic scale of the maps qualitatively shows the increasing intensity of the band as follows: green < yellow < red. Beside each chromatic map, the corresponding image under visible light is shown. Map A (700 × 700 μm²): untreated travertine; Map B (2800 × 2000 μm²): travertine sulfated and then cleaned with the HVPDs; Map C (1400 × 2100 μm²): travertine sulfated.



untreated and the cleaned tiles. It must be noted that, according to the literature, the FPA detector allows enhanced sensitivity as compared to attenuated total reflection (ATR) measurements, as for instance in cases where the lowest detectable concentration of drugs passed from 0.35% (ATR) down to 0.075% (FPA) [33]. The intensity of the gypsum band at 3572 cm^{-1} (imaged as the area of the peak between 3692 and 3542 cm^{-1}) decreases dramatically upon cleaning, becoming comparable to that of untreated travertine. Namely, the gypsum peak absorbance is evenly decreased all across the surface, indicating the homogeneous removal of gypsum after the application of the HVPDs.

Conclusions

In the present work, the effectiveness of 80PVAc-borax HVPDs embedded with three different chelators (EDTA, $(\text{NH}_4)_2\text{CO}_3$ and Rochelle salt) in the removal of gypsum from a carbonatic matrix was explored.

As confirmed by the rheological measurements, upon the addition of the chelating agents the mechanical properties of the HVPDs resulted still adequate for their removal from the treated surface in one step by a simple peeling action, minimizing the potential residues. As concern the systems containing $(\text{NH}_4)_2\text{CO}_3$ or Rochelle salt, the viscoelastic behavior was invariant for chelator concentrations respectively up to 0.5 and 0.9 wt%. However, a further increase of Rochelle salt concentration to 1, wt% determined the formation of a true gel. At concentrations around 0.3 wt% and 0.9 wt%, for $(\text{NH}_4)_2\text{CO}_3$ and Rochelle salt, respectively, the addition of these salts had a structuring effect on the HVPDs as indicated by the increase of their intrinsic elasticity (G_0). For higher amounts of additive, a lowering of G_0 was recorded, indicating a reduction of the entanglements density of the PVA network.

The cleaning efficacy and the easiness of removal of the systems embedded with 0.25 wt% disodium EDTA, 0.5 wt% $(\text{NH}_4)_2\text{CO}_3$, 1 wt% Rochelle salt were tested through several applications on artificially sulfated travertine tiles: they were removed easily in one step (with the aim of plastic rings) without leaving any visible residue. Optical micrographs of the sulfated surfaces before and after the cleaning tests revealed their effectiveness in the thinning of the gypsum patina. The quantification of the sulfates extracted was achieved through IC and ICP techniques by setting up suitable measuring protocols for the pre-treatment and the analysis of samples. Regardless of the additive, the extracting power increased with the contact time between the surface and the cleaning systems, confirming their gradual, gentle action. The $(\text{NH}_4)_2\text{CO}_3$ resulted the most effective, removing 37% of sulfates after an application of 1380'.

Acknowledgments: Financial support from the University of Florence, from Consorzio Interuniversitario per lo Sviluppo dei Sistemi a Grande Interfase (CSGI), Florence, and SICAMOR Project PAR-FAS (Tuscany Region, Action Line 1.1.a.3) is gratefully acknowledged. This project has received funding from the European Union's Horizon 2020 research and innovation programme under grant agreement No 646063.

References

- [1] R. Steudel. *Angew. Chem.* **34**, 1313 (1995).
- [2] L. Borgioli. *Polimeri di sintesi per la conservazione della pietra*, Collana I Talenti, Il Prato (2002).
- [3] E. Ferroni, P. Baglioni. In *Proceedings of the Symposium on Scientific Methodologies Applied to Works of Art*, Firenze (1984), Montedison Progetto Cultura, Milano, 108 (1986).
- [4] M. Ciatti. *Appunti per un manuale di storia e di teoria del restauro. Dispense per gli studenti*, Edifir (2009).
- [5] M. Matteini, S. Scuto. *Consolidamento di manufatti lapidei con idrossido di bario*, Arkos **1** (2001).
- [6] L. Campanella, A. Casoli, M. P. Colombini, R. M. Bettolo, M. Matteini, L. M. Migneco, A. Montenero, L. Nodari, C. Piccioli, M. P. Zappalà, G. Portalone, U. Russo, M. P. Sammartino. *Chimica per l'arte*, Zanichelli Editore (2007).
- [7] P. Baglioni, E. Carretti, L. Dei, R. Giorgi. Nanotechnology in wall painting conservation, in *Self-Assembly*, B. H. Robinson (Ed.), IOS Press, Amsterdam (2003).

- [8] A. Giovagnoli, C. Meucci, M. Tabasso Laurenzi. In: *Deterioration and preservation of stones, Proceedings of the 3rd International Congress*, Venezia, October 24–27, 1979, Università degli Studi – Istituto di Chimica Industriale, Padova, 499 (1982).
- [9] M. Matteini, A. Moles, M. Oeter, I. Tosini. In: *The cleaning of architectural surfaces, Proceedings of a symposium*, Bressanone, July 3–6, 1995, Libreria Progetto, Padova, 283 (1995).
- [10] P. Fiorentino, M. Marabelli, M. Matteini, A. Moles. In *Studies in Conservation* **27**, 145 (1982).
- [11] N. Berlucchi, R. G. Corradini, R. Bonomi, E. Bemporad, M. Tisato. In: *Proceedings of the 9th International Congress on Deterioration and conservation of stone*, Venezia, 23 (2000).
- [12] G. Carbonara. *Trattato di Restauro Architettonico*, Torino (1996).
- [13] H. Burgess. *The Paper Conservator* **15**, 36 (1991).
- [14] A. Phenix, A. Burnstock. In *The Conservator* **16**, 28 (1992).
- [15] J. Heuman. In *The Conservator* **16**, 12 (1992).
- [16] I. D. MacLeod. In *Studies in conservation* **32**, 25 (1987).
- [17] L. Carlyle, J. H. Townsend, S. Hackney. In *Dirt and Pictures Separated*, United Kingdom Institute for Conservation, London, 44 (1990).
- [18] R. Wolbers. *Cleaning painted surfaces: aqueous methods*, Archetype Publications, London (2000).
- [19] Materiali tradizionali ed innovativi nella pulitura dei dipinti e delle opere policrome mobili, in: *Proceedings of Primo Congresso Internazionale – Colore e conservazione: materiali e metodi nel restauro delle opere policrome mobili*, Piazzola sul Brenta, October 25–26, 2002, Il prato (2003).
- [20] A. Onesti. *CAB newsletter* **2**, 10 (1993).
- [21] D. Stulik, V. Dorge. *Solvent gels for the cleaning of works of art: the residue question*, Getty Publications, Los Angeles, USA (2004).
- [22] E. Carretti, I. Natali, C. Matarrese, P. Bracco, R. G. Weiss, P. Baglioni, A. Salvini, L. Dei. *J. Cult. Herit.* **11**, 373 (2010).
- [23] C. Y. Chen, T. L. Yu. *Polymer* **38**, 2019 (1997).
- [24] A. Koike, N. Nemoto, T. Inoue, K. Osaki. *Macromolecules* **28**, 2339 (1995).
- [25] L. V. Angelova, P. Terech, I. Natali, L. Dei, E. Carretti, R. G. Weiss. *Langmuir* **27**, 11671 (2011).
- [26] E. Carretti, M. Bonini, L. Dei, B. H. Berrie, L. V. Angelova, P. Baglioni, R. G. Weiss. *Acc. Chem. Res.* **43**, 751 (2010).
- [27] E. Carretti, C. Matarrese, E. Fratini, P. Baglioni, L. Dei. *Soft Matter* **10**, 4443 (2014).
- [28] I. Natali, E. Carretti, L. Angelova, P. Baglioni, R. G. Weiss. L. Dei. *Langmuir* **27**, 13226 (2011).
- [29] L. Piculell, M. Egermayer. J. Sjostrom. *Langmuir* **19**, 3643 (2003).
- [30] M. Chen, R. Stephen Reid. *Can. J. of Chem.* **71**, 763 (1993).
- [31] S. Grassi, E. Carretti, P. Pecorelli, F. Iacopini, P. Baglioni, L. Dei. *J. Cult. Herit.* **8**, 119 (2007).
- [32] G. Anbalagan, S. Mukundakumari, K. Sakthi Murugesan, S. Gunasekaran. *Vibrational Spectroscopy* **50**, 226 (2009).
- [33] K. L. Andrew Chan and Sergei G. Kazarian. *Analyst* **131**, 126 (2006).

8

GOLD NANOSTRUCTURES AT A PDMS SURFACE

In this Chapter are reported the results on the two-step in situ growth of AuNPs on a PDMS surface, with enhanced bulk sensitivity.

Tunable growth of gold nanostructures at a PDMS surface to obtain plasmon rulers with enhanced optical features

Simona Scarano¹  · Chiara Berlangieri¹ · Emiliano Carretti¹ · Luigi Dei¹ · Maria Minunni¹

Received: 27 January 2017 / Accepted: 3 May 2017 / Published online: 13 May 2017
© Springer-Verlag Wien 2017

Abstract Efficient coupling of plasmonic nanomaterials to optically transparent polymers still is a challenge in order to obtain affordable, versatile, and sensitive surface plasmonic devices. The in-situ fabrication of gold and silver nanoparticles on PDMS has been reported, but the resulting bulk sensitivities (of up to 70 nm RIU⁻¹) may still be improved. The authors report that few simple modifications to the general preparation of these composites (AuNPs@PDMS) can result in substantial improvements of the optical features. A two-steps growth of AuNPs@PDMS is found to be particularly effective. It includes chemical treatment of the PDMS surface before the formation of well-exposed and densely-packed 3D conglomerates of gold spheroids with enhanced bulk sensitivity. Differently from available approaches, the structures obtained by this method display sensitivity to refractive index change of about 250 nm per RIU. This is 3.5 times higher than spherical nanoparticles prepared by similar protocols and is near the optical performance of anisotropic NPs. Due to the strong 3D character of the structures, excellent plasmon coupling is realized on PDMS surface. The authors also show that these nanocomposite substrates can be subjected to external stimuli and then exhibit red shifts or blue shifts typical of induced plasmon coupling and uncoupling. Hence, the method represents a major step forward in terms of high-

performance composite plasmonic nanomaterials for use in biosensing.

Keywords Localized surface plasmon resonance · Optical transducers · Polydimethylsiloxane · Biosensing · Nanostructures · Plasmon coupling · Bulk sensitivity

Introduction

The fabrication of plasmonic composite substrates for LSPR-based (bio)sensing has recently gained great attention, and cheap and versatile polymeric substrates such as polydimethylsiloxane (PDMS) for the in-situ growth of metal nanoparticles (mNPs) has been reported. These can be obtained by the spontaneous reduction of Au(III) or Ag(I) ions by simple immersion of cured PDMS films/blocks into metal salt solutions [1–6], without the need of additional reducing/capping agents. The formation of NPs at PDMS surface (hereafter NPs@PDMS) is attributed to residual curing agent present in the PDMS matrix after polymerization [4, 6, 7]. Gold and silver NPs formed at PDMS surface are generally spherical, with size and surface distribution depending on PDMS preparation (base monomer/curing agent ratio, η), Au(III) concentration ([Au]), and growth time. Afterward, cost and time consuming post-processing treatments such as thermal annealing and/or swelling/shrinking cycles are required to obtain final moderate refractive index sensitivity (RIS, ~ 70 nm RIU⁻¹). Until now, AuNPs@PDMS have been exploited for traditional LSPR biosensing, in which mNPs are further modified with bioreceptors (antibodies, nucleic acids *etc.*) targeting specific analytes [1–6], as well as for their direct testing upon external chemical/physical stimuli [8, 9]. The optical behavior of these substrates lead to the recording of red shifts of the NPs maximum wavelength (λ_{\max}) and/or the absorbance intensity,

Electronic supplementary material The online version of this article (doi:10.1007/s00604-017-2323-z) contains supplementary material, which is available to authorized users.

✉ Simona Scarano
simona.scarano@unifi.it

¹ Department of Chemistry Ugo Schiff and CSGI, University of Florence, via della Lastruccia 3-13, Sesto Fiorentino, 50019 Florence, Italy

proportional to the concentration of the bound analyte and dielectric constant change at the near field [10]. The LSPR signal is hence the exclusive consequence of the NPs near field perturbation due to the biorecognition event occurring within its depth (in the order of few tens of nm). In fact, mean distances among NPs obtained by basic protocols exclude the contribution of inter-particle plasmon coupling. This phenomenon occurs only when mNPs are separated by short distances (from 1 to 2.5 folds their diameter), through the overlapping of their localized fields along dimer axis [11–14]. The overlapped near fields are characterized by extremely enhanced intensity, with obvious applicative advantages [15]. Under these conditions, the progressive shift of λ_{max} and/or band intensity is observed in a distance-dependent manner. Decrease of inter-particle separation leads to red shifts and enhanced intensity, whereas if NPs are pushed apart, a blue shift is recorded with loss in extinction peak intensity [16–19]. Therefore, the optical behavior can be directly related to mNPs distances in their environment. This band shift in the LSPR of coupled NPs found its nicest expression in the so-called plasmon rulers (PRs). This fascinating and emerging class of nanometrology devices is based on the exquisite, atomic-bond-length sensitivity to distance and their transduction of signal as a simple spectrophotometric measurement [19–22].

A two-steps growth of AuNPs@PDMS is here optimized, evidencing that PDMS surface chemical cleaning before the second growth is the key step in driving the formation of well-exposed and densely-packed 3D conglomerates of spheroids at the PDMS surface. These structures achieve sensitivity to refractive index change of about 250 nm RIU^{-1} . This value results about 360% higher than spherical nanoparticles prepared with similar protocols, and near the optical performances of anisotropic NPs. Due to the strong 3D character and near field intensity of the structures, the establishment of plasmon coupling effects among AuNPs is supposed. To confirm this assumption, plasmonically coupled or not AuNPs@PDMS substrates have been directly compared in their optical response through a classic immuno-based assay as reference approach. In fact, such a design performed on non-coupled AuNPs@PDMS leads only to red-shifted spectra. The local RI increment elicited by biomolecule binding at AuNPs surface is in fact the sole event occurring at the nanoscale. Conversely, coupled NPs subjected to the same biomodification react as plasmon rulers after protein absorption. As a consequence, the biofilm formed at the resonant nanostructured surface induces plasmon uncoupling. Typically, blue-shifted spectra and band intensity decrease are observed in this case.

The results here reported represent a step forward in understanding and controlling mNPs optical properties during their in-situ synthesis @PDMS surface, and represent a valid alternative to time and cost expensive existing approaches. A

variety of applications from (bio)sensing to nanometrology can be envisaged, accounting for the design of new smart and cheap composite materials for nanophotonics. The whole AuNPs@PDMS fabrication process has been developed by modifying disposable UV-Vis cuvettes with PDMS films and then performing Au(III) reduction to NPs directly in-situ with the unique advantage of having a cheap, simple and highly stable composite substrates that can be interrogated by conventional spectrophotometry or portable spectrometers (Fig. 1).

Experimental section

Preparation of ‘plasmonic’ cuvettes

PDMS base monomer and curing agent (SYLGARD184 Silicone Elastomer kit, Dow Corning, Midland, MI, USA, <https://www.dowcorning.com>) were carefully weighted and thoroughly mixed in a weight proportion of 10:1, then degassed under vacuum for 20 min to eliminate air bubbles. Modification of UV-Vis cuvettes (Sigma-Aldrich, Milan, Italy, <https://www.sigmaaldrich.com/italy.html>) with PDMS was hence carried out as represented in Fig. S1A: a PDMS layer of $400 \pm 20 \mu\text{m}$ was obtained keeping the cuvette lying on one of the two transparent sides and by casting known weight (35 mg) of the polymer on it. Borders were delimited by paper tape to confine the polymer into the cuvette. After deposition, the cuvette was placed in oven at $80 \text{ }^\circ\text{C}$ for 20 min. The procedure was repeated to modify the second transparent side of the cuvette. After PDMS coating, cuvettes were subjected to the in-situ growth of AuNPs@PDMS by incubation of aqueous HAuCl_4 (Sigma-Aldrich, Milan, Italy, <https://www.sigmaaldrich.com/italy.html>) at different concentrations for 96 h, sealed and in the dark at room temperature. To stop the AuNPs growth, Au(III) solutions were removed and cuvettes were washed three times with MilliQ water.

AuNPs@PDMS obtained from the first growth were subjected to a second growth with Au(III) solution to obtain plasmonically coupled nanostructures. To this aim, before the second growth, cuvettes are repeatedly washed with 96% ethanol. This treatment displayed the ability to tune the growth of plasmonically coupled AuNPs on the polymer surface during the second growth step. Substrates not subjected to ethanol washings were also prepared for comparison. Finally, cuvettes were dried under nitrogen flow and stored at $4 \text{ }^\circ\text{C}$ until use. Figure 1b reports the image of frontal and side view of the cuvettes.

Optical measurements

Extinction spectra of AuNPs@PDMS were recorded by a Perkin-Elmer Lambda 900 spectrophotometer. Refractive

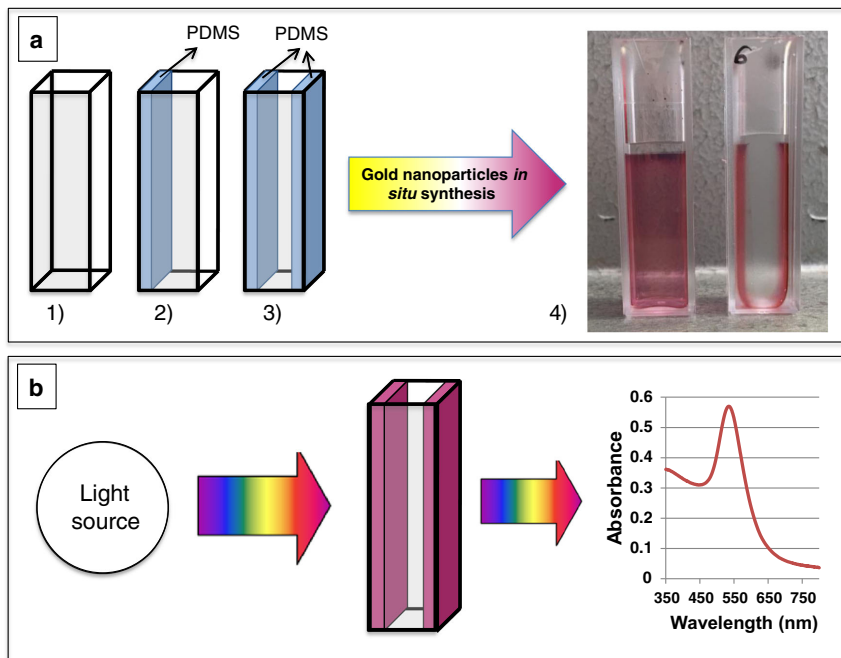


Fig. 1 **a** Sketched representation of 'photonic' cuvettes preparation. The transparent walls of disposable UV-Vis cuvettes (1) are coated with a PDMS layer (400 μm) in two steps (2–3). Then are filled with aqueous Au(III) solution at different concentrations and incubated for 96 h. Once the gold solution is removed, bright pale red color due to AuNPs

formation is clearly evident by naked eye (4). **b** Optical interrogation of 'photonic' cuvettes is finally performed by classic spectrophotometry for LSPR measurements. The two modified walls both contribute to the LSPR reading as shown in the figure

index sensitivity (RIS) of substrates was tested in water-glycerol solutions by increasing the glycerol percentage from 0% to 70% with 10% steps. Non-modified cuvettes filled with the same solutions were tested to assess possible bulk contributions and baselines subtracted accordingly, if necessary. Before measurements, the modified cuvettes were treated several times by alternating ethanol/water washings, until stabilization of the plasmon band.

Extinction spectra were collected in the range 300–700 nm, with 1 nm resolution. RIS values were inferred from maximum wavelength shift (S_{λ} , nm RIU^{-1}) and/or absorbance intensity change at fixed λ (S_{Abs} , a.u. RIU^{-1}), against refractive index unit change (RIU). $\Delta\lambda_{\text{max}}$ is the difference of the maximum absorbance wavelength (nm) recorded in glycerol solutions and water; ΔAbs is the difference of the absolute absorbance intensity (a.u.) at λ_{max} recorded under the same conditions. Δn is the corresponding variation of refractive index, i.e. $n_{\text{glycerol}(\%)} - n_{\text{water}}$. RI of deionized water was taken as 1.333.

Morphological analysis

The morphology of the substrates were investigated by Scanning electron microscopy (SEM). Images of PDMS layers modified with AuNPs were acquired by a FEI Quanta-200 ESEM at 25 kV. Mean size of AuNPs@PDMS surface were estimated by digital image analysis of SEM micrographies by ImageJ software (<https://imagej.net/>).

Bio-analytical assays

The optical behavior of the substrates was tested by an immuno-based assay. Chicken ovalbumin (100 $\mu\text{g mL}^{-1}$ OVA, Sigma-Aldrich, Italy, <https://www.sigmaaldrich.com/italy.html>) was immobilized on AuNPs via spontaneous adsorption in saline phosphate buffer (0.1 M PBS, 0.1 M NaCl), and incubated 1 h at room temperature, then thoroughly washed with the same buffer prior recording spectral responses. To assess the saturation of AuNPs after

OVA immobilization, 400 $\mu\text{g mL}^{-1}$ casein was subsequently incubated. Afterward, the binding of the specific antibody, i.e. anti-OVA IgG (Rockland Immunochemicals Inc., Tebu-bio, Milan, Italy, www.tebu-bio.com), was performed in cuvettes for 30 min, then the spectral variations were recorded in PBS. Regeneration of substrates was performed by short (2 min) washes of cuvettes with 10 mM NaOH. The regeneration step allowed the recovery of the initial λ_{max} and confirms the reversibility of the specific biorecognition.

Results and discussion.

Effect of [Au(III)] on AuNPs@PDMS bulk sensitivity

The in-situ reduction of Au(III) on PDMS generally leads to spherical NPs of different size, distribution, and penetration depth as function of the curing agent to monomer ratio (η) [1–6]. In particular, Zhang et al. [6] investigated the influence of different η values at constant Au(III) concentration (25 mM). They found that the increase of curing agent ($\eta > 0.1$) leads to the formation of bigger particles well-exposed on the surface of the polymer. However, $\eta = 0.1$ is generally reported in literature, with [Au(III)] varying only between 0.5% and 2% (25–100 mM). Under these conditions, the obtained NPs display negligible RIS. Therefore, cost and time consuming post-processing treatments such as thermal annealing and/or swelling/shrinking cycles are required. Final substrates reach however only moderate RIS around 70 nm RIU $^{-1}$, likely ascribed to the growth of partially embedded AuNPs within the polymer bulk. Starting from these findings, we explored suitable modifications of the growth strategy to enhance the bulk sensitivity of these nanocomposites. To this aim, we tuned the formation of well-exposed AuNPs displaying plasmon coupling effects at the polymer surface. This in turn allows to enhance the RIS of the substrate. Differently from literature, for all the PDMS preparations, here the Au(III) concentration was changed keeping constant the η value ($\eta = 0.1$). The curing agent/[Au(III)] ratio (η^{-1} , w mM $^{-1}$) was thus increased from 0.02 (1:50, 50 mM) up to 1 (1:1, 1 mM). Within the explored range, the substrates displayed a progressive change in color, gradually shifting from pale to purple red (Fig. 2a). Direct comparison of extinction spectra from the highest (50 mM, ‘Type I’) and the lowest (1 mM, ‘Type II’) Au(III) concentration shows a well defined peak centered at 537.5 ± 1.2 nm ($n = 6$, CV% 0.2) for Type I. This confirms fast reduction kinetics at high [Au(III)] (Fig. 2b). Contrarily, Type II is characterized by a broader and asymmetric extinction spectrum with $\lambda_{\text{max}} = 565.6 \pm 1.5$ nm ($n = 6$, CV% 0.3). This is compatible with a slower growth rate which favors the formation of larger particles. SEM images support spectra behaviors and show that substrates differ for AuNPs density on PDMS surfaces.

Therefore, gold concentration drives AuNPs growth both in terms of average particle size and distribution on the polymer surface.

Effect of PDMS thickness on AuNPs growth

PDMS thickness is also a key parameter to be taken into account: when lowered down to ~ 100 μm , the correlation between [Au(III)] and tunability of NPs is lost, and similar behaviors are obtained, despite from the initial [Au(III)]. This effect is likely related to the scarce availability of the reducing agent on the PDMS surface, which limits AuNPs growth. Spectra obtained from thin PDMS layers are characterized by a high and broad extinction band linearly increasing from red to blue wavelengths (Fig. S2). This is probably related to the observed partial loss of transparency of the modified PDMS. This additional finding indicates an important role of PDMS thickness in AuNPs@PDMS preparation.

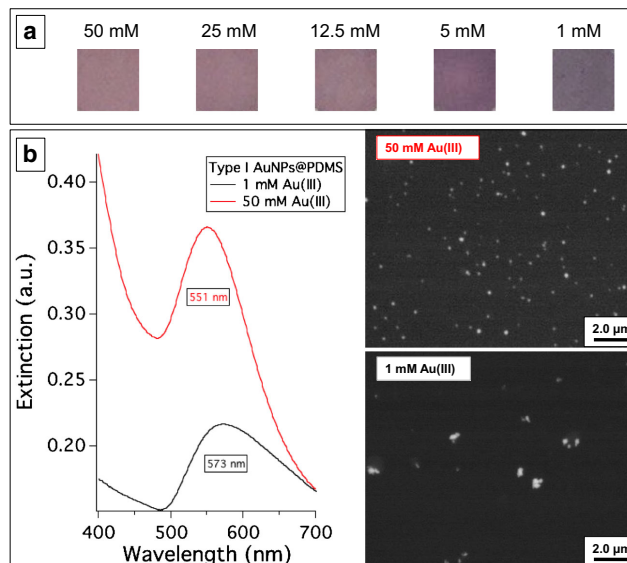
Refractive index sensitivity after the first growth

The evaluation of refractive index sensitivity (RIS) is a common and informative way to estimate the susceptibility of localized plasmons toward refractive index changes in the surrounding medium [10]. Cuvettes modified with AuNPs@PDMS were therefore tested in water at increasing glycerol content (0–70%). Type I AuNPs@PDMS displayed a marked response of absorbance intensity change at fixed λ ($S_{\text{Abs}} = 0.3170 \pm 0.0007$ a.u. RIU $^{-1}$), associated to the negligible presence of wavelength shift ($S_{\lambda} < 10$ nm RIU $^{-1}$) (Fig. S3). This behavior is sustained by the need of post-processing treatments of pristine AuNPs@PDMS (thermal annealing, plasma etching, swelling/shrinkage treatments, etc.) to enhance bulk sensitivity before their use for sensing purposes, as reported in literature [2–4, 6].

In fact, metallic NPs supported on solid substrates (e.g. glass or polymers) show a decrease of S_{λ} which is proportional to the NPs fraction volume in contact with the surface [23, 24]. Therefore, since PDMS surface is susceptible to local deformation of the polymeric network during AuNPs growth, the observed scarce S_{λ} bulk sensitivity of Type I indicates that NPs can be partially embedded into the polymer. Moreover, Au nanostructures densely distributed on solid substrates display a progressive disappearance of S_{λ} bulk sensitivity in favor of S_{Abs} . These kind of AuNPs thus express RIS prevalently by plasmon band intensity change rather than wavelength shift [25]. This is thus compatible with our morphological evaluation of Type I substrates.

On the contrary, Type II showed both absorbance intensity and maximum wavelength change. The absolute absorbance intensity of the peak at λ_{max} displayed a progressive change, well-described by an exponential fit (Fig. S4), corresponding to S_{Abs} of 0.2671 ± 0.0011 a.u. RIU $^{-1}$. The associated $\Delta\lambda_{\text{max}}$

Fig. 2 **a** digital images of color change of AuNPs@PDMS by decreasing [Au(III)] from 50 mM to 1 mM. **b** extinction spectra and SEM images of AuNP@PDMS substrates relative to AuNPs prepared from 50 mM and 1 mM Au(III) for 96 h, hereafter named Type I and II



was 12 ± 1 nm within the whole RI interval, corresponding to $S = 126 \pm 10$ nm RIU⁻¹, with a linear correlation up to 1.40 RI (Fig. 3). This value is significantly higher than those reported in literature for similar composites (< 70 nm RIU⁻¹). The achievement is probably due to the combination of the high η' value used ($\eta' = 1$, i.e. curing agent:Au(III) ratio (w/mM)) respect to other approaches [3], and a longer growth time (96 h). The latter results indicate therefore that AuNPs@PDMS of Type II samples are well exposed over the PDMS surface and suitable for (bio)sensing applications.

In both the cases, the observed trend of absorbance intensity change is negative in terms of absolute change, but corresponds to the increase of the relative plasmon peak height, as expected as consequence of the refractive index increase (Fig. S5).

Inducing plasmon coupling by second growth

AuNPs are plasmonically coupled only if the inter-particle distance is comparable to their diameters [11–14]. Therefore, we attempted the tuning of AuNPs@PDMS to obtain the formation of proximal nanostructures to enhance the bulk sensitivity and to evidence plasmon coupling. To achieve the purpose, a second growth step on both Type I and II substrates (hereafter Type I² and Type II²) was carried out. Cuvettes were subjected to ethanol washings before the addition of new Au(III) solution and its subsequent incubation. The target of ethanol treatment is the removal of residual surface curing/reducing agent after the first growth. This step is effective in obtaining different distributions of the nanostructures at

PDMS surface. In case of ethanol treatment, the second growth of AuNPs is limited by the scarce availability of the reducing agent at the surface. Therefore, substrates subjected to ethanol treatment between growths show large particles at low density (Fig. S6). Contrarily, if ethanol treatment is avoided, particles appear smaller and more homogeneously-distributed over the polymer surface. Spectra of Type I² samples (Fig. S7) confirm SEM images. In absence of ethanol treatment the plasmon peak results significantly higher and narrow, with $\lambda_{\max} = 535.3 \pm 1.1$ nm. On the contrary, when the treatment is performed the peak is lower, broad, and red-shifted to 542 nm (Fig. S7). This trend is more evident in case of Type II² substrate. The relative spectrum is well-compatible with NPs clustering, since a large red shift from 565.6 ± 1.5 to 648.3 ± 8.4 nm along with a marked absorbance intensity enhancement is observed (Fig. S8). The averaged dimensions of Au clusters have been evaluated from SEM micrographs, and image analysis supports the spectral behaviors. In particular, the estimated average size of nanostructures resulted around 120 nm and 200 nm for Type I² and Type II² respectively (Fig. S9). The substrates differ also for AuNPs density on PDMS surface and size distribution. In case of Type II² the analysis shows a wider dispersion of particle size, in accord to the prevalence of metallic clusters at the surface.

The morphological differentiation is particularly evident on Type II substrates, displaying densely-packed sub-micrometer conglomerates after ethanol treatment. This morphology is likely the result of a fine interplay between kinetics and thermodynamics of underlying nucleation and growth on the first

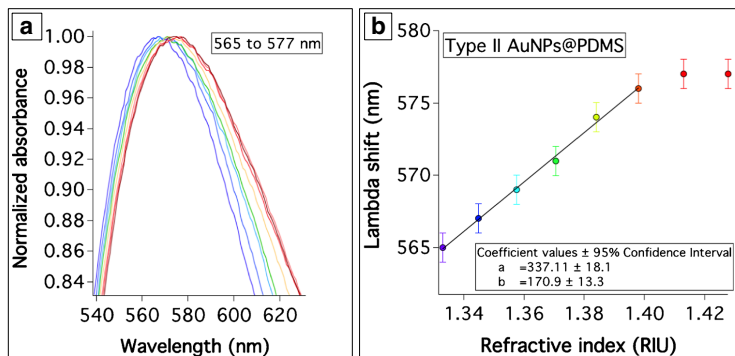


Fig. 3 a Transmission spectra recorded at different glycerol % in water (0–70%). RI sensitivity of Type II AuNPs@PDMS is evidenced as maximum wavelength red shift (S_{λ}), with an overall $\Delta\lambda_{\max} = 12$ nm. **b**

Plot of the linear correlation between $\Delta\lambda_{\max}$ and Δn , where S_{λ} is obtained as $\Delta\lambda_{\max}/\Delta n$ ratio. Standard deviations are obtained from independent measurements on the same cuvette ($n = 3$)

AuNPs generation. However, as it can be observed by Fig. 4a, NPs composing the conglomerates have roughly comparable size and shape. Therefore, we can hypothesize that the large red-shift and intensity increase observed for Type II² can be prevalently ascribed to plasmon coupling effects among proximal NPs on the surface. This is in agreement not only with NPs densely packed and well exposed toward the bulk [25], but also with the enhancing effect elicited by the near field overlapping. The RIS of both substrates has been evaluated. Type I² samples did not display RIS increase in terms of S_{λ} (Fig. S10), but only in terms of S_{Abs} , from 0.3170 to 0.3725 ± 0.0017 a.u. RIU⁻¹. Contrarily, the S_{λ} of Type II² resulted greatly improved compared to the first growth (Fig. 4b-d), whereas the associated S_{Abs} increased only from 0.2671 to 0.2887 ± 0.0032 a.u. RIU⁻¹.

In particular, within the RI change associated to the binding of the biomolecules on mNPs, NPs are characterized by an enhancement of more than 200% the initial sensitivity, i.e. 254 ± 11 nm RIU⁻¹ ($\Delta n = 1.3448$ – 1.3330 , Fig. 4d). The obtained sensitivity is also noticeably higher than those obtained by classic spherical NPs supported on solid/polymeric surfaces (~ 70 nm RIU⁻¹). In particular, it results similar to sensitivities of pre-formed nanostars immobilized on PDMS via silanization [26]. Attempts in obtaining in-situ growth of non-spherical AuNPs@PDMS are still limited [27] and deserve to be improved. Therefore, these results represent a step forward in fabricating sensitive plasmonic nanostructures without the need of post-processing treatments.

Behavior of AuNPs@PDMS as plasmon rulers

To verify that Type II² substrates support plasmon coupling among AuNPs, we directly compared the optical behavior of the two nanocomposites (Type I² and Type II²) through a classic immuno-based assay. As proof-of-principle test, we

used ovalbumin (OVA) as antigen and anti-ovalbumin antibody (anti-OVA) as specific antibody for its biorecognition. This with perspective application of the approach to the identification of egg proteins on artwork surfaces by optical biosensing, as recently reported [28]. The rationale is that such a design performed by plasmonic substrates in which coupling effects are negligible, i.e. Type I² in this case, leads only to red-shifted spectra. This effect is due to the local RI increment elicited by biomolecule binding at AuNPs surface, that is the sole event occurring at the nanoscale. Conversely, coupled NPs subjected to the same biomodification may act as plasmon rulers [16–22] after protein adsorption. This is due to the formation of a biofilm at the nanostructured surface which may cause steric hindrance, plasmon uncoupling, and related blue-shifted spectra of lower intensity. Therefore, the adsorption of OVA ($100 \mu\text{g mL}^{-1}$) on Types I² and II² AuNPs@PDMS followed by buffer washing to eliminate unbound protein is carried out. Accordingly to previous findings and considerations on Type II² substrate, a marked blue-shift from 648 nm to 605 nm occurred, whereas Type I² showed a classical (from 543 to 547 nm) red shift (Fig. 5a).

These results confirm that, depending on their own features, Type II² AuNPs@PDMS may act as stimuli-responsive nanomaterial. In particular, it can be assumed that the protein diameter (5.4 nm) is small enough to penetrate in interstitial spaces among AuNPs conglomerates and elicit mesospacing variation, evidenced by the characteristic blue shift, as sketched in Fig. 5a (right). Furthermore, the expected decrease of extinction intensity (Fig. S11) sustains the plasmon ruler behavior and is associated to inter-particle distance increase induced by protein binding. Contrarily, on Type I² OVA adsorption induces a red shift, which is well-compatible with a classical LSPR-based biosensing. This can be accounted by the absence of plasmon coupling among NPs at the surface (Fig. 5a).

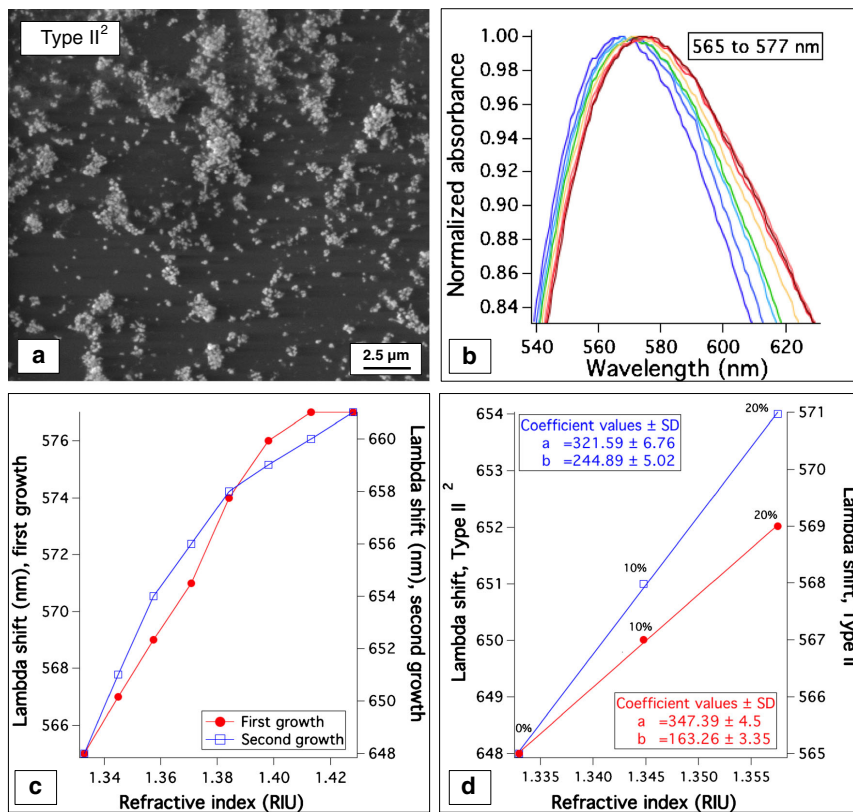


Fig. 4 **a** SEM image of Type II² AuNPs@PDMS when ethanol treatment is performed between the two growths. The 3D sub-micrometer AuNPs clusters are clearly visible at the polymer surface; **b** transmission spectra of Type II² showing λ_{\max} shift with RI increase (0–

70% glycerol); **c** comparison of λ_{\max} shifts obtained on Type II (red) and Type II² (blue) substrates; **d** Zoom in of the RIU range of interest for biomolecular interaction studies

To further sustain this assumption, anti-OVA ($1 \mu\text{g mL}^{-1}$) was incubated on the adsorbed OVA on both substrates. After a saturation step with casein and washing with buffer, the spectral response of the substrates was compared. Interestingly, the binding of the antibody is able to induce red-shifted spectra in both cases (Fig. 5b–c). In particular, the marked red shift recorded on Type II² (6 nm) is strongly informative of a classic LSPR response. It clearly indicates that the antibody prevalently binds the exposed surface of the immobilized OVA, but it does not induce further plasmon uncoupling among NPs. This finds further confirmation in the opposite variation of absorbance intensity, i.e. an intense (0.04 a.u.) increase instead of the decrease recorded during OVA immobilization (Fig. S12). The result is coherent with data elsewhere reported for bovine serum albumin binding by classic molecular

LSPR reading, in which antibody binding elicits the expected intensity increase [29, 30]. After anti-OVA binding, a brief (2 min) treatment with 10 mM NaOH is able to regenerate the biochip surface and to recover the starting wavelength and intensity recorded before anti-OVA interaction (data not shown). As expected from data obtained on its bulk sensitivity, Type II² demonstrated scarce near-field sensitivity to anti-OVA binding in terms of λ_{\max} . This result supports that AuNPs@PDMS require dedicated post-treatments to enhance the S_{λ} [2–4, 6].

As a whole, Type II² substrates display not only excellent bulk sensitivity ($>250 \text{ nm RIU}^{-1}$) respect to the available literature ($\sim 70 \text{ nm RIU}^{-1}$), but also the specialized ability in sensing mesospacing variation at the nanoscale upon external stimulus. Moreover, the specific biorecognition of the adsorbed protein can be further performed by classical

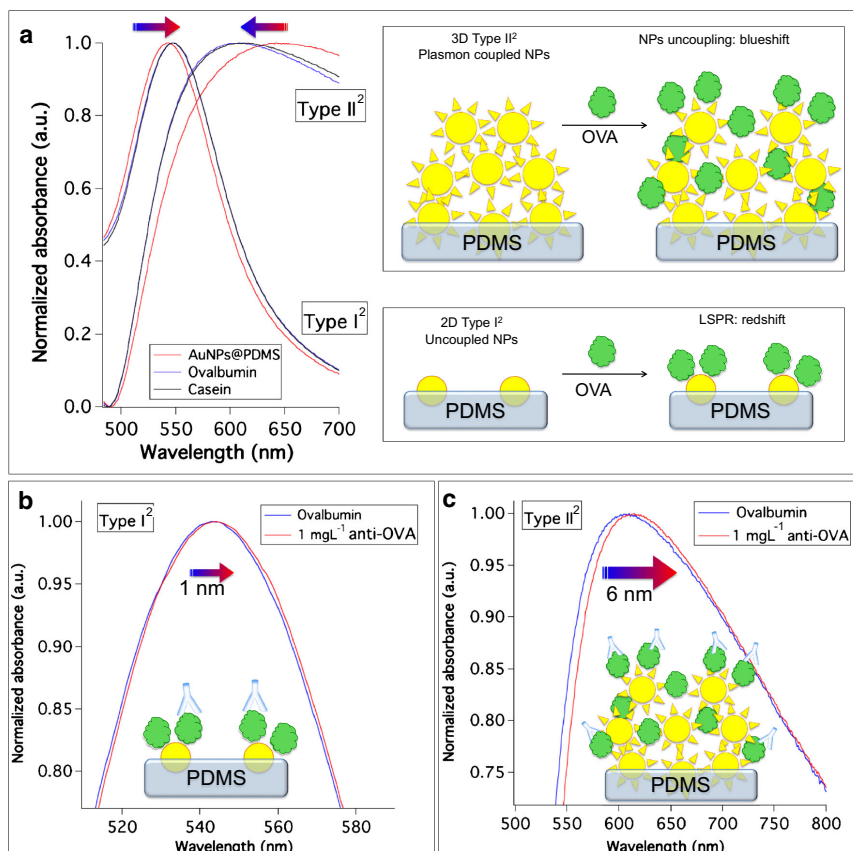


Fig. 5 **a** Spectra of Type I² and Type II², in which the opposite behavior of the two substrates is directly compared after ovalbumin (OVA) adsorption and casein saturation. Plasmonically coupled substrate, Type II², displays a marked *blue shift* whereas Type I², in which this feature is absent, shows the classical *red shift*. On the right, sketched

representations of the two different optical effects induced by OVA adsorption. **b, c** *Red shifts* induced by the specific binding of anti-OVA IgG on Type I² and Type II², respectively. In this case both substrates react with a *red shift* of the wavelength, marked for Type II² as consequence of plasmon coupling at the surface

LSPR, distinguishing the recognition step from the former by the opposite blue/red spectral shift.

Classical LSPR measurements on AuNPs immobilized on glass after their modification with Bovine serum albumin (BSA) at the same concentration give up to ~30 nm of λ_{\max} shifts at the saturation point of the sensor [29]. Therefore, as preliminary evaluation, the sensitivity of Type II² results roughly 2.5 folds higher in terms of λ_{\max} shift (80 ± 3 nm). A remarkable gain of signal is also obtained in terms of absorbance intensity change ($\Delta Abs (10^{-2}) = 4$ a.u.). This variation is about one order of magnitude higher respect to the response obtained through immuno-based albumin recognition by classical substrate preparation (pre-formed AuNPs immobilized on glass) [30].

It should be noted that the structures used in these experiments have not yet been optimized to obtain the lowest limits of detection, but already demonstrate that these substrates can display enhanced analytical performances. Moreover, they are able to differentiate molecular interactions from bulk index changes at the metallic surface.

Conclusions

Spherical AuNPs@PDMS obtained by available protocols display intrinsic RI sensitivity below 70 nm RIU^{-1} . This limits their use in LSPR-based applications at the forefront of the research. Herein we investigated the

possibility to tune and enhance the optical performance of AuNPs@PDMS composites. This goal has been pursued by avoiding long and expensive post-processing treatments, and by playing only on the synthetic route. We showed that there is room for new approaches in controlling morphology and functioning of these smart and promising stimuli-responsive materials. The intriguing finding is that low Au(III) concentration (1 mM) coupled to an extended growth time (96 h) is a key strategy to favor the growth of large and well-exposed spherical AuNPs with improved sensitivity ($>120 \text{ nm RIU}^{-1}$). The use of high (50 mM) or low (1 mM) Au(III) concentration deeply influences the RIS observed. In the first case, a predominant absorbance-dominated RIS is obtained, whereas low Au(III) availability produces larger nanostructures dominated by scattering phenomena. The flexibility and the partial permeability of PDMS to Au(III) gold solution during NPs growth has to be taken into account. In fact, high [Au(III)] induces the growth of AuNPs with scarce RIS, as also reported by other authors. The reproducibility and the stability of the substrates strongly depend on their preparation, e.g. PDMS thickness and batch-to-batch variation of Au(III) solutions. The removal of the reducing agent at the PDMS surface can strongly modulate the morphology of the new generation of AuNPs during a second growth step. In particular, it triggers the appearance of well-exposed 3D conglomerates characterized by a strong enhancement of the bulk sensitivity ($>250 \text{ nm RIU}^{-1}$) due to plasmon coupling effects at the surface. The molecular sensitivity of these substrates results significantly enhanced compared to classical AuNPs immobilized on glass substrates, both in terms of wavelength and absorbance shift.

These nanocomposite materials represent therefore a fruitful direction accounting for the design of new smart substrates to be applied to (bio)sensing. Further work can be done in the direction of controlling morphology and function of these promising stimuli-responsive materials, to obtain the controlled in-situ growth of anisotropic NPs expressing different spectral fingerprints to be used in microarray format. We foresee the rational use of these substrates as plasmon rulers for nanometrology, an exciting and emerging topic of broad interest in different fields. Plasmon rulers represent a challenging tool to achieve the precise measurement of distance variations, down to few tens of Ångströms, by exploiting the plasmon coupling/uncoupling dynamics.

Acknowledgements The authors thank the Ministry of Education, University and Research (MIUR) for the scientific program SIR2014 Scientific Independence of young Researchers (RBSI1455LK).

Compliance with ethical standards The author(s) declare that they have no competing interests.

References

- Dunklin JR, Forcherio GT, Berry KR Jr, Roper DK (2013) Asymmetric reduction of gold nanoparticles into Thermoplasmonic polydimethylsiloxane thin films. *ACS Appl Mater Interfaces* 5:8457–8466. doi:10.1021/am4018785
- Ozhikandathil J, Badilescu S, Packirisamy M (2012) Gold nanostructure-integrated silica-on-silicon waveguide for the detection of antibiotics. In milk and milk products. Proceedings of SPIE, photonics north conference, 800707
- Sad Abadi H, Badilescu S, Packirisamy M, Wüthrich R (2012) PDMS-gold nanocomposite platforms with enhanced sensing properties. *J Biomed Nanotechnol* 8:539–549. doi:10.1166/jbn.2012.1418
- Sad Abadi H, Badilescu S, Packirisamy M, Wüthrich R (2013) Integration of gold nanoparticles in PDMS microfluidics for lab-on-a-chip plasmonic biosensing of growth hormones. *Biosens Bioelectron* 44:77–84. doi:10.1016/j.bios.2013.01.016
- Wu WY, Bian ZP, Wang W, Zhu JJ (2010) PDMS gold nanoparticle composite film-based silver enhanced colorimetric detection of cardiac troponin. *Sens Actuatur B-Chem* 147:298–303. doi:10.1016/j.snb.2010.03.027
- Zhang Q, Xu JJ, Liu Y, Chen HY (2008) In-situ synthesis of poly(dimethylsiloxane)-gold nanoparticles composite films and its application in microfluidic systems. *Lab Chip* 8:352–357. doi:10.1039/b716295m
- Goyal A, Kumar A, Patra PK, Mahendra S, Tabatabaei S, Alvarez PJJ, John G, Ajayan PM (2009) In situ synthesis of metal nanoparticle embedded free standing multifunctional PDMS films. *Macromol. Rapid Commun* 30:1116–1122. doi:10.1002/marc.200900174
- Li X, Gao Y, Serpe M (2016) Stimuli-responsive polymers and their applications. *Gels* 2:8–28. doi:10.1039/C6PY01585A
- Cataldi U, Caputo R, Kurylyak Y, Klein G, Chekini M, Umeton C, Bürgi T (2014) Growing gold nanoparticles on a Flexible substrate to enable simple mechanical control of their Plasmonic coupling. *J Mater Chem C* 37:7927–7933. doi:10.1039/C4TC01607F
- Szunerits S, Boukherroub R (2012) Sensing using localised surface Plasmon resonance sensors. *Chem Commun* 48:8999–9010. doi:10.1039/C2CC33266C
- Maier SA, Brongersma ML, Kik PG, Atwater HA (2002) Observation of near-field coupling in metal nanoparticle chains using far-field polarization spectroscopy. *Phys. Rev. B: Condens. Matter Mater. Phys* 65:193408. doi:10.1103/PhysRevB.65.193408
- Rechberger W, Hohenau A, Leitner A, Krenn JR, Lamprecht B, Aussenegg FR (2003) Optical properties of two interacting gold nanoparticles. *Opt Commun* 220:137–141. doi:10.1016/S0030-4018(03)01357-9
- Nordlander P, Oubre C, Prodan E, Li K, Stockman MI (2004) Plasmon hybridization in nanoparticle dimers. *Nano Lett* 4:899–903. doi:10.1021/nl049681c
- Su KH, Wei QH, Zhang X, Mock JJ, Smith DR, Schultz S (2003) Interparticle coupling effects on Plasmon resonances of Nanogold particles. *Nano Lett* 3:1087–1090. doi:10.1021/nl034197f
- Guo L, Jackman JA, Yang HH, Chen P, Cho NJ, Kim DH (2015) Strategies for enhancing the sensitivity of Plasmonic nanosensors. *Nano Today* 10:213–239. doi:10.2217/ntnm.09.48
- Sönnichsen C, Reinhard BM, Liphardt J, Alivisatos AP (2005) A molecular ruler based on Plasmon coupling of single gold and silver nanoparticles. *Nat Biotechnol* 23:741–745. doi:10.1038/nbt1100
- Jiang N, Ruan Q, Qin F, Wang J, Lin HQ (2015) Switching Plasmon coupling through the formation of dimers from polyaniline-coated gold Nanospheres. *Nano* 7:12516–12526. doi:10.1039/C5NR02619

18. Mahmoud MA (2015) Polarized Optomechanical response of silver Nanodisc monolayers on an elastic substrate induced by stretching. *J Phys Chem C* 119:19359–19366. doi:10.1021/acs.jpcc.5b05359
19. Mahmoud MA (2016) Silver Nanodisk monolayers with surface coverage gradients for use as optical rulers and protractors. *Langmuir* 32:11631–11638. doi:10.1021/acs.langmuir.6b03211
20. Hill RT, Mock JJ, Hucknall A, Wolter SD, Jokerst NM, Smith DR, Chilkoti A (2012) Plasmon ruler with angstrom length resolution. *ACS Nano* 6:9237–9246. doi:10.1021/nn3035809
21. Chen T, Hong Y, Reinhard BM (2015) Probing DNA stiffness through optical fluctuation analysis of Plasmon rulers. *Nano Lett* 15:5349–5357. doi:10.1021/acs.nanolett.5b01725
22. Lee SE, Chen Q, Bhat R, Petkiewicz S, Smith JM, Ferry VE, Correia AL, Alivisatos P, Bissell MJ (2015) Reversible aptamer-*au* Plasmon rulers for secreted single molecules. *Nano Lett* 15:4564–4570. doi:10.1021/acs.nanolett.5b01161
23. Martinsson E, Shahjamali MM, Large N, Zraee N, Zhou Y, Schatz GC, Mirkin CA, Aili D (2016) Influence of surfactant bilayers on the refractive index sensitivity and catalytic properties of anisotropic gold nanoparticles. *Small* 12:330–342. doi:10.1002/sml.201502449
24. Martinsson E, Otte MA, Shahjamali MM, Sepulveda B, Aili D (2014) Substrate effect on the refractive index sensitivity of silver nanoparticles. *J Phys Chem C* 118:24680–24687. doi:10.1021/jp5084086
25. Tesler AB, Chuntunov L, Karakouz T, Bendikov TA, Haran G, Vaskevich A, Rubinstein I (2011) Tunable localized plasmon transducers prepared by thermal dewetting of percolated evaporated gold films. *J Phys Chem C* 115:24642–24652. doi:10.1021/jp209114j
26. Shiohara A, Langer J, Polavarapu L, Liz-Marzán LM (2014) Solution processed polydimethylsiloxane/gold Nanostar Flexible substrates for plasmonic sensing. *Nano* 6:9817–9823. doi:10.1039/c4nr02648a
27. Chekini M, Cataldi U, Maroni P, Guénée L, Černý R, Bürgi T (2015) Preparation of anisotropic and oriented particles on a Flexible substrate. *Langmuir* 31:13221–13229. doi:10.1021/acs.langmuir.5b03524
28. Scarano S, Carretti E, Dei L, Baglioni P, Minunni M (2016) Coupling non invasive and fast sampling of proteins from work of art surfaces to surface Plasmon resonance Biosensing: differential and simultaneous detection of egg components for cultural heritage diagnosis and conservation. *Biosens Bioelectron* 85:83–89. doi:10.1016/j.bios.2016.04.093
29. Jia K, Khaywah MY, Li Y, Bijeon JL, Adam PM, Déturche R, Guelorget B, François M, Louarn G, Ionescu RE (2013) Strong improvements of localized surface plasmon resonance sensitivity by using *au/ag* bimetallic nanostructures modified with polydopamine films. *ACS Appl Mater Interfaces* 6:219–227. doi:10.1021/am403943q
30. Fujiwara K, Watarai H, Itoh H, Nakahama E, Ogawa N (2006) Measurement of antibody binding to protein immobilized on gold nanoparticles by localized surface plasmon spectroscopy. *Anal Bioanal Chem* 386:639–644. doi:10.1007/s00216-006-0559-2

Supplementary material

Tunable growth of gold nanostructures at a PDMS surface to obtain plasmon rulers with enhanced optical features

*Simona Scarano^{*a}, Chiara Berlangieri^a, Emiliano Carretti^a, Luigi Dei^a and Maria Minunni^a*

^aDepartment of Chemistry 'Ugo Schiff' and CSGI, University of Florence, via della Lastruccia 3-13, Sesto Fiorentino, 50019, Firenze, Italy.

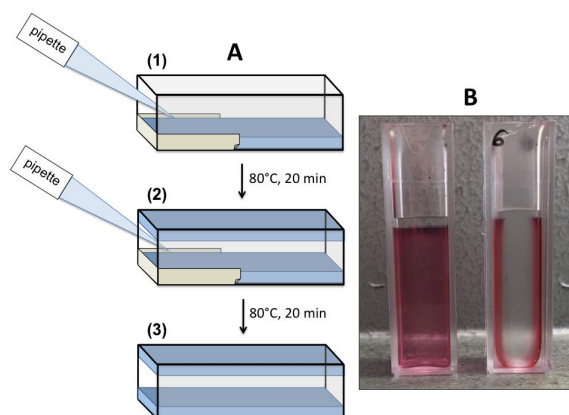


Figure S1. A: Sketched preparation of PDMS layers in polystyrene cuvettes. After polymerization in oven, the tape was removed and the cuvette is ready to be modified with gold nanoparticles (3). On the right, B, the obtained AuNPs@PDMS, frontal and lateral view.

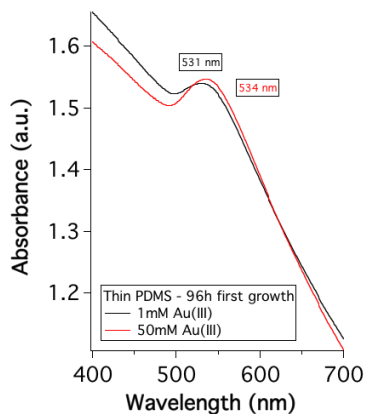


Figure S2. Extinction spectra relative to thin (130 μm) PDMS after AuNPs growth at 1 mM and 50 mM Au(III) for 96 hours and recorded in deionized water.

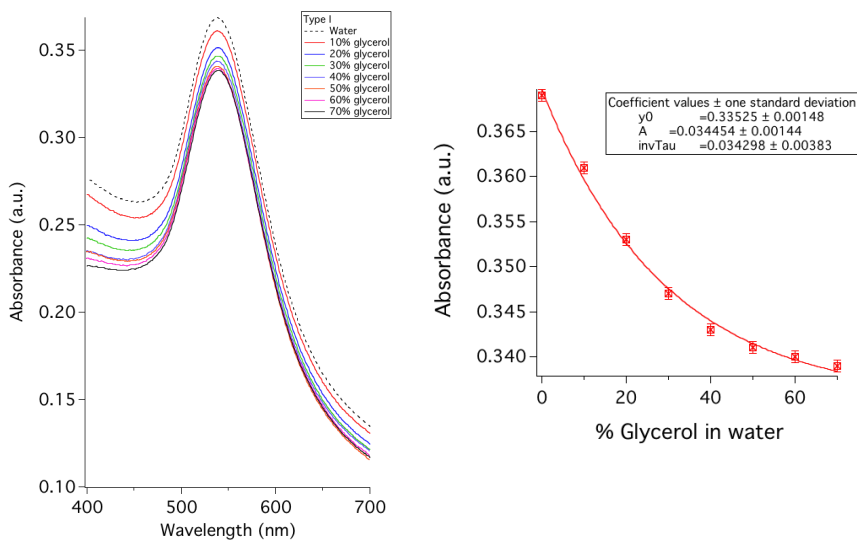


Figure S3. On the left, bulk sensitivity test carried out on Type I AuNPs@PDMS grown with 50 mM Au(III) for 96 hours. On the right, absolute absorbance change at λ_{max} is reported as function of the refractive index change (S_{Abs}). Standard deviations are obtained from independent measurements on the same cuvette ($n=3$) to evaluate the stability of plasmonic source.

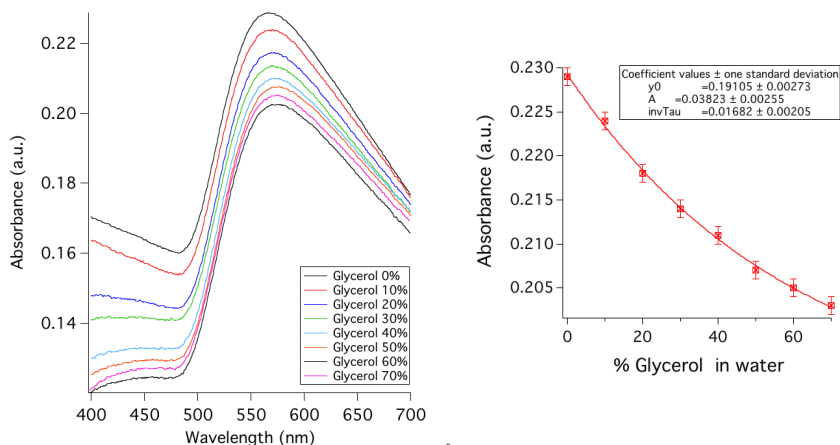


Figure S4. On the left, bulk sensitivity test on Type II AuNPs@PDMS (subtracted respect unmodified cuvette in the same solution). On the right, the absolute absorbance change at λ_{max} is reported as function of the refractive index change (S_{Abs}). Standard deviations are obtained from independent measurements on the same cuvette ($n=3$) to evaluate the stability of the plasmonic source.

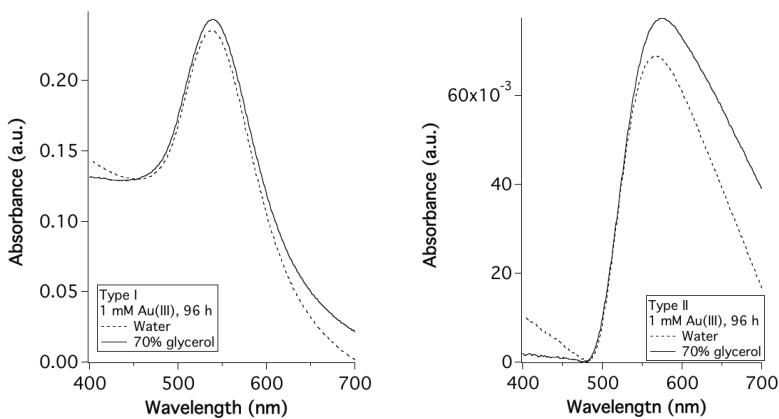


Figure S5. Absorbance spectra of Type I (left) and Type II (right) substrates are overlapped at the left baseline of the plasmon bands to evidence the peak height increase with RI change. Y-axis are arbitrary shifted to better visualize the results.

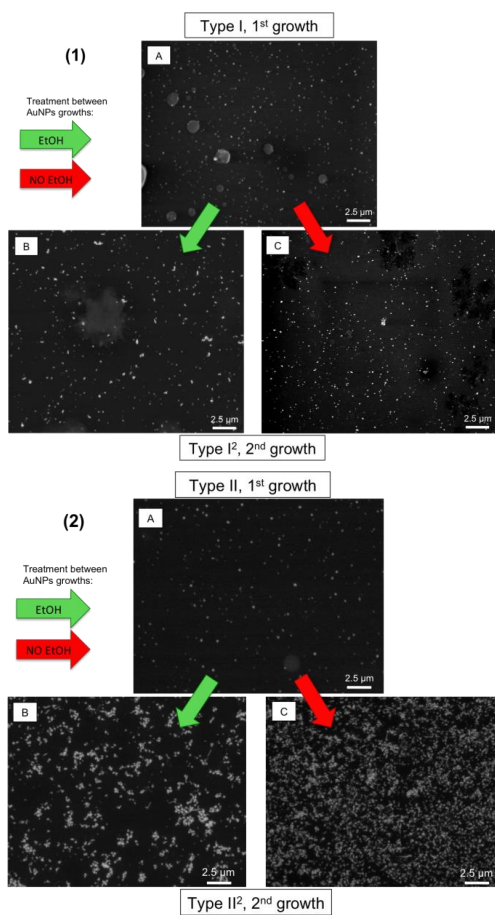


Figure S6. Effect of ethanol treatment between the first and the second growth on Type I and Type II substrates. On the left (1) SEM images relative to Type I (A) and Type I² (B,C) are reported. On the right (2), the same comparison is reported for Type II substrate (A) and Type II² substrates (B,C).

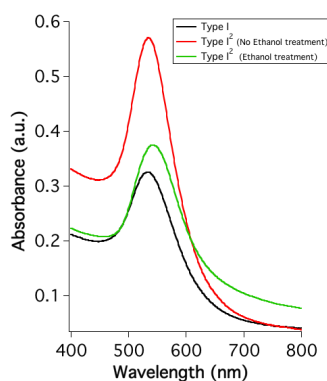


Fig. S7. Spectral behavior of Type I substrate subjected to the second growth with (green) or without (red) ethanol treatment.

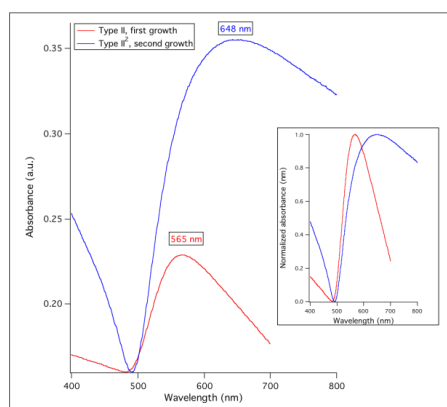


Figure S8. Extinction spectra comparing the first (Type II) and the second (Type II²) growth of AuNPs@PDMS by performing the ethanol treatment between growths. The onset plot shows normalized spectra to evidence the large red-shift (83 nm) occurred between the two growth steps. Absorbance spectra are overlapped at the left baseline of the plasmon bands to evidence the peak height relative increase with RI change. Y-axis are arbitrary shifted to better visualize the results.

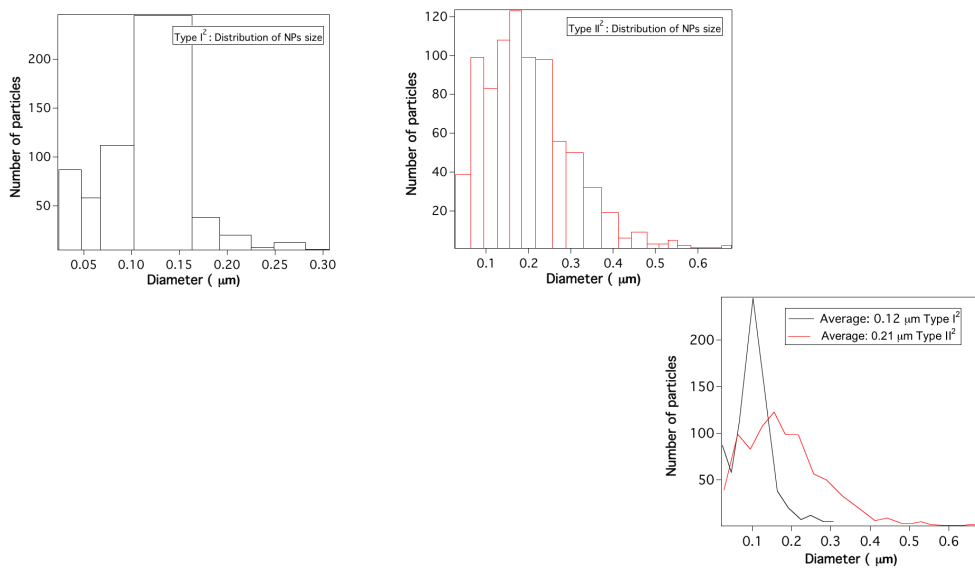


Figure S9. Size distribution analysis of Type I² and Type II² substrates. From left to right: Type I² substrate displays a prevalent population of AuNP@PDMS with a narrow distribution within 0.10 and 0.15 µm; Type II² shows a significantly broader the mean size and its distribution (0.1-0.4 µm), well compatible with the 3D sub-micrometer clusters observed by SEM analysis.

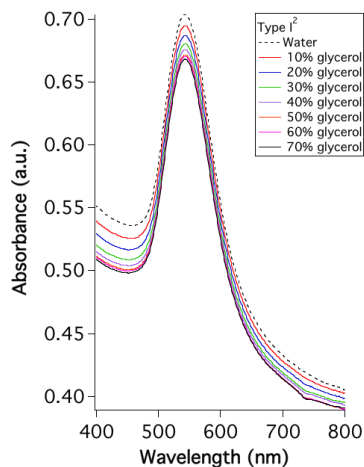


Figure S10. Bulk sensitivity test carried out on Type I² AuNPs@PDMS, from which can be inferred that the S_λ of this substrate is negligible (< 1 nm over the tested range of RI change).

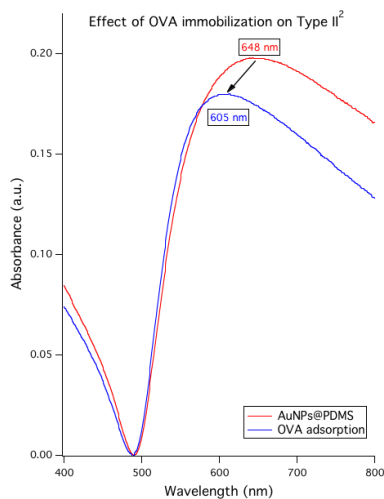


Figure S11. Absolute absorbance decrease of the plasmon peak due to OVA adsorption on Type II² substrate. This effect is related to mesosporing increase among Au nanostructures at PDMS surface, typical of plasmon rulers.

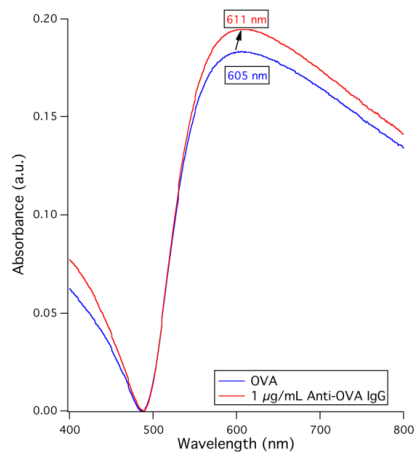


Figure S12. Absorbance increase of the plasmon peak due to anti-OVA specific binding on Type Π^2 substrate modified with OVA.

Part IV

CONCLUSIONS

9

CONCLUSIONS

Advancement in new technologies offers more and more opportunities for improvements in all research fields. The aim of this project was to study, from different points of view, the potentiality of new technologies in the field of the diagnostic, restoration and conservation of cultural heritage.

In particular, among the restoration procedures, cleaning of works of art surfaces is considered one of the most critical and delicate step. In this perspective, efficacy, high selectivity, controllable action and low toxicity are fundamental features that a system should have to allow an efficient and harmless cleaning performance. Moreover, the assessment of a cleaning treatment is very crucial in order to achieve even more advantages and to investigate the critical issues connected with a particular situation.

As a matter of facts, the use of neat solvents in cleaning procedures is nowadays considered potentially harmful, mainly because of the lack in control of solvent penetration and spreading on artistic substrates and the scarce selectivity. Colloids and Surface research played a crucial role in the development of new materials for the cleaning. Among them, in this work we focused on gels and gel-like systems as polymer matrixes for the confinement of water or other liquid solvents. The use of confining systems allows a controlled release of cleaning agents onto the artifact surface, leading to more selective and controlled treatments. In this work we studied water-based systems containing hydroxypropyl guar (HPG) crosslinked by borax and we investigated the viscoelastic and dynamic features that can be tuned by changing the components amount. In particular we deeper investigated systems behavior after the addition of glycerol, focusing on its effect on systems viscoelastic properties and structure, connected to its role in the network formation.

The characterization and the preliminary applicative test for the removal of a dark patina from a stucco decoration belonging to La Fenice theatre (Venice) suggest that these systems have a great potential in the field of restoration, due to their viscoelastic properties and the capability to upload organic solvents. In particular, the viscoelastic behavior allows a good handling of the system and at the same time a good adhesion onto the surface to be treated. In addition, the elasticity of this material determines a well peelability from the surface after the treatment.

Among the advantages originated from the use of gel and gel-like systems in cleaning, there is the capability to upload a large variety of cleaning agents. The second topic of this dissertation regards the application of previously developed HVPD containing PVAc crosslinked by borax, embedded with three different chelating agents, for the removal of a gypsum patina from an artificially sulfated travertine tiles. The viscoelastic properties of HVPD containing different amounts of chelator were investigated to study how the additive influence their elastic response. The efficacy of the cleaning treatments was assessed thanks to the set-up of an analytical protocol for the pre-treatment and the analysis of HVPD samples collected after the cleaning tests. Indeed, in order to determine the sulfate amount removed, HVPD samples collected after the cleaning tests were analyzed through Ion Chromatography and Inductively Coupled Plasma techniques, allowing the quantification of the gypsum extracted.

The assessment of a cleaning treatment is very crucial in order to achieve even more improvements in the cleaning efficacy and to investigate the critical issues connected with a particular situation. This study highlighted how analytical technologies associated with innovative cleaning systems can help in the development of a secure restoration performance. At the same time, the development of a sample preparation protocol for IC and ICP analysis can be a very interesting input to study also different situations connected to the use of HVPD in conservation.

Among analytical technologies recently developed, SPR and LSPR spectroscopies potential is still little exploited in the field of preservation and restoration of cultural heritage. During the last decade biotechnological applications to artwork preservation have been introduced with promising prediction of future innovations. In particular, the third topic of the present work takes as a starting point a recent work, which involved CSGI research group, in which the union between LSPR and gel technologies in the field of cultural heritage resulted very promising [6]. In this work, a LSPR biosensor based on a classical immuno assay was used to distinguish albumen and yolk collected from a painted surface by using HVPD based on PVA and borax.

The application of the HVPD was performed in order to remove a superficial protective layer, mainly made by albumen in this case of study. The intriguing scope was to determine when the cleaning action has to be stopped: the critical point is determined when the biosensor registered the presence of yolk, which was used as binder in the paint layer.

The aim of our work was to obtain devices easier to use, versatile and sensitive at the same time, with a perspective of a possible use even in the field of cultural heritage. We focused on the study of plasmonic composite substrates for LSPR sensing, using PDMS as a cheap and versatile polymeric substrate for the in-situ growth of Au nanoparticles (AuNPs). Indeed, the fabrication process was performed by modifying disposable UV-Vis cuvettes with a PDMS film and performing the in-situ growth of AuNPs, obtaining the interesting advantage of a stable device whose LSPR signal can be investigated by conventional or portable spectrophotometers.

The main outcome is that low Au(III) concentration (1 mM) coupled to an extended growth time determine the growth of large and well-exposed spherical AuNPs with improved sensitivity, in particular by using a double growth approach, preceded by the removal of the reducing agent at the PDMS surface. In particular, it allows the formation of well-exposed 3D conglomerates characterized by a strong enhancement of the bulk sensitivity due to plasmon coupling effects at the surface. In addition, we used a classical immuno-based assay for the biorecognition of ovalbumin.

The promising performances of these devices suggest their interesting potential both in the field of (bio)sensing and in the field of cultural heritage. In the last one, they could be used as portable innovative tools for controlling the progress of a cleaning action, but also for the detection of specific compounds on an artistic surface, thanks to the combination with the gel technology.

10

BIBLIOGRAPHY

- [1] P. Baglioni and D. Chelazzi. *Nanotechnology for the conservation of works of art*. London: RSC Publishing, 2013.
- [2] P. Baglioni, D. Berti, M. Bonini, E. Carretti, L. Dei, E. Fratini, and R. Giorgi. “Micelle, microemulsions, and gels for the conservation of cultural heritage”. In: *Advances in Colloid and Interface Science* 205 (2014), pp. 361–371.
- [3] P. Baglioni, D. Chelazzi, and R. Giorgi. *Nanotechnologies in the Conservation of Cultural Heritage*. Springer Netherlands, 2015.
- [4] K. M. Mayer and J. H. Hafner. “Localized Surface Plasmon Resonance Sensors”. In: *Chemical Reviews* 111.6 (June 2011), pp. 3828–3857.
- [5] C.-S. Cheng, Y.-Q. Chen, and C.-J. Lu. “Organic vapour sensing using localized surface plasmon resonance spectrum of metallic nanoparticles self assemble monolayer”. In: *Talanta* 73.2 (Sept. 2007), pp. 358–365.
- [6] S. Scarano, E. Carretti, L. Dei, P. Baglioni, and M. Minunni. “Coupling non invasive and fast sampling of proteins from work of art surfaces to surface plasmon resonance biosensing: Differential and simultaneous detection of egg components for cultural heritage diagnosis and conservation”. In: *Biosensors and Bioelectronics* 85 (Nov. 2016), pp. 83–89.
- [7] D. Jordan Lloyd. *Colloid Chemistry*. Vol. 1. The Chemical Catalog Co.: New York: J. Alexander, 1926.
- [8] C. Brinker and G. Scherer. *Sol-Gel Science: The Physics and Chemistry of Sol-Gel Processing*. Gulf Professional Publishing, 1990.
- [9] J. V. Alemán, A. V. Chadwick, J. He, M. Hess, K. Horie, R. G. Jones, P. Kratochvíl, I. Meisel, I. Mita, G. Moad, S. Penczek, and R. F. T. Stepto. “Definitions of terms relating to the structure and processing of sols, gels, networks, and inorganic-organic hybrid materials (IUPAC Recommendations 2007)”. In: *Pure and Applied Chemistry* 79.10 (Jan. 2007).

- [10] S. S. Büchler, G. Kummerlöwe, and B. Luy. “Naturally occurring biodegradable polymers as the basis of chiral gels for the distinction of enantiomers by partially oriented NMR spectroscopy”. In: *The International Journal of Artificial Organs* 34.2 (2011), pp. 134–138.
- [11] R. Cheng, J. Liu, P. Xie, Y. Wu, and J. Deng. “Chiral, pH-sensitive polyacrylamide hydrogels: Preparation and enantio-differentiating release ability”. In: *Polymer* 68.Supplement C (June 2015), pp. 246–252.
- [12] Y. Shin, J. Liu, J. H. Chang, and G. J. Exarhos. “Sustained drug release on temperature-responsive poly(N-isopropylacrylamide)-integrated hydroxyapatite”. In: *Chemical Communications* 0.16 (July 2002), pp. 1718–1719.
- [13] D. Geisthardt and J. Kruppa. “Polyacrylamide gel electrophoresis: reaction of acrylamide at alkaline pH with buffer components and proteins”. In: *Anal. Biochem.* 160.1 (1987), pp. 184–191.
- [14] S. B. Ross-Murphy. “Physical Gelation of Synthetic and Biological Macromolecules”. In: *Polymer Gels*. Springer, Boston, MA, 1991, pp. 21–39.
- [15] R. Wolbers. “Workshop on New Methods in the Cleaning of Paintings and other Decorative Surfaces”. In: Marina del Rey, California, USA, 1990, pp. 188–210.
- [16] G. Pizzorusso, E. Fratini, J. Eiblmeier, R. Giorgi, D. Chelazzi, A. Chevalier, and P. Baglioni. “Physicochemical Characterization of Acrylamide-Bisacrylamide Hydrogels and Their Application for the Conservation of Easel Paintings”. In: *Langmuir* 28.8 (Feb. 2012), pp. 3952–3961.
- [17] O. Wichterle and D. Lim. “Hydrophilic Gels for Biological Use”. In: *Nature* 185 (Jan. 1960), pp. 117–118.
- [18] H. A. Barnes, J. Hutton, and K. Walters. *An Introduction to Rheology*. Elsevier, 1993.
- [19] J. D. Ferry. *Viscoelastic Properties of Polymers*. New York: Wiley, 1980.
- [20] I. Natali, E. Carretti, L. Angelova, P. Baglioni, R. G. Weiss, and L. Dei. “Structural and mechanical properties of “peelable” organoaqueous dispersions with partially hydrolyzed poly(vinyl acetate)-borate networks: Applications to cleaning painted surfaces”. In: *Langmuir* 27 (2011), pp. 13226–13235.
- [21] K. Almdal, J. Dyre, S. Hvidt, and O. Kramer. “Towards a phenomenological definition of the term ‘gel’”. In: *Polymer Gels and Networks* 1 (1993), pp. 5–17.
- [22] J. Rouquerol, D. Avnir, C. W. Fairbridge, D. H. Everett, J. M. Haynes, N. Pernicone, J. D. F. Ramsay, K. S. W. Sing, and K. K. Unger. “Recommendations for the characterization of porous solids (Technical Report)”. In: *Pure and Applied Chemistry* 66.8 (1994), pp. 1739–1758.

-
- [23] P. De Gennes. *Scaling concepts in polymer physics*. New York: Cornell University Press, Ithaca, 1979.
- [24] P. Baglioni and D. Chelazzi, eds. *Nanoscience for the Conservation of Works of Art*. Cambridge: Royal Society of Chemistry, 2013.
- [25] A. Casoli, Z. Di Diego, and C. Isca. "Cleaning painted surfaces: evaluation of leaching phenomenon induced by solvents applied for the removal of gel residues". In: *Environmental Science and Pollution Research* 21.23 (Dec. 2014), pp. 13252–13263.
- [26] R. Wolbers. *Cleaning Painted Surfaces: Aqueous Methods*. Archetype, London, 2000.
- [27] A. Burnstock and T. Kieslich. "A study of the clearance of solvent gels used for varnish removal from paintings". In: Scotland: James & James, London, 1996, pp. 253–262.
- [28] D. Stulik. *Solvent Gels for the Cleaning of Works of Art: The Residue Question*. Getty Publications, 2004.
- [29] E. Campani, A. Casoli, P. Cremonesi, I. Sacconi, and E. Signorini. *L'uso di agarosio e agar per la preparazione di "gel rigidi" - Use of agarose and agar for preparing "rigid gels"*. Il Prato, 2007.
- [30] S. Iannuccelli and S. Sotgiu. *Wet treatment of works of art on paper with rigid gellan gums*. Book Paper Group Annu, 2010.
- [31] D. Gulotta, D. Saviello, F. Gherardi, L. Toniolo, M. Anzani, A. Rabbolini, and S. Goidanich. "Setup of a sustainable indoor cleaning methodology for the sculpted stone surfaces of the Duomo of Milan." In: *Herit. Sci.* 2 (2014), pp. 1–13.
- [32] F. Gorel. *Assessment of agar gel loaded with micro-emulsion for the cleaning of porous surfaces*. CeROArt Conserv. Expo. Restaur. Obj. Art., 2010.
- [33] J. A. L. Domingues, N. Bonelli, R. Giorgi, E. Fratini, F. Gorel, and P. Baglioni. "Innovative hydrogels based on semi-interpenetrating p(HEMA)/PVP networks for the cleaning of water-sensitive cultural heritage artifacts." In: *Langmuir : the ACS journal of surfaces and colloids* 29.8 (Feb. 2013), pp. 2746–55.
- [34] E. Carretti, L. Dei, P. Baglioni, and R. G. Weiss. "Synthesis and characterization of gels from polyallylamine and carbon dioxide as gellant". In: *Journal of the American Chemical Society* 125.17 (Apr. 2003), pp. 5121–5129.
- [35] E. Carretti, L. Dei, A. Macherelli, and R. G. Weiss. "Rheoreversible Polymeric Organogels: The Art of Science for Art Conservation". In: *Langmuir* 20.20 (Sept. 2004), pp. 8414–8418.

- [36] E. Carretti, L. Dei, and R. G. Weiss. “Soft matter and art conservation. Rheoreversible gels and beyond”. In: *Soft Matter* 1.1 (May 2005), pp. 17–22.
- [37] E. Carretti, M. Bonini, L. Dei, B. H. Berrie, L. V. Angelova, P. Baglioni, and R. G. Weiss. “New Frontiers in Materials Science for Art Conservation: Responsive Gels and Beyond”. In: *Accounts of Chemical Research* 43.6 (June 2010), pp. 751–760.
- [38] E. Carretti, L. Dei, R. G. Weiss, and P. Baglioni. “A new class of gels for the conservation of painted surfaces”. In: *Journal of Cultural Heritage* 9.4 (Sept. 2008), pp. 386–393.
- [39] M. Bonini, S. Lenz, E. Falletta, F. Ridi, E. Carretti, E. Fratini, A. Wiedenmann, and P. Baglioni. “Acrylamide-Based Magnetic Nanosponges: A New Smart Nanocomposite Material”. In: *Langmuir* 24.21 (Nov. 2008), pp. 12644–12650.
- [40] M. Bonini, S. Lenz, R. Giorgi, and P. Baglioni. “Nanomagnetic Sponges for the Cleaning of Works of Art”. In: *Langmuir* 23.17 (Aug. 2007), pp. 8681–8685.
- [41] J. Domingues, N. Bonelli, R. Giorgi, and P. Baglioni. “Chemical semi-IPN hydrogels for the removal of adhesives from canvas paintings”. In: *Applied Physics A* 114.3 (Mar. 2014), pp. 705–710.
- [42] E. Carretti, S. Grassi, M. Cossalter, I. Natali, G. Caminati, R. G. Weiss, P. Baglioni, and L. Dei. “Poly(vinyl alcohol)-Borate Hydro/Cosolvent Gels: Viscoelastic Properties, Solubilizing Power, and Application to Art Conservation”. In: *Langmuir* 25.15 (2009), pp. 8656–8662.
- [43] E. Carretti, I. Natali, C. Matarrese, P. Bracco, R. G. Weiss, P. Baglioni, A. Salvini, and L. Dei. “A new family of high viscosity polymeric dispersions for cleaning easel paintings”. In: *JOURNAL OF CULTURAL HERITAGE* 11 (2010), pp. 373–380.
- [44] L. V. Angelova, P. Terech, I. Natali, L. Dei, E. Carretti, and R. G. Weiss. “Cosolvent Gel-like Materials from Partially Hydrolyzed Poly (vinyl acetate) s and Borax”. In: *Langmuir* (2011), pp. 11671–11682.
- [45] E. Carretti, C. Matarrese, E. Fratini, P. Baglioni, and L. Dei. “Physicochemical characterization of partially hydrolyzed poly(vinyl acetate)-borate aqueous dispersions”. In: *Soft Matter* (2014).
- [46] C. Berlangieri, E. Andrina, C. Matarrese, E. Carretti, R. Traversi, M. Severi, D. Chelazzi, L. Dei, and P. Baglioni. “Chelators confined into 80pvac-borax highly viscous dispersions for the removal of gypsum degradation layers”. In: *Pure and Applied Chemistry* 89.1 (2017), pp. 97–109.
- [47] A. Tudos and R. Shasfoort. “Introduction to surface plasmon resonance”. In: *Handbook of surface plasmon resonance*. 2008, pp. 1–15.

-
- [48] J. Homola, S. S. Yee, and G. Gauglitz. "Surface plasmon resonance sensors: review". In: *Sensors and Actuators B: Chemical* 54.1 (Jan. 1999), pp. 3–15.
- [49] H. Nguyen, J. Park, S. Kang, and M. Kim. "Surface Plasmon Resonance: A Versatile Technique for Biosensor Applications". In: *Sensors* 15.5 (May 2015), pp. 10481–10510.
- [50] P. A. Van Der Merwe. "Surface plasmon resonance". In: *Protein-ligand interactions: hydrodynamics and calorimetry* 1 (2001), pp. 137–170.
- [51] C. Campbell. *Surface Plasmon Resonance (SPR) Biosensor Development*. Tech. rep., pp. 1–11.
- [52] D. Stuart, A. Haes, C. Yonzon, E. Hicks, and R. Van Duyne. "Biological applications of localised surface plasmonic phenomena". In: *IEE Proceedings - Nanobiotechnology* 152.1 (2005), p. 13.
- [53] K. A. Willets and R. P. Van Duyne. "Localized Surface Plasmon Resonance Spectroscopy and Sensing". In: *Annual Review of Physical Chemistry* 58.1 (May 2007), pp. 267–297.
- [54] M. D. Malinsky, K. L. Kelly, G. C. Schatz, and R. P. Van Duyne. "Chain Length Dependence and Sensing Capabilities of the Localized Surface Plasmon Resonance of Silver Nanoparticles Chemically Modified with Alkanethiol Self-Assembled Monolayers". In: *J. Am. Chem. Soc.* 123.7 (Feb. 2001), pp. 1471–1482.
- [55] T. R. Jensen, M. L. Duval, K. L. Kelly, A. A. Lazarides, G. C. Schatz, and R. P. Van Duyne. "Nanosphere Lithography: Effect of the External Dielectric Medium on the Surface Plasmon Resonance Spectrum of a Periodic Array of Silver Nanoparticles". In: *J. Phys. Chem. B* 103.45 (Nov. 1999), pp. 9846–9853.
- [56] J. J. Mock, D. R. Smith, and S. Schultz. "Local Refractive Index Dependence of Plasmon Resonance Spectra from Individual Nanoparticles". In: *Nano Letters* 3.4 (Apr. 2003), pp. 485–491.
- [57] J. J. Mock, M. Barbic, D. R. Smith, D. A. Schultz, and S. Schultz. "Shape effects in plasmon resonance of individual colloidal silver nanoparticles". In: *The Journal of Chemical Physics* 116.15 (Apr. 2002), pp. 6755–6759.
- [58] Y. Sun and Y. Xia. "Increased Sensitivity of Surface Plasmon Resonance of Gold Nanoshells Compared to That of Gold Solid Colloids in Response to Environmental Changes". In: *Anal. Chem.* 74.20 (Oct. 2002), pp. 5297–5305.
- [59] J. Burgin, M. Liu, and P. Guyot-Sionnest. "Dielectric Sensing with Deposited Gold Bipyramids". In: *J. Phys. Chem. C* 112.49 (Dec. 2008), pp. 19279–19282.

- [60] M. J. Banholzer, N. Harris, J. E. Millstone, G. C. Schatz, and C. A. Mirkin. “Abnormally Large Plasmonic Shifts in Silica-Protected Gold Triangular Nanoprisms”. In: *J. Phys. Chem. C* 114.16 (Apr. 2010), pp. 7521–7526.
- [61] A. Madeira, E. Vikeved, A. Nilsson, B. Sjögren, P. E. Andren, and P. Svenningsson. “Identification of protein-protein interactions by surface plasmon resonance followed by mass spectrometry”. In: *Curr Protoc Protein Sci* Chapter 19 (Aug. 2011).
- [62] J. Majka and C. Speck. “Analysis of protein-DNA interactions using surface plasmon resonance”. In: *Adv. Biochem. Eng. Biotechnol.* 104 (2007), pp. 13–36.
- [63] R. L. Rich, L. R. Hoth, K. F. Geoghegan, T. A. Brown, P. K. LeMotte, S. P. Simons, P. Hensley, and D. G. Myszka. “Kinetic analysis of estrogen receptor/ligand interactions”. In: *PNAS* 99.13 (June 2002), pp. 8562–8567.
- [64] M. Nuopponen and H. Tenhu. “Gold Nanoparticles Protected with pH and Temperature-Sensitive Diblock Copolymers”. In: *Langmuir* 23.10 (May 2007), pp. 5352–5357.
- [65] C. L. Nehl, H. Liao, and J. H. Hafner. “Optical properties of star-shaped gold nanoparticles”. In: *Nano Lett.* 6.4 (Apr. 2006), pp. 683–688.
- [66] Y. Xia and N. J. Halas. “Shape-Controlled Synthesis and Surface Plasmonic Properties of Metallic Nanostructures”. In: *MRS Bulletin* 30.5 (May 2005), pp. 338–348.
- [67] Y. Sun and Y. Xia. “Shape-controlled synthesis of gold and silver nanoparticles”. In: *Science* 298.5601 (Dec. 2002), pp. 2176–2179.
- [68] B. Wiley, Y. Sun, B. Mayers, and Y. Xia. “Shape-controlled synthesis of metal nanostructures: the case of silver”. In: *Chemistry* 11.2 (Jan. 2005), pp. 454–463.
- [69] Q. Xu, J. Bao, F. Capasso, and G. M. Whitesides. “Surface Plasmon Resonances of Free-Standing Gold Nanowires Fabricated by Nanoskiving”. In: *Angewandte Chemie International Edition* 45.22 (May 2006), pp. 3631–3635.
- [70] G. Carotenuto, G. L. Peruta, and L. Nicolais. “Thermo-chromic materials based on polymer-embedded silver clusters”. In: *Sensors and Actuators B: Chemical* 114.2 (Apr. 2006), pp. 1092–1095.
- [71] P. H. C. Camargo, K. G. Satyanarayana, and F. Wypych. “Nanocomposites: synthesis, structure, properties and new application opportunities”. In: *Materials Research* 12.1 (Mar. 2009), pp. 1–39.

-
- [72] A. Scott, R. Gupta, and G. U. Kulkarni. “A Simple Water-Based Synthesis of Au Nanoparticle/PDMS Composites for Water Purification and Targeted Drug Release”. In: *Macromolecular Chemistry and Physics* 211.15 (2010), pp. 1640–1647.
- [73] A. Bal, F. E. Cepni, O. Cakir, I. Acar, and G. Guclu. “Synthesis and Characterization of Copolymeric and Terpolymeric Hydrogel-Silver Nanocomposites Based on Acrylic Acid, Acrylamide and Itaconic Acid: Investigation of their Antibacterial Activity Against Gram-Negative Bacteria”. In: *Brazilian Journal of Chemical Engineering* 32.2 (June 2015), pp. 509–518.
- [74] D. Li, C. Li, A. Wang, Q. He, and J. Li. “Hierarchical gold/copolymer nanostructures as hydrophobic nanotanks for drug encapsulation”. In: *J. Mater. Chem.* 20.36 (Aug. 2010), pp. 7782–7787.
- [75] L. L. Beecroft and C. K. Ober. “Nanocomposite Materials for Optical Applications”. In: *Chem. Mater.* 9.6 (June 1997), pp. 1302–1317.
- [76] H. Sadabadi, S. Badilescu, M. Packirisamy, and R. Wuthrich. “PDMS-Gold Nanocomposite Platforms with Enhanced Sensing Properties”. In: *Journal of Biomedical Nanotechnology* 8.4 (2012), pp. 1–11.
- [77] R. Gradess, R. Abargues, A. Habbou, J. Canet-Ferrer, E. Pedrueza, A. Russell, J. L. Valdes, and J. P. Martinez-Pastor. “Localized surface plasmon resonance sensor based on Ag-PVA nanocomposite thin films”. In: *Journal of Materials Chemistry* 19.48 (2009), pp. 9233–9240.
- [78] M. Tagaya and M. Nakagawa. “Incorporation of Decanethiol-Passivated Gold Nanoparticles into Cross-Linked Poly(Dimethylsiloxane) Films”. In: *Smart Materials Research* (2011).
- [79] Q. Zhang, J.-j. Xu, Y. Liu, and H.-y. Chen. “In-situ synthesis of poly (dimethylsiloxane) - gold nanoparticles composite films and its application in microfluidic systems”. In: *Lab on a Chip* 184 (2008), pp. 352–357.
- [80] P. Devi, A. Y. Mahmoud, S. Badilescu, M. Packirisamy, P. Jeevanandam, and V.-V. Truong. “Synthesis and Surface Modification of Poly (dimethylsiloxane) - Gold Nanocomposite Films for Biosensing Applications”. In: *IEEE*, Mar. 2010, pp. 1–5.
- [81] H. Sadabadi, S. Badilescu, M. Packirisamy, and W. Rolf. “Integration of gold nanoparticles in PDMS microfluidics for lab-on-a-chip plasmonic biosensing of growth hormones”. In: *Biosensors and Bioelectronics* 44 (2013), pp. 77–84.
- [82] A. Goyal, A. Kumar, P. K. Patra, S. Mahendra, S. Tabatabaei, P. J. J. Alvarez, G. John, and P. M. Ajayan. “In situ Synthesis of Metal Nanoparticle Embedded Free Standing Multifunctional PDMS Films”. In: *Macromolecular Rapid Communications* 30.13 (July 2009), pp. 1116–1122.

- [83] M. Wei, Y. Gao, X. Li, and M. J. Serpe. “Stimuli-responsive polymers and their applications”. In: *Polym. Chem.* 8.1 (Dec. 2016), pp. 127–143.
- [84] M. Gavrilescu and Y. Chisti. “Biotechnology: a sustainable alternative for chemical industry”. In: *Biotechnology Advances* 23 (Nov. 2005), pp. 471–499.
- [85] A. Schmid, F. Hollmann, J. B. Park, and B. Buhler. “The use of enzymes in the chemical industry in Europe”. In: *Current Opinion in Biotechnology* 13.4 (Aug. 2002), pp. 359–366.
- [86] J. L. Ramirez, M. A. Santana, I. Galindo-Castro, and A. Gonzalez. “The role of biotechnology in art preservation”. In: *Trends in Biotechnology* 23.12 (Dec. 2005), pp. 584–588.
- [87] P. Fernandes. “Applied microbiology and biotechnology in the conservation of stone cultural heritage materials”. In: *Applied Microbiology and Biotechnology* 73.2 (Nov. 2006), pp. 291–296.
- [88] L. Micheli, C. Mazzuca, A. Palleschi, and G. Palleschi. “Combining a hydrogel and an electrochemical biosensor to determine the extent of degradation of paper artworks”. In: *Analytical and Bioanalytical Chemistry* 403.6 (June 2012), pp. 1485–1489.
- [89] F. Bottari, P. Oliveri, and P. Ugo. “Electrochemical immunosensor based on ensemble of nanoelectrodes for immunoglobulin IgY detection: Application to identify hen’s egg yolk in tempera paintings”. In: *Biosensors and Bioelectronics* 52 (Feb. 2014), pp. 403–410.
- [90] S. Scarano, C. Berlangieri, E. Carretti, L. Dei, and M. Minunni. “Tunable growth of gold nanostructures at a PDMS surface to obtain plasmon rulers with enhanced optical features”. In: *Microchimica Acta* 184 (2017), pp. 3093–3102.
- [91] H. A. Barnes. *Handbook of Elementary Rheology*. 2000.
- [92] G. Schramm. *A Practical Approach to Rheology and Rheometry*. 1998.
- [93] R. Suriano, G. Griffini, M. Chiari, M. Levi, and S. Turri. “Rheological and mechanical behavior of polyacrylamide hydrogels chemically crosslinked with allyl agarose for two-dimensional gel electrophoresis”. In: *Journal of the Mechanical Behavior of Biomedical Materials* 30 (2014), pp. 339–346.
- [94] “Modulus of elasticity, E”. In: *IUPAC Compendium of Chemical Terminology*. Research Triangle Park, NC: IUPAC, June 2009.
- [95] M. Shibayama. “Structure-mechanical property relationship of tough hydrogels”. In: *Soft Matter* 8 (2012), pp. 8030–8038.